UNIVERSITI TEKNOLOGI MARA

COPPER ALUMINUM OXIDE AND CHROMIUM GALIUM CARBIDE IN POLYVINYL ALCOHOL BASED PASSIVE Q-SWITCHER AND MODE-LOCKER

MUHAMMAD NUR AL HAFIZ BIN MOHAMAD HUSAINI

PhD

July 2026

UNIVERSITI TEKNOLOGI MARA

COPPER ALUMINUM OXIDE AND CHROMIUM GALIUM CARBIDE IN POLYVINYL ALCOHOL BASED PASSIVE Q-SWITCHER AND MODE-LOCKER

MUHAMMAD NUR AL HAFIZ BIN MOHAMAD HUSAINI

Thesis submitted in fulfilment
of the requirements for the degree of
Doctor of Philosophy
(Electrical Engineering)

Faculty of Electrical Engineering

July 2026

CONFIRMATION BY PANEL OF EXAMINERS

I certify that a Panel of Examiners has met on 8th May 2026 to conduct the final examination of Muhammad Nur Al Hafiz bin Mohamad Husaini on his Doctor of Philosophy thesis entitled "Copper Aluminum Oxide And Chromium Galium Carbide In Polyvinyl Alcohol Based Passive Q-Switcher And Mode-Locker" in accordance with Universiti Teknologi MARA Act 1976 (Akta 173). The Panel of Examiners recommends that the student be awarded the relevant degree. The Panel of Examiners was as follows:

Zakiah Mohd Yusoff, PhD
Associate Professor
Faculty of Electrical Engineering
Universiti Teknologi MARA
(Chairman)

Nani Fadzlina Naim, PhD
Associate Professor
Faculty of Electrical Engineering
Universiti Teknologi MARA
(Internal Examiner)

Fauzan Ahmad, PhD
Associate Professor
Malaysia-Japan International Institute of Technology
(External Examiner)

PROF DR HJH ZURAEDA IBRAHIM
Dean
Institute of Postgraduate Studies
Universiti Teknologi MARA

Date: 30 July 2026

AUTHOR'S DECLARATION

I declare that the work in this thesis was carried out in accordance with the regulations of Universiti Teknologi MARA. It is original and is the results of my own work, unless otherwise indicated or acknowledged as referenced work. This thesis has not been submitted to any other academic institution or non-academic institution for any degree or qualification.

I, hereby, acknowledge that I have been supplied with the Academic Rules and Regulations for Postgraduate, Universiti Teknologi MARA, regulating the conduct of my study and research.

Name of Student	:	Muhammad Nur Al Hafiz bin Mohamad Husaini
Student ID. No.	:	2023720477
Programme	:	Doctor Of Philosophy (Electrical Engineering) – CEEE950
Faculty	:	Electrical Engineering
Thesis Title	:	Copper Aluminum Oxide And Chromium Galium Carbide In Polyvinyl Alcohol Based Passive Q-Switcher And Mode-Locker
Signature of Student	:	
Date	:	July 2026

ABSTRACT

Passively Q-switched and mode-locked fiber lasers based on saturable absorbers (SAs) provide an efficient and flexible platform for generating short and ultrashort optical pulses. These lasers offer important advantages, including high beam quality, compact and alignment-free configuration, low cost, and strong compatibility with all-fiber systems. However, many conventional SA materials still face limitations such as wavelength-restricted operation due to bandgap dependence, narrow lasing bandwidths, low optical damage thresholds, and weak nonlinear absorption. To address these issues, this study explores emerging materials, specifically transparent conducting oxides and MAX-phase compounds, as alternative SAs. Copper Aluminium Oxide ($CuAlO_2$) and Chromium Gallium Carbide (Cr_2GaC) are investigated as new SA candidates. Both materials are mixed with polyvinyl alcohol (PVA) to form thin-film SAs using a simple casting method. The films are placed between fiber ferrules and integrated into an erbium-doped fiber laser (EDFL) ring cavity to enable passive Q-switching and mode-locking. Using the $CuAlO_2$ thin-film SA, stable Q-switched operation was achieved with pump powers from 132.15 mW to 210.62 mW. As the pump increased, the repetition rate rose from 66.09 kHz to 84.96 kHz, while the pulse width decreased from 6.31 μs to 5.03 μs. The laser operated at 1563.3 nm, delivering a maximum pulse energy of 43.55 nJ and a slope efficiency of 1.95%. For mode-locking, a 100 m single-mode fiber (SMF) spool was added to lengthen the cavity and enhance nonlinear effects. Self-starting mode-locking was obtained between 141.38 mW and 233.7 mW. At the threshold of 141.38 mW, pulses centered at 1560 nm were generated with a repetition rate of 1.792 MHz and a pulse duration of 3.17 ps. The Cr_2GaC thin-film SA also enabled both Q-switched and mode-locked operation. In the Q-switched regime, stable pulses were produced at 1530.6 nm with pump powers from 49.06 mW to 72.14 mW. The repetition rate reached 76.92 kHz, with a minimum pulse width of 5.03 μs and an SNR of 60.14 dB. For mode-locking using Cr_2GaC, soliton pulses centered at 1558.2 nm were generated. With an additional 100 m of SMF, a long-cavity configuration produced a stable pulse train at 1.82 MHz, matching the calculated cavity length. Mode-locking was sustained from 53.7 mW to 95.2 mW, yielding 3.04 ps pulses and a maximum pulse energy of 3.74 nJ. High stability was confirmed by an SNR of 71.7 dB. Furthermore, dark-pulse generation was demonstrated using the Cr_2GaC SA by extending the cavity with 150 m of SMF under net anomalous dispersion. A stable dark-pulse train was obtained between 83.68 mW and 99.83 mW, operating at 1.27 MHz with pulse widths of about 300 ns and dual spectra at 1529.6 nm and 1531.6 nm. At 99.83 mW, the average output power reached 4.56 mW with an SNR of 69.30 dB. These results confirm that $CuAlO_2$ and Cr_2GaC are effective SAs for both Q-switching and mode-locking in EDFLs, showing strong potential for applications in ultrafast lasers, nonlinear optics, and advanced photonic systems.

ACKNOWLEDGEMENT

I begin by expressing my deepest gratitude to Allah for granting me the opportunity to embark on my PhD journey and for giving me the strength, patience, and determination to complete this long and demanding work. This journey has been filled with challenges, learning experiences, and personal growth, and every step of the way has been guided by His blessings. Without His mercy and guidance, it would not have been possible for me to overcome the difficulties and remain steadfast in completing this thesis.

I am profoundly thankful to my supervisors, Prof. Madya Ir. Dr. Zulzilawati Binti Jusoh, Prof. Sulaiman Wadi Harun, Prof. Madya Ts. Dr. Arni Munira Binti Markom, and Dr. Amri Bin Ab Rahman, for their continuous guidance, patience, and encouragement throughout this research. Their expertise, dedication, and commitment to excellence have greatly shaped my academic development. They consistently provided insightful advice, constructive feedback, and thoughtful direction, which helped refine my ideas and strengthen the quality of this thesis. Their willingness to guide me through every stage of this work, from the early planning to the final writing, has been invaluable.

I would also like to sincerely acknowledge the Photonic Engineering Laboratory at the University of Malaya for providing the facilities, equipment, and technical resources required for this study. The supportive research environment made it possible for me to carry out experiments and analyses effectively. My heartfelt appreciation goes to the members of the photonic lab—Ts. Dr. Aeriyn D., Izzah, Athirah, Dr. Haziq, Dr. Imran, Dr. Hasanain, and Dr. Aina—for their kind assistance, meaningful discussions, and helpful suggestions. Their collaboration, encouragement, and readiness to share knowledge greatly improved both this research and my understanding of the field of photonics.

I am also grateful to all friends, colleagues, and fellow researchers who have directly or indirectly contributed to this journey. Their companionship, moral support, and shared experiences made this demanding period more manageable and enjoyable. The friendships built along the way have been a source of motivation and strength during difficult times.

Finally, this thesis is lovingly dedicated to my parents, whose sacrifices, prayers, and endless support have guided me throughout my academic life. Their unwavering belief in me, constant encouragement, and unconditional love gave me the confidence to face every challenge and to keep moving forward despite obstacles. They have always been my greatest source of strength, and this achievement belongs to them as much as it belongs to me.

TABLE OF CONTENTS

		Page
CONFIRMATION BY PANEL OF EXAMINERS		**ii**
AUTHOR'S DECLARATION		**iii**
ABSTRACT		**iv**
ACKNOWLEDGEMENT		**v**
TABLE OF CONTENTS		**vi**
LIST OF TABLES		**ix**
LIST OF FIGURES		**x**
LIST OF SYMBOLS		**xiv**
LIST OF ABBREVIATIONS		**xvi**
CHAPTER 1 INTRODUCTION		**1**
1.1	Research Background	1
1.2	Problem Statement	3
1.3	Research Objectives	5
1.4	Research Questions	6
1.5	Scope Of Study	6
1.6	Significance Of Study	7
1.7	Thesis Outline	8
CHAPTER 2 LITERATURE REVIEW		**11**
2.1	Introduction	11
2.2	Optical Fiber	12
2.3	Fiber Laser	13
2.4	Erbium-Doped Fiber Laser	14
2.5	Pulse Generation In Fiber Laser	16
	2.5.1 Q-Switching	19
	2.5.2 Mode-Locking	20
2.6	Description Of Laser Pulses	23
2.7	Pulse Propagation In A Fiber	25

2.7.1 Dispersion 25
2.7.2 Nonlinear Effect 26
2.7.3 Formation Of Kelly Sidebands 27
2.8 Dark Pulses 28
2.9 Saturable Absorber (SA) 30
2.10 SA Materials 32
2.11 Summary 34

CHAPTER 3 RESEARCH METHODOLOGY 39

3.1 Introduction 39
3.2 Material 40
3.2.1 Polyvinyl Alcohol 40
3.2.2 Copper Aluminum Oxide ($CuAlO_2$) 41
3.2.3 Chromium Gallium Carbide (Cr2GaC) 43
3.3 Fabrication Of SA 44
3.3.1 Preparation Of The $CuAlO_2$ Film 45
3.3.2 Preparation Of The Cr_2GaC Film 46
3.4 Characterization Of The Prepared Thin Film SA 47
3.5 Laser Configuration 49
3.6 Summary 51

CHAPTER 4 RESULTS AND DISCUSSION I: COPPER ALUMINUM OXIDE–BASED Q-SWITCHING AND MODE-LOCKING 53

4.1 Introduction 53
4.2 Characteristics Of The $CuAlO_2$ Film. 55
4.3 Laser Configuration 58
4.4 Q-Switching Performance 60
4.5 Mode-Locking Performance 65
4.6 Chapter Summary 70

CHAPTER 5 RESULTS AND DISCUSSION II: CHROMIUM GALIUM CARBIDE–BASED Q-SWITCHING AND MODE-LOCKING 71

5.1 Introduction 71
5.2 Characteristics Of The Cr_2GaC Film. 72
5.3 Laser Configuration. 74
5.4 Q-Switching Performance With Cr_2GaC SA 76
5.5 Mode-Locking Performance With Cr_2GaC SA 82
5.6 Dark Pulse Generation In Mode-Locked EDFL Using Cr_2GaC SA 88
5.7 Chapter Summary 93

CHAPTER 6 CONCLUSION 97

6.1 Research Outcome 97
6.2 Recommendation & Limitation Of Work 100
REFERENCES 102
AUTHOR'S PROFILE 112

LIST OF TABLES

Tables	Title	Page
Table 2.1	Q-Switched EDFL With 2D Materials As SA	33
Table 2.2	Mode-locked EDFL With 2D Materials As SA	34
Table 4.1	Performance Comparison Of Proposed $CuAlO_2$-Based Q-Switched EDFL With Other Works.	63
Table 4.2	Performance Comparison Of Proposed $CuAlO_2$-Based Mode-Locked Lasers With Other Works.	69
Table 5.1	Comparison Of Q-Switched Laser Performance Using The Cr_2GaC SA With Other Reported SAs.	82
Table 5.2	Mode-Locking Performance For Various SA Materials	87
Table 5.3	Performance Comparison Of The Dark Pulse Mode-Locked EDFL With Other Eeported Studies.	93
Table 5.4	Performance Of Difference SA Materials.	95

LIST OF FIGURES

Figures	Title	Page
Figure 2.1	The Structure Of An Optical Fiber (Ahmad, &, Mokhtar, 2025).	13
Figure 2.2	Energy-Level Diagram Of Erbium Ions Illustrating The Pumping Process And Stimulated Emission Mechanism (Ahmad, &, Salam 2024).	15
Figure 2.3	Illustration of material removal mechanisms: (a) melt ejection and vaporization under short-pulse laser irradiation; (b) phase explosion induced by ultrashort-pulse laser irradiation (Ahmad, H., Rusni, 2024)..	18
Figure 2.4	Illustrations showing the random phase and locked phase(Ahmed, & Latiff, 2016)	21
Figure 2.5	Illustration of pulse duration (τL) defined by the full width at half maximum (FWHM), and the period T between two successive laser pulses. The pulse energy (EL) corresponds to the area under the power–time curve.	24
Figure 2.6	Schematic representation of the saturable absorption process based on a two-level electronic model(Chen, H., Yin, 2017)..	31
Figure 3.1	Basic process flowchart of the research methodology adopted in this study	40
Figure 3.2	PVA powder used in this study	41
Figure 3.3	Crystal structure of delafossite $CuAlO_2$. The lattice parameter a represents the basal (horizontal) plane, c denotes the lattice parameter along the vertical stacking direction, and cz corresponds to the height of one structural block, typically associated with a single Cu–O layer.	43

Figure 3.4 Crystal structure of a MAX-phase material with the general formula M_2AX (illustrated for Cr_2GaC). The structure consists of alternating M–X octahedral layers (green: M = Cr; blue: X = C) and A-element atomic layers (purple: A = Ga) stacked along the c-axis. 44

Figure 3.5 The procedure for preparing the $CuAlO_2$-PVA film. The inset figure displays an image of the produced film. 46

Figure 3.6 Complete fabrication flow for Cr_2GaC film SA. 47

Figure 3.7 Experimental setups for (a) linear absorption and (b) nonlinear absorption characterization. 48

Figure 3.8 Schematic of the erbium-doped fiber laser (EDFL) cavity employed in this study for the generation of Q-switched and mode-locked pulses using a passive modulation technique based on a thin-film SA. 50

Figure 4.1 (a) EDX analysis results, with an inset showing the FESEM image at 3000x magnification. (b) XRD pattern of d 56

Figure 4.2 (a) Linear, and (b) non-linear absorption characteristics 58

Figure 4.3 Schematic of the proposed EDFL incorporating a $CuAlO_2$ film as a SA. An additional 100 m spool of single-mode fiber was included to enable mode-locking operation. 59

Figure 4.4 (a) Oscilloscope trace, (b) RF spectrum with a span of 1000 kHz, (c) Output spectrum, and (d) Output spectrum measured over time. 61

Figure 4.5 Q-switched laser performance showing (a) output power and pulse energy as functions of pump power, and (b) repetition rate and pulse width versus pump power. 62

Figure 4.6 Analysis of Mode-Locked Laser Parameters (a) Output power and pulse energy versus pump power, (b) Autocorrelation trace, (c) Output spectrum, (d) Typical oscilloscope trace. 66

Figure 4.7 (a) Variation of peak power with pump power, (b) corresponding RF spectrum at 233.7 mW. Inset highlights the fundamental mode featuring an SNR of 71.75 dB, and (c) stability test result. 68

Figure 5.1 (a) Real image of Cr_2GaC film transducer, (b) The Integration of Cr_2GaC film onto the tip of fiber ferrule, (c) Cr_2GaC transducer mechanism, (d) its corresponding FESEM image, and (e) EDX analysis results 73

Figure 5.2 Optical characterization of Cr_2GaC film transducer (a) linear absorption, (b) nonlinear absorption. 74

Figure 5.3 Schematic representation of the EDFL employing a Cr_2GaC SA. A 100-meter-long SMF is also inserted between the SA and coupler to effectively manage dispersion and enhance nonlinear effects, crucial for achieving mode-locking. 76

Figure 5.4 Q-switched pulse trains recorded at pump powers of (a) 49.06 mW, (b) 62.91 mW, and (c) 72.14 mW. 77

Figure 5.5 Performance characteristics of the Q-switched EDFL: (a) optical spectrum, (b) RF spectrum, (c) dependence of pulse width and repetition rate on pump power, and (d) output power and pulse energy as functions of pump power. 79

Figure 5.6 Output spectrum stability monitored over a 60-minute duration. 81

Figure 5.7 (a) output spectrum, (b) typical pulse train. Inset shows the envelope of two-pulse. (c) RF spectrum. Inset displays the fundamental frequency, and (d) autocorrelator trace. 85

Figure 5.8 The Cr_2GaC SA performance with pump power variation (a) average output power and pulse energy, and (b) peak power. 86

Figure 5.9 The output spectrum evolution over time 87

Figure 5.10 Performance of Cr_2GaC dark pulse mode-locked (a) OSA spectrum (b) pulse train (c) RF spectrum 91

Figure 5.11 Average output power as a function of pumping strength for the Cr_2GaC-based mode-locked laser 92

LIST OF SYMBOLS

Symbols

n_1 .	Refractive Index of the Core
n_2	Refractive Index of the Cladding
T_r	Round-trip Time of the Resonator
n	Refractive Index of the Medium
L	Length of Laser Resonator
c	Speed of Light
f	Frequency
τ_p	Pulse Width
S_p	Pulse Shape
q_0	Saturable Absorber Loss Coefficient
δ	Ratio of Saturable to Non-Saturable Loss
η	Energy Extraction Efficiency
E_p	Pulse Energy
P_{ave}	Average Output Power
P_p	Peak Power
v_m	Speed of Light in Material
k	Frequency-Dependant Wave Number
v_g	Group Velocity
ω	Angular Frequency

β^2	Group Velocity Dispersion Coefficient
D_m	Wavelength-Dependent Fiber Dispersion
λ	Wavelength
λ_D	Dispersion Wavelength
n_{eff}	Effective Refraction Index
l_{int}	Optical Intensity
ϕ_{nl}	Non-linear Phase Constant
$\alpha(I)$	Intensity-Dependant Absorption
α_s	Saturable Absorption
α_{ns}	Non-saturable Absorption
I	Intensity of Light
I_{sat}	Saturation Intensity
λ_{3dB}	3-dB Spectral Width
τ_{FWHM}	FWHM of the Pulse
α	Loss of the Resonator
Δv	Frequency Spacing Between Adjacent Longitudinal Modes

LIST OF ABBREVIATIONS

Abbreviations

2D	Two Dimensional
Al	Aluminium
ASE	Amplified Spontaneous Emission
AZO	Aluminium Zinc Oxide
BP	Black Phosphorus
Bi_2Te_3	Bismuth Telluride
Bi_2Se_3	Bismuth Selenide
C	Carbon
CeO_2	Cerium Oxide
CNT	Carbon Nanotube
CuNW	Copper Nanowires
CuPc	Copper Phthalocyanine
CVD	Chemical Vapour Deposition
CW	Continuous Wave
DI	Deionized
EDF	Erbium-Doped Fiber
EDFA	Erbium-Doped Fiber Amplifier
EDX	Energy-Dispersive X-ray

Er^{3+}	Erbium
FC	Ferrule Connector / Fibre Channel
FePc	Iron Phthalocyanine
PC	Physical Contact
FESEM	Field Emission Scanning Electron Microscopy
FWHM	Full Width Half-Maximum
FWM	Four-wave Mixing
GVD	Group Velocity Dispersion
ISO	Optical Isolator
LASER	Light Amplification By Stimulated Emission Of Radiation
L	Length
LPE	Liquid-phase Exfoliation
LD	Laser Diode
LEDs	Light-emitting Diodes
MMF	Multimode Ffibre
MnPc	Manganese Phthalocyanine
MoS_2	Molybdenum Disulfide
$MoSe_2$	Molybdenum Selenide
MPc	Metal Phthalocyanine
NA	Numerical Aperture
NPR	Nonlinear Polarization Rotation

OLEDs	Organic Light-Emitting Diodes
OPM	Optical Power Meter
O	Oxygen
OSA	Optical Spectrum Analyzer
OSC	Oscilloscope
PC	Polarization Controller
PVA	Polyvinyl Alcohol
Q-factor	Quality Factor
Q-switched	Quality-Switched
REE	Rare-Earth Element
RF	Radio Frequency
SA	Saturable Absorber
SEM	Scanning Electron Microscopy
SESAMs	Semiconductor Saturable Absorber Mirrors
Si	Silicon
SMF	Single Mode Fibre
SNR	Signal-to-Noise Ratio
SPM	Self-Phase Modulation
TBP	Time-Bandwidth Product
Ti_3AlC_2	Titanium Aluminum Carbide
TMD	Transition Metal Dichalcogenide

TIR	Total Internal Reflection
ZnO	Zinc Oxide
ZnPc	Zinc Phthalocyanine
Bi_2Se_3	Bismuth Selenide
$ZrSe_2$	Zirconium Diselenide
ReS_2	Rhenium Disulfide
$NbTe_2$	Niobium Ditelluride
$MoWS_2$	Molybdenum Tungsten Disulfide Alloy
SnS_2	Tin Disulfide

CHAPTER 1
INTRODUCTION

1.1 Research Background

Fiber technology has evolved into a mature and highly influential industrial sector, driven largely by the rapid expansion of optical communication systems. As global demand for high-speed data transmission continues to rise, conventional non-optical technologies can no longer meet performance requirements, making optical communication indispensable. The maturity of this technology has significantly reduced the cost of optical components, which in turn has accelerated progress in related fiber-optic applications, particularly fiber lasers that use rare-earth-doped fibers as the gain medium. Fiber lasers have attracted considerable attention due to their compact and alignment-free architecture, excellent beam quality, high efficiency, and cost-effectiveness, outperforming many traditional bulk solid-state lasers ,((N., & Al-Samuraee, A.,2011). ,(Eskandarian, P., & Zabolian, H. , 2022). For applications such as material micro-processing, optical communications, biochemistry, and metrology, lasers are typically required to operate in a pulsed regime. Short, high-peak-power pulses can be generated through Q-switching, which produces microsecond-to-nanosecond pulses, or through mode-locking, which enables ultrafast pulses in the picosecond-to-femtosecond range (Ahmad, & Elseman, 2026)

Pulsed fiber lasers can be realized using either active or passive techniques. Active methods employ acousto-optic or electro-optic modulators to control pulse formation, offering precise tunability but at the cost of bulky, complex, and expensive components. In contrast, passive techniques rely on saturable absorbers (SAs), which provide simpler, more compact, and self-starting laser systems, benefiting from low saturation intensity and fast recovery time ., (Kamangar, S., & Harun, S. W. ,2025)Among various SAs, semiconductor saturable absorber mirrors (SESAMs) are widely used due to their reliability; however, they suffer from limited operating bandwidth and high fabrication cost (Ahmad, &, Mokhtar, 2025).

These limitations have driven strong interest in alternative materials, especially two-dimensional (2D) materials such as graphene (Ahmad, A. D., Mokhtar, 2024) black phosphorus (BP) (Ahmad, &, Salam 2024), topological insulators (TIs) ., (Kamangar,

S., & Harun, S. W. ,2025)such as Bi2Te3, Sb2Te3, Bi2Se3, and transition metal dichalcogenides (TMDs) (Ahmad, A. D., Salam, 2014), (Rusni, N., & Samion, M. , 2025) including MoS2, ZrSe2, ReS2, NbTe2, MoWS2, and SnS2. These materials exhibit ultrafast carrier dynamics, strong optical nonlinearity, and broad absorption bandwidth, making them attractive for pulsed laser generation (Ahmad, A. D., Mokhtar, 2024). Despite its broadband operation and ultrafast recovery, graphene suffers from low modulation depth and zero bandgap. Other 2D materials such as BP, TIs, and TMDs have demonstrated impressive pulsed-laser performance; for example, $NbTe_2$ enabled vector soliton generation (Aidit, S. N., & Ismail, M. F. , 2018), while SnS_2 produced 623 fs pulses at 29.33 MHz Manaf, M., & Arof, H. (2015). However, many of these materials possess relatively low optical damage thresholds, limiting their long-term laser performance. Consequently, the search for new, robust SA materials remains an active research direction.

In contrast to previous saturable absorber, $CuAlO_2$, a stable delafossite oxide, and Cr_2GaC, a mechanically strong MAX-phase material, exhibit better resistance to heat accumulation and optical stress, making them promising candidates for more durable and stable long-term pulsed laser operation. Many conventional nanomaterial-based saturable absorbers can degrade under prolonged high-intensity laser exposure, leading to oxidation, structural defects, increased insertion loss, or unstable pulse generation. These restrictions could lower laser performance and reliability over time. On the other hand, $CuAlO_2$, a stable delafossite oxide, and Cr_2GaC, a mechanically robust MAX-phase material, have superior resistance to heat accumulation and optical stress, which makes them viable options for more stable and long-term pulsed laser operation as $CuAlO_2$ and Cr_2GaC offer higher optical damage thresholds due to their superior thermal stability, stronger chemical durability, and robust crystal structures.

Recently, the development of efficient and low-cost absorber materials has also attracted attention in renewable-energy and photonic technologies. Metal-oxide-based composites are particularly promising due to their excellent thermal stability, chemical durability, and tunable optical properties (Ahmad, H., & Harun, S. W, 2016), (Ahmed, M. H. M., Latiff, , 2016). Among them, aluminium–copper oxide composites have shown strong potential for solar thermal collectors, photothermal devices, and energy conversion systems ., (Arof, H., & Harun, S. W., 2016). Aluminium offers lightweight structure and high thermal conductivity, while copper oxide, a p-type semiconductor with a narrow bandgap, exhibits strong absorption in the visible and

near-infrared regions (Diblawe, A. M., & Harun, S. W., 2025). Their combination can form nanostructured or multilayer absorbers with enhanced optical absorption, heat transfer, and mechanical stability (Yasin, M., Harun, 2025),(Aljunid, & Ghafar,2024). Copper aluminium oxide ($CuAlO_2$)-based absorbers have been synthesized using techniques such as chemical vapor deposition(Alrebdi, & Sadiq.2025) sputtering, sol-gel processing (Apandi, & Ahmad, ,2017, and thermal oxidation (Barmenkov, & Kir'yanov,2014), with their properties tunable through control of thickness, composition, and morphology (Olsson,., & Simpson, J. R. ,1999), (Rosaiah, P., & Jeon, C.-W. ,2023).

In parallel, MAX phase materials have emerged as attractive alternatives for photonic applications. Unlike MXenes, which require costly and hazardous etching processes, MAX phases are easier and cheaper to fabricate. They exhibit a unique combination of ceramic and metallic properties, including oxidation resistance, radiation tolerance, high-temperature stability, excellent electrical conductivity, good nonlinear saturation, high damage tolerance, and strong thermal shock resistance (K.-H., & Hsieh, W.-F. ,2014),(Chen, & Yin,2017),(Chen, & Cheak, 2024),(Czyzyk,2018), (Dacey, G. ,1962). . These features make MAX phases promising candidates for saturable absorber applications. Among them, Chromium Gallium Carbide (Cr_2GaC) stands out due to its good oxidation resistance and mechanical robustness (Apsari, R., & Harun, S. W., 2023).

In this work, two novel materials—Copper Aluminium Oxide ($CuAlO_2$) and Chromium Gallium Carbide (Cr_2GaC)—are investigated as potential saturable absorbers for Q-switched and mode-locked fiber lasers. Both materials are mixed with polyvinyl alcohol (PVA) to form thin-film SAs using a simple casting technique. The films are then inserted between fiber ferrules and integrated into an erbium-doped fiber laser (EDFL) ring cavity to function as passive Q-switchers and mode-lockers for pulsed laser generation.

1.2 Problem Statement

Owing to their high stability, reliability, and compact size together with their wide-ranging applications in optical communication, nonlinear optics, biomedicine, and defense technologies, fiber lasers have attracted considerable research interest (Dong, L., & Samson, B, 2016), (Zhao, C., & Zhong, J ,2020).

Achieving high-quality pulse generation in fiber lasers requires careful optimization at multiple levels (Moussa, M. E., & Harun, S. W. , 2026). In this work, pulse generation is realized using a passive approach for both Q-switching and mode-locking, due to its simplicity, robustness, and cost effectiveness compared with active techniques, which rely on additional electronic components and are therefore more complex and expensive. Generation through passive done by using saturable absorber, SA as loss modulator.

In passive pulsed lasers, the key element responsible for pulse formation is the SA. Numerous materials have been proposed and demonstrated as SAs, as discussed in the previous section. However, many of these materials suffer from inherent limitations. For instance, SESAMs, although widely studied, are restricted by narrow operating bandwidth and high fabrication cost (Feng, M., Silverman, 2010), (. Fu, & Hua,2014). Other candidates, such as two-dimensional materials including graphene [32, 33], BP (Hamida, B. A., & Harun, S. W. W. , 2024)), (Hammadi, & Mansour,2018) TIs (Haris, & Arof, 2018) and TMDs (Ahmad, &, Salam 2024), have also been reported to exhibit drawbacks such as low modulation depth and poor thermal stability (Feng, & Silverman, 2010), (Haris, & Batumalay,2019). These limitations highlight the need to explore and develop new materials for use as SAs. A saturable absorber is a material whose optical absorption decreases with increasing incident light intensity. To function effectively, it must exhibit a fast and reversible change in absorption in response to intensity variations. This fundamental requirement must be carefully evaluated when investigating new materials for SA applications.

Recently, transparent conducting oxides (TCOs) have attracted growing attention because of their wide range of potential applications. These materials combine electrical conductivity with relatively low absorption of electromagnetic radiation in the visible region. Commonly fabricated using thin-film technologies, TCOs are widely used in optoelectronic devices such as optoelectronic interfaces, solar cells, light-emitting diodes, displays, and semiconductor lasers (37. Hasegawa, A., & Tappert, F., 1973). Among them, copper-based delafossite oxides are especially promising as p-type TCOs, which are essential for the development of transparent semiconductor technologies. The reported bandgap of $CuAlO_2$ spans a wide range, from about 1.9 eV to 13 eV. In earlier work, Salah et al. investigated the low-energy electronic structure of copper aluminum oxide ($CuAlO_2$) using angle-resolved photoemission spectroscopy

(Hecht, J., 2010). However, to date, there have been no reports on the application of $CuAlO_2$ in fiber laser systems.

In parallel, MXene-based heterostructures have been actively studied to improve mode-locking performance. For instance, Liu et al. employed a $Ti_3C_2T_x$/graphene vertical heterostructure with a modulation depth of up to 28%, enabling stable mode-locked operation with pulse durations as short as 356 fs at 1559.16 nm [39]. More recently, MAX phases, which are precursors to MXenes, have attracted increasing interest as optical transducers (Chen, & Tsai, 2014). These materials follow the general formula $M_{n+1}AX_n$ (n = 1–3), where M denotes a transition metal (e.g., Cr, Nb, Ti), X represents carbon and/or nitrogen, and A is an element from groups 13–16 (e.g., Sn, Si, Ga) [40]. MAX phases possess a unique layered atomic structure that gives them a combination of metallic and ceramic characteristics. They exhibit excellent thermal stability and oxidation resistance typical of ceramics, while retaining high electrical and thermal conductivity characteristic of metals.

Together, these developments open a promising pathway to explore the largely untapped potential of $CuAlO_2$ and the Cr_2GaC MAX phase for applications in nonlinear optics and advanced laser technologies.

1.3 Research Objectives

The primary objective of this work is to fabricate novel saturable absorber (SA) devices based on transparent conducting oxides (TCOs) and MAX-phase materials for improving Q-switched and mode-locked operation in an erbium-doped fiber laser (EDFL) cavity. The achievement of this research will be evaluated through three main objectives, as outlined below:

a) To fabricate $CuAlO_2$ and Cr_2GaC thin-film saturable absorbers using the solution casting technique with polyvinyl alcohol (PVA) as the host polymer.

b) To characterize the optical and physical properties of the fabricated SAs using field-emission scanning electron microscopy (FESEM), energy-dispersive X-ray spectroscopy (EDX) and the balanced twin-detector technique.

c) To evaluate the performance of the fabricated SA films by demonstrating Q-switched and mode-locked pulse generation in an erbium-doped fiber laser (EDFL) cavity.

1.4 Research Questions

The above objectives were formulated based on the following research questions:

i) Can $CuAlO_2$ and Cr_2GaC be successfully fabricated into uniform, flexible thin-film SAs using the solution casting method with polyvinyl alcohol (PVA) as the host polymer?

ii) What are the surface morphology and elemental composition of the fabricated $CuAlO_2$ and Cr_2GaC thin-film saturable absorbers as revealed by FESEM and EDX analysis?

iii) What are linear transmission spectrum and nonlinear optical absorption characteristics of the fabricated saturable absorbers in the 1.55 μm region, as determined using linear transmission and the balanced twin-detector technique?

iv) Are the fabricated $CuAlO_2$ and Cr_2GaC thin-film saturable absorbers capable of enabling stable Q-switched and mode-locked pulse generation in an erbium-doped fiber laser cavity?

v) How do the key laser performance parameters such as pulse width, repetition rate, pulse energy, average output power, operating wavelength, and signal-to-noise ratio depend on the type of saturable absorber used?

vi) To what extent do $CuAlO_2$ and Cr_2GaC differ in their effectiveness as Q-switchers and mode-lockers in terms of stability, efficiency, and pulse quality in the EDFL system by results parameter acquire?

1.5 Scope of Study

This study is dedicated to demonstrating Q-switched and mode-locked pulse generation in an EDFL using $CuAlO_2$- and Cr_2GaC-based SAs. The work is systematically carried out in three main phases: fabrication of SA devices, characterization of the fabricated SAs, and laser operation experiments. Each phase serves a distinct purpose and contributes directly to fulfilling the overall research objectives, with the analysis and results in each stage providing clear evidence of the outcomes.

In the first phase, the SA devices are fabricated using a solution-casting method. The active materials are dispersed in a polymer host to form a homogeneous solution, which is then cast and dried to produce thin-film SAs. This approach enables simple,

low-cost, and reproducible fabrication of flexible SA films that can be easily integrated into fiber laser cavities. The successful formation of uniform thin films marks the foundation for subsequent characterization and laser experiments.

The second phase focuses on comprehensive physical and optical characterization of the fabricated SAs. Physical characterization is performed using field-emission scanning electron microscopy (FESEM) and energy-dispersive X-ray (EDX) spectroscopy. FESEM analysis provides detailed information on surface morphology, particle distribution, and film uniformity, while EDX reveals the elemental composition and confirms the presence of the intended materials. Optical characterization is conducted in the 1.55 μm region, which is relevant to EDFL operation. Linear absorption spectra are measured using a white light source combined with an optical spectrum analyzer (OSA), allowing evaluation of broadband absorption behavior. Nonlinear absorption characteristics, which are critical for saturable absorption, are determined using the balanced twin-detector technique to extract key parameters such as modulation depth, saturation intensity, and non-saturable loss.

In the final phase, the prepared SA films are incorporated into a ring-configured EDFL cavity to investigate their effectiveness in generating pulsed laser operation through Q-switching and mode-locking. The laser performance is systematically evaluated by measuring key parameters, including pulse duration, repetition rate, pulse energy, average output power, operating wavelength, and radio-frequency (RF) signal-to-noise ratio (SNR). These measurements provide a comprehensive assessment of pulse stability and quality. The results from this stage are analyzed and discussed in detail to verify that the fabricated SAs successfully enable stable Q-switched and mode-locked operation, thereby validating the effectiveness of $CuAlO_2$ and Cr_2GaC as functional saturable absorbers for ultrafast fiber laser applications.

1.6 Significance of Study

Although pulsed fiber lasers have been widely developed and investigated, their high cost and complex fabrication processes continue to limit large-scale application and widespread adoption. The use of passive Q-switching and mode-locking in EDFL cavities offers clear advantages for facilitating the industrialization and commercialization of pulsed fiber laser systems due to their lower cost, simpler design, and higher operational stability. This research therefore seeks to develop alternative

pulse-generation approaches by introducing new SAs based on $CuAlO_2$ and Cr_2GaC thin films. These SA devices offer advantages in terms of simple fabrication, mechanical robustness, and operational stability, making them promising candidates for a wide range of practical applications. In addition, this work aims to enhance pulsed laser performance, particularly in terms of pulse duration, repetition rate, efficiency, single-pulse energy, and overall stability. The market potential for passively Q-switched and mode-locked fiber lasers is substantial, especially in applications such as material processing, remote sensing, sensing technologies, and medical diagnostics.

This study is motivated by the extensive recent research on various advanced materials, including graphene, black phosphorus, topological insulators, transition metal oxides (TMOs), and TMDs. Although these materials have demonstrated excellent optical properties—such as broadband linear absorption, ultrafast recovery time, and strong optical nonlinearity—further development is still required to achieve consistently high performance and superior pulse quality in Q-switched and mode-locked fiber lasers using alternative novel materials. The investigation of $CuAlO_2$ and Cr_2GaC thin-film SAs is therefore expected to improve laser performance while providing deeper insight into the optical behavior of passive Q-switchers and mode-lockers. Moreover, this work aims to contribute positively to future research by enhancing understanding of material selection and guiding the development of high-potential saturable absorbers for pulsed laser applications.

1.7 Thesis outline

This thesis is devoted to the development of Q-switched and mode-locked fiber laser systems operating in the 1.5 μm wavelength region using two novel SA materials, namely $CuAlO_2$ and Cr_2GaC. These materials are investigated for their potential to enable stable and efficient pulsed laser operation with improved performance characteristics. The overall structure of the thesis is organized into six chapters, each addressing a specific aspect of the research. The present chapter serves as the introductory chapter. It provides a comprehensive overview of the research background and highlights the motivation for pursuing this study. The problem statement is clearly defined to identify existing limitations and research gaps in pulsed fiber laser development. The chapter also presents the research objectives and corresponding research questions that guide the direction of the study. In addition, the scope of the

research is outlined to clarify the boundaries of the investigation, while the significance of the study is discussed in terms of its academic, technological, and practical contributions. Finally, this chapter concludes with an overview of the thesis structure, offering readers a clear roadmap of how the subsequent chapters are organized and how they collectively address the aims of the research.

Chapter 2 presents a comprehensive review of the existing literature, covering the fundamental theory of optical fibers, the role of erbium-doped fiber as a gain medium, and the basic operating principles of fiber lasers. It further discusses the mechanisms underlying passive Q-switching and mode-locking, as well as important performance parameters of pulsed lasers and pulse propagation in optical fibers. In addition, this chapter surveys various materials that have previously been used as saturable absorbers. The chapter concludes with an introduction to the $CuAlO_2$ and Cr_2GaC materials, highlighting their properties and relevance to this study.

Chapter 3 describes in detail the research methodology adopted in this work. It explains the fabrication process of $CuAlO_2$ and Cr_2GaC thin-film SAs using PVA as the host polymer. The procedure involves dispersing the powdered active materials into a PVA solution to form a homogeneous mixture, which is then cast and dried to produce flexible thin films. The fabrication steps, materials preparation, and handling processes are systematically presented to ensure reproducibility. This chapter also focuses on the characterization of the fabricated SAs. It discusses the techniques used to evaluate both the physical and optical properties of the SAs, with particular emphasis on linear and nonlinear absorption behavior. Methods for measuring linear absorption using broadband light sources and optical spectrum analysis, as well as nonlinear absorption using the balanced twin-detector technique, are described in detail. The chapter further outlines the use of FESEM and EDX for investigating surface morphology and elemental composition. Finally, the chapter introduces the experimental setup of the erbium-doped fiber laser system used to demonstrate Q-switched and mode-locked operation. The laser cavity configuration, key optical components, and measurement instruments are described, providing a complete overview of the experimental arrangement for pulse generation and performance evaluation.

The results of this study are comprehensively presented and discussed in Chapters 4 and 5. Chapter 4 presents the experimental demonstration of $CuAlO_2$ as an effective SA for both Q-switched and ultrafast mode-locked pulse generation in an EDFL system. The SA was inserted into two different laser configurations designed for

pulsed operation. In the Q-switched configuration, stable pulse generation was obtained through modulation of intracavity loss and gain, with pump power varied from 132.15 mW to 210.62 mW. For mode-locked operation, a 100 m single-mode fiber spool was added to extend the cavity length and enhance nonlinear effects, enabling self-starting mode-locking over a pump power range of 141.38 mW to 233.7 mW. The results obtained confirm that $CuAlO_2$ is a viable and effective pulse transducer for Q-switched and mode-locked fiber laser applications.

Chapter 5 presents the demonstration of Q-switched and mode-locked pulse generation in EDFL cavities using a Cr_2GaC-based SA. In the Q-switched regime, stable pulsed operation was obtained at a central wavelength of 1530.6 nm with pump powers ranging from 49.06 to 72.14 mW. For mode-locked operation, bright soliton pulses centered at 1558.2 nm were generated using the same Cr_2GaC thin-film SA. By extending the EDFL cavity with an additional 100 m of single-mode fiber (SMF), a long-cavity configuration was achieved, producing a stable soliton pulse train at a repetition rate of 1.82 MHz, in close agreement with the calculated cavity length. In addition, dark-pulse generation was successfully realized in a mode-locked EDFL incorporating the Cr_2GaC SA under net anomalous dispersion by further extending the cavity length with 150 m of SMF. The formation of dark pulses was attributed to the combined effects of anomalous dispersion and strong intracavity nonlinearities. The results establish Cr_2GaC as a highly promising and versatile SA capable of supporting Q-switched, bright-soliton, and dark-pulse regimes, with strong potential for applications in ultrafast optics, optical communications, biomedical diagnostics, and advanced material processing.

Chapter 6 concludes the thesis by summarizing the key findings obtained throughout this study and highlighting their scientific and technological significance. The main outcomes related to the fabrication, characterization, and application of $CuAlO_2$ and Cr_2GaC SAs in Q-switched and mode-locked EDFLs are revisited and synthesized to demonstrate how the research objectives have been successfully achieved. In addition, this chapter discusses few recommendations for future work, with emphasis on improving the temporal characteristics of pulsed fiber lasers.

CHAPTER 2
LITERATURE REVIEW

2.1 Introduction

Laser is an acronym for “Light Amplification by Stimulated Emission of Radiation”, referring to a process in which light is amplified through stimulated emission after initial photons are generated. The first practical laser was demonstrated in 1960 by Theodore H. Maiman at Hughes Research Laboratories using a ruby crystal as the gain medium. Unlike conventional light sources, laser light possesses several unique properties, including high directionality, coherence, and monochromaticity [Abbas & Shehab ,2011]. Because of these characteristics, lasers are not typically used for general lighting such as streetlamps, household bulbs, flashlights, or vehicle headlights. As noted by Singh, lasers exhibit a much narrower frequency distribution, significantly higher intensity, and the ability to produce extremely short pulses compared to ordinary light sources [Abbasi,& Ghorashi ,2022]. Owing to these exceptional features, lasers are widely applied in barcode scanners, compact disc players, medical instruments such as surgical scalpels, and in industrial cutting and welding systems.

The conceptual foundation of the laser dates back to 1953, when Charles Townes developed the maser (microwave amplification by stimulated emission of radiation) based on Albert Einstein’s theory of stimulated emission. The maser functioned as a microwave amplifier but was initially unable to provide continuous output. Over time, improvements in maser technology led to a wide range of applications, including its use as a low-noise oscillator in radio astronomy and communication systems [Ahmad,& Elseman ,2026]. In 1958, Townes and Arthur Schawlow extended the maser concept to optical frequencies by proposing the use of an optical resonator consisting of mirrors surrounding an optical gain medium to enhance light amplification. Their pioneering theoretical work later earned them a Nobel Prize. This idea was experimentally realized in 1960 when Maiman built the first laser using a ruby crystal and a flashlamp as the pumping source [Ahmad, &, Mokhtar 2025]. Shortly thereafter, A. Javan, W. Bennet, and D. Harriott at Bell Laboratories developed the first gas laser using a helium–neon mixture. In the same period, L. F. Johnson and K. Nassau introduced the first neodymium-based laser, which became well known for its robustness and reliability. In

1962, Robert N. Hall developed the first laser diode, emitting near-infrared radiation at around 850 nm. In the same year, Nick Holonyak demonstrated the first visible semiconductor laser (Ahmad, &, Mokhtar, 2025).

Further advances rapidly followed. Optical resonators were demonstrated by Krupke and Sooy in 1969, while Q-switching techniques were first achieved by McClung and Hellwarth in 1962 and later theoretically explained by Wagner and Lengyel (Ahmad, &, Mokhtar, 2025). The first mode-locked laser was realized in 1964 by Hargrove, Fork, and Pollack (Ahmad, &, Mokhtar, 2025). Since then, intensive research has focused on improving laser cavity designs, operational stability, efficiency, and reliability, leading to the diverse laser technologies used today.

Building on this historical and scientific foundation, the present study explores the potential of $CuAlO_2$ and Cr_2GaC as saturable absorbers (SAs) for achieving Q-switched and mode-locked operation in erbium-doped fiber lasers (EDFLs).

This chapter provides a comprehensive literature review relevant to the thesis. It begins with an overview of the basic principles of optical fibers and erbium-doped fiber lasers. The fundamental mechanisms of Q-switching and mode-locking for pulsed laser generation are then discussed, with special emphasis on the critical role of saturable absorbers within the laser cavity. Key pulse parameters used to evaluate pulsed laser performance are subsequently introduced. Finally, this chapter reviews commonly used SA materials, discussing their reported experimental performances as well as their limitations, thereby establishing the motivation for investigating $CuAlO_2$ and Cr_2GaC as alternative SA materials.

2.2 Optical Fiber

An optical fiber is defined as a transparent, thin, and flexible strand of glass or plastic capable of transmitting light over long distances. It forms the backbone of local, regional, national, and international communication networks and has revolutionized telecommunications by enabling high-speed and high-capacity data transmission. Structurally, an optical fiber has a cylindrical geometry consisting of a central core surrounded by a transparent cladding layer with a lower refractive index. The difference in refractive indices between the core and cladding enables total internal reflection (TIR), which confines light within the core and minimizes signal loss during propagation.

Outside the cladding, an additional protective layer known as the buffer coating is applied. This layer is typically made of polymer materials and serves to protect the fiber from moisture, mechanical stress, and physical damage. Figure 2.1 illustrates the basic structure of an optical fiber, where the core has a refractive index $n_1$and the surrounding cladding has a lower refractive index n_2. For efficient light guidance, $n_1$must be greater than n_2, ensuring that light remains confined within the core.

Total internal reflection is the fundamental mechanism that governs light propagation in optical fibers. When light traveling in a medium with higher refractive index reaches the boundary with a lower-index medium at an angle greater than the critical angle, it is completely reflected back into the higher-index medium. This repeated internal reflection allows light to be guided along the length of the fiber with minimal attenuation, enabling reliable long-distance optical communication.

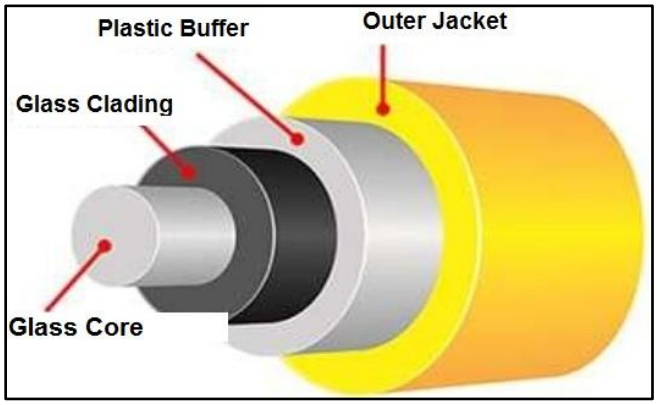


Figure 2.1 The Structure of An Optical Fiber (Ahmad, &, Mokhtar, 2025).

2.3 Fiber laser

A fiber laser is a type of laser in which the gain medium is an optical fiber doped with rare-earth elements such as erbium (Er), ytterbium (Yb), neodymium (Nd), or thulium (Tm). Unlike conventional bulk lasers that rely on solid crystals or gases, fiber lasers use a long, thin, and flexible optical fiber to generate and amplify light. In operation, pump light from a laser diode is coupled into the doped fiber, exciting the rare-earth ions. As these ions return to lower energy states, they emit light at characteristic wavelengths. This light is amplified as it propagates back and forth within the fiber between reflectors—such as fiber Bragg gratings or other cavity components—

forming a laser resonator. Because the light is guided within the fiber core, it remains tightly confined, resulting in high efficiency and excellent beam quality.

Fiber lasers were developed as an alternative to conventional bulk solid-state lasers, which often suffer from bulky configurations, sensitivity to misalignment, and high maintenance requirements. In contrast, fiber lasers are compact, robust, and alignment-free. They also offer a broad operational wavelength range, typically from 1 to 2 μm. Among the various types, erbium-doped fiber lasers (EDFLs) are the most widely studied, particularly for emission around 1.55 μm, which lies in the low-loss window of silica fibers and is ideal for telecommunication applications.

Overall, fiber lasers provide numerous advantages, including compact size, high electrical-to-optical efficiency, excellent thermal management, and low maintenance. They can operate in continuous-wave or pulsed regimes, such as Q-switching and mode-locking, and are extensively used in telecommunications, material processing, medical technology, sensing, and scientific research.

2.4 Erbium-doped Fiber laser

In this thesis, fibre-laser development is centred on operation in the 1.5-μm wavelength region, which is the characteristic emission band of erbium ions (Er^{3+}). Erbium is employed as the active dopant in the gain medium, while silicate glass is used as the host material for the erbium-doped fibre (EDF). A 980-nm laser diode is selected as the pumping source due to its high pumping efficiency compared with other available pump wavelengths. The use of a 980-nm pump enables lower electrical power consumption and reduces excess heat generation inside the fibre, which in turn minimizes thermal loading and may eliminate the need for complex cooling systems. In addition, weaker thermal effects contribute to improved beam quality and enhanced laser stability (Ahmad, A. D., Mokhtar 2024).

The operating principle of the erbium-doped fibre laser (EDFL) can be described using the energy-level diagram of Er^{3+} ions, as illustrated in Figure 2.2 (Ahmad, &, Salam 2024). The energy manifolds E1, E2, and E3 correspond to the ground state, the metastable state, and the excited state, respectively. When the EDF is pumped with a 980-nm laser diode, Er^{3+} ions are excited from the ground state (E1) to a higher-energy excited state (E3), which has a relatively short lifetime. These ions then relax non-radiatively to the intermediate metastable level (E2) by releasing energy in the form of

phonons associated with lattice vibrations. The metastable level has a long lifetime of approximately 10 ms, allowing a large number of Er^{3+} ions to accumulate at this level. This accumulation leads to population inversion between the metastable state (E2) and the ground state (E1), which is a necessary condition for laser action.

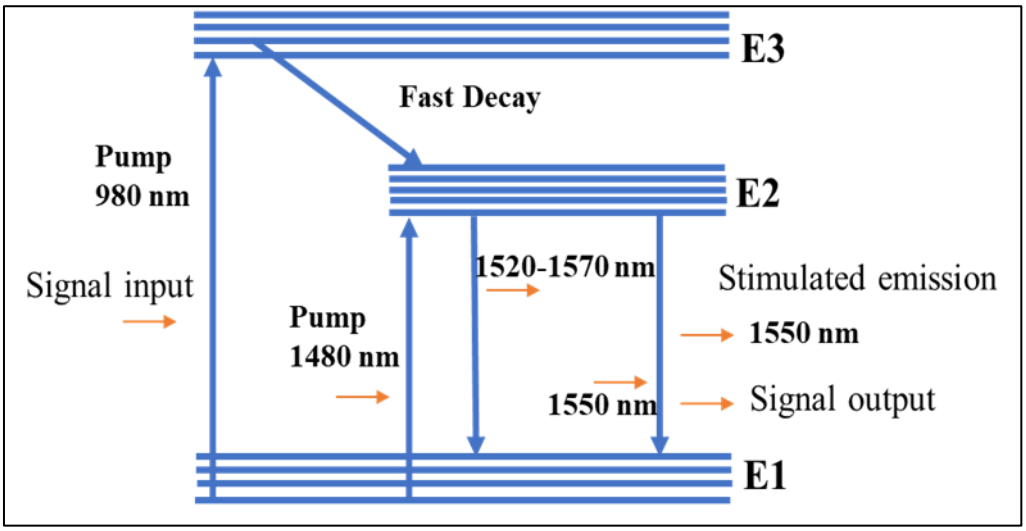


Figure 2.2 Energy-Level Diagram of Erbium Ions Illustrating The Pumping Process And Stimulated Emission Mechanism (Ahmad, &, Salam 2024).

Once population inversion is established, some Er^{3+} ions spontaneously decay from E2 to E1, emitting photons with wavelengths in the 1525–1565 nm range through spontaneous emission. If optical energy already exists within this wavelength band—such as a signal propagating through the EDF—this incoming light can trigger further transitions from E2 to E1. This process, known as stimulated emission, produces additional photons that are identical in phase, direction, and wavelength to the stimulating photons, thereby amplifying the signal. When both the pump wavelength and a signal wavelength propagate simultaneously through the EDF, energy is transferred from the pump to the signal through the erbium ions, resulting in optical gain.

In a laser cavity, the amplified spontaneous emission (ASE) generated in the EDF is repeatedly reflected by feedback elements, forcing the light to oscillate within the cavity. Through this feedback and amplification process, coherent laser radiation is produced, typically around the 1550-nm wavelength region.

Erbium-doped fibres are essential components in fibre-optic technology and form the core of erbium-doped fibre amplifiers (EDFAs), which are widely used in

long-haul optical communication systems. When pumped by 980-nm or 1480-nm laser diodes, EDFAs provide optical amplification through stimulated emission. By incorporating suitable feedback elements into an EDFA configuration, the system can be converted into a laser source, known as an EDFL, capable of generating laser output in the 1.55-μm wavelength region. EDFLs offer numerous advantages, including wide wavelength tunability, compact and alignment-free structure, excellent beam quality, and relatively low cost, making them attractive for applications in communications, sensing, and photonics research.

2.5 Pulse Generation in Fiber laser

Standard fibre-laser operation can be broadly classified into two main regimes: continuous-wave (CW) and pulsed operation. In CW operation, the laser emits a constant and uninterrupted output power over time, producing a steady optical beam. In contrast, pulsed lasers deliver energy in the form of discrete bursts of light, where each pulse has a much higher peak power than a CW beam but is emitted at a lower average frequency. Pulsed laser operation is particularly important for applications that require high peak power, precise energy delivery, or time-resolved measurements. Pulsed fibre lasers can be generated using two principal techniques: Q-switching and mode-locking. In both cases, the laser emits a train of pulses with specific pulse widths and repetition rates. Pulses can be generated either actively, using external modulators such as electro-optic or acousto-optic devices, or passively, by inserting a saturable absorber (SA) into the cavity. Passive pulse generation is often preferred because it eliminates the need for bulky and expensive external modulators, resulting in a simpler, more compact, and more stable laser system.

Q-switching is a technique in which the quality factor (Q) of the laser resonator is periodically varied by modulating the intracavity losses. When the cavity is kept in a low-Q (high-loss) state, energy from the gain medium is stored. Once the cavity is rapidly switched to a high-Q (low-loss) state, the stored energy is released in the form of a short and intense pulse. This process significantly enhances the pulse energy and peak power compared to CW operation. Typically, Q-switched lasers generate pulses with repetition rates in the kilohertz range and pulse durations in the nanosecond to microsecond regime. Although Q-switching was first demonstrated in solid-state lasers, it has since been successfully implemented in fibre lasers. Q-switched fibre lasers are

widely used in applications such as second-harmonic generation, optical time-domain reflectometry (OTDR), laser ranging and radar systems, material processing, and various industrial and scientific applications.

In a fibre-laser cavity, many longitudinal modes are supported by the resonator. In CW operation, these modes oscillate independently with random and uncorrelated phases, and there is no fixed phase relationship between them. The total electromagnetic field at any point in the cavity is simply the vector sum of all these modes. However, if appropriate mechanisms are introduced into the cavity to enforce a fixed phase relationship among the longitudinal modes, the modes can interfere constructively at regular intervals. This interference leads to periodic intensity modulation and results in a train of short optical pulses at the laser output. This process is known as mode-locking.

Mode-locking is an optical technique that forces the longitudinal modes of the laser cavity to oscillate with a constant phase difference. Through this phase synchronization, the laser can produce ultrashort pulses, typically in the picosecond or femtosecond range, although nanosecond pulses can also be obtained in some configurations. Mode-locked fibre lasers are of great interest because of their extremely short pulse duration and high peak power, making them suitable for applications in nonlinear optics, terahertz generation, precision micromachining, biomedical imaging, and ultrafast spectroscopy.

The interaction between laser pulses of different temporal regimes and materials is illustrated in Figure 2.3, which compares laser–material interactions for short-pulse (Q-switched) lasers and ultrashort-pulse (picosecond/femtosecond) lasers. For short-pulse lasers operating in the microsecond to nanosecond range, the ablation mechanism is mainly governed by thermal processes. In this regime, there is sufficient time for heat to diffuse into the metal or semiconductor target, leading to the formation of a relatively thick molten layer. As shown in Figure 2.3 (a), material removal occurs in both vapour and liquid phases: surface vaporization generates a strong recoil pressure that expels the underlying molten material.

In contrast, in the ultrashort-pulse regime (Figure 2.3(b)), energy is deposited into the material on an extremely short timescale. The energy is delivered faster than thermal diffusion can occur, preventing continuous evaporation during the pulse. As a result, very high temperatures and pressures rapidly build up beneath the surface. Much of the energy dissipation and material ejection takes place after the laser pulse has ended, through complex non-equilibrium processes that are still not fully understood.

Ultrafast pulses in the picosecond and femtosecond range therefore produce the smallest heat-affected zone (HAZ), and in some cases no observable HAZ at all, because heat has insufficient time to spread into the surrounding material. This leads to minimal thermal damage, clean and smooth ablation features, and superior processing quality.

The interaction between laser pulses of different temporal regimes and materials is illustrated in Figure 2.3, which compares short pulse (Q-switched laser), and ultrashort pulses (picosecond/femtosecond laser) laser-material interactions. The laser ablation mechanism of short pulse duration lasers in the microsecond to nanosecond range is dominated by thermal effects. There is sufficient time for heat to propagate into the semiconductor or metal target and to subsequently create a relatively large molten layer. As depicted in Fig. 2.3, the target material is removed both in vapor and liquid phases, since the vaporization process creates a recoil pressure that expels the molten liquid. In the ultrashort pulse duration regime, the rate of energy deposition is so rapid that the material cannot evaporate continuously, and extremely high temperature and pressure are built up beneath the evaporating surface. The dissipation of the absorbed energy in bulk material and the corresponding material removal take place mostly after pulse duration, which remains poorly understood. It shows that ultrafast pulses in the picosecond or femtosecond regime produce the smallest heat heat-affected zone (HAZ), or even no observable HAZ, because the material is removed so rapidly that heat does not have time to diffuse into the surrounding region. This results in clean, smooth features and superior processing quality

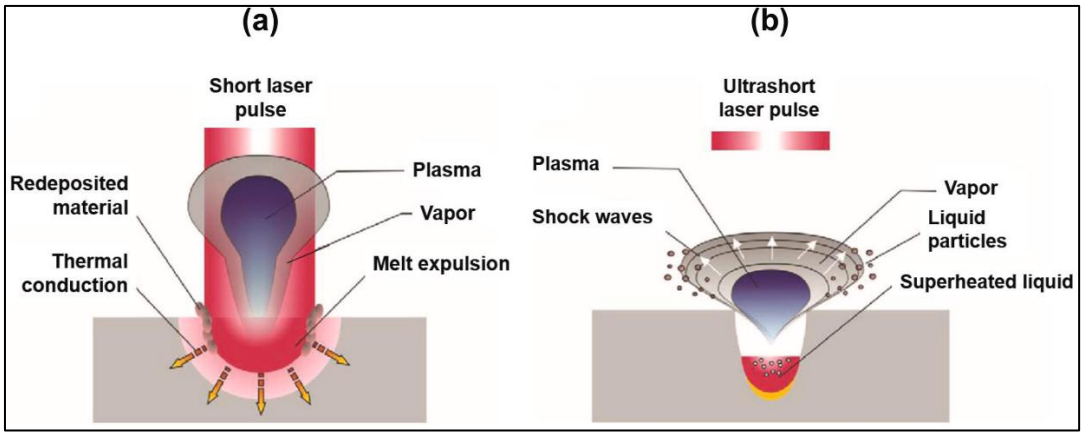


Figure 2.3 Illustration Of Material Removal Mechanisms: (A) Melt Ejection And Vaporization Under Short-Pulse Laser Irradiation; (B) Phase Explosion Induced By Ultrashort-Pulse Laser Irradiation (Ahmad, H., Rusni, 2024).

Due to their extremely short pulse duration and high repetition rates, ultrashort pulsed lasers enable high-precision micromachining with excellent spatial resolution, minimal thermal damage, and high processing speed. These advantages make ultrafast fibre lasers particularly attractive for advanced manufacturing, microelectronics fabrication, biomedical device processing, and other applications requiring high accuracy and minimal material damage.

2.5.1 Q-switching

Q-switching is a technique used to generate short and intense laser pulses by controlling the losses in the optical resonator, or equivalently, by varying the quality factor (Q-factor) of the laser cavity. The Q-factor is defined as

$$Q=\frac{2\pi nL}{\lambda\alpha} \tag{2.1}$$

where n is the refractive index of the medium, L is the cavity length, λ is the operating wavelength, and α represents the one-way loss of the resonator. From this expression, it is clear that the Q-factor is inversely proportional to the cavity loss. Hence, by adjusting the loss inside the resonator, the Q-factor can be controlled: lower cavity loss corresponds to a higher Q-factor, while higher loss results in a lower Q-factor. When the cavity has high loss (low Q-factor), laser oscillation is suppressed even though the gain medium is being pumped. During this period, stimulated emission is inhibited and the population inversion in the gain medium is allowed to build up to a high level. Once a large inversion is achieved, the cavity losses are suddenly reduced, restoring a high Q-factor. This rapid change allows the stored energy in the gain medium to be released almost instantaneously, producing a very short and intense laser pulse, typically with a pulse duration in the microsecond or nanosecond range.

The Q-switching process begins by pumping the gain medium while maintaining high intracavity losses, which prevents significant energy extraction from the cavity. As pumping continues, the gain increases until it greatly exceeds the losses. When the losses are abruptly reduced, the intracavity optical power rises exponentially until the gain is depleted and saturation is reached. In this way, Q-switching converts the energy stored in the gain medium into a single, high-energy laser pulse. The choice of gain medium is crucial for efficient Q-switched laser operation. Important considerations include a high concentration of laser-active ions, a suitable upper-state lifetime, and

moderate gain efficiency. If the gain is too high, excessive amplified spontaneous emission (ASE) may occur, which can limit the amount of energy that can be stored in the gain medium before Q-switching. Therefore, a balanced gain medium is required to achieve high pulse energy without premature energy loss. Q-switching can be implemented using either active elements, such as electro-optic or acousto-optic modulators, or passive elements, such as saturable absorbers (Ahmad, & Samion 2018, Ahmed, &, Ali, 2015).

2.5.2 Mode-Locking

Mode-locking is a technique used to generate ultrashort laser pulses by forcing all the longitudinal modes of a laser cavity to oscillate with a fixed phase relationship. When the phases of these modes are locked together, constructive interference occurs at regular time intervals, producing a train of pulses with very high repetition rates, typically in the megahertz (MHz) range. This process results in extremely narrow pulses that are evenly spaced in time. Figure 2.4 illustrates the difference between random-phase and phase-locked operation by comparing intensity versus time. In normal laser operation, multiple longitudinal modes oscillate independently with random and uncorrelated phases. There is no fixed phase relationship between these modes, and the total electromagnetic field at any point in the cavity is simply the vector sum of all the individual modes. As a result, the output intensity fluctuates randomly and appears as a noisy or irregular signal, as shown in the right side of Figure 2.4.

Under mode-locking conditions, a fixed phase relationship is imposed among the longitudinal modes. When these phase-locked modes interfere, they add constructively at specific times and destructively at others, leading to the formation of a periodic train of short pulses at the laser output. Depending on the laser configuration and gain medium, these pulses can reach extremely short durations, often in the picosecond or femtosecond range.

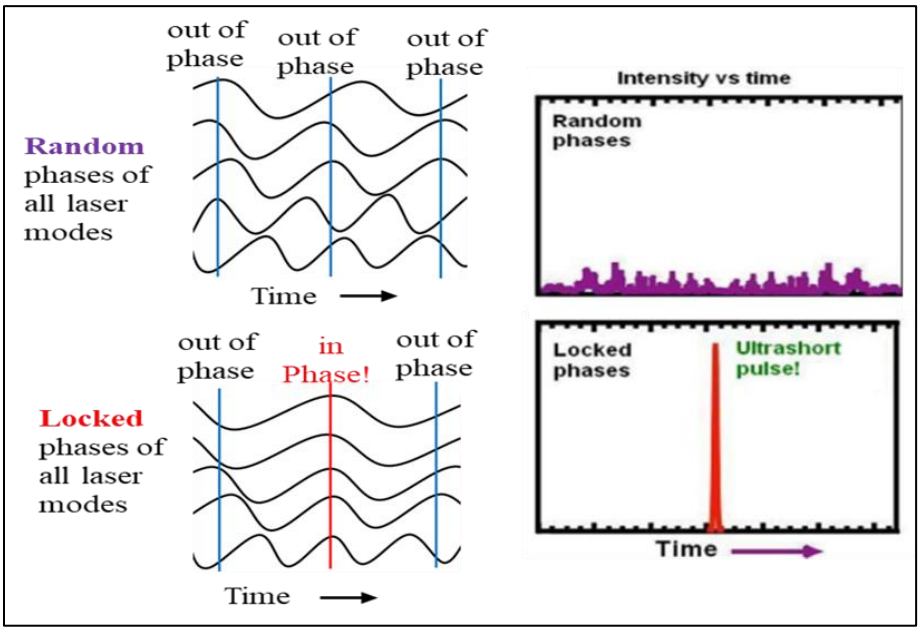


Figure 2.4 Illustrations Showing The Random Phase And Locked Phase(Ahmed, & Latiff, 2016)

In a Fabry–Perot cavity, the frequency spacing between adjacent longitudinal modes is given by

$$\Delta\nu = \frac{c}{2L} \tag{2.2}$$

where L is the cavity length and c is the speed of light. For a ring cavity, the mode spacing becomes

$$\Delta\nu = \frac{c}{L} \tag{2.3}$$

The duration of the mode-locked pulses is strongly influenced by the number of longitudinal modes that are phase-locked. If Nmodes are locked together, the total optical bandwidth is approximately $N\Delta\nu$. This shows that a broader spectral bandwidth corresponds to a shorter pulse duration. For a Gaussian-shaped pulse, the minimum achievable pulse width is given by

$$\tau = \frac{0.441}{N\Delta\nu} \tag{2.4}$$

The constant 0.441 is known as the time–bandwidth product (TBP) for a Gaussian pulse. The TBP depends on the pulse shape. For ultrashort pulses that are better described by a hyperbolic secant-squared (sech^2) profile, the TBP is 0.315 (Ahmed,& Latiff, 2016).

As the number of interacting phase-locked modes increases, the total bandwidth becomes wider, the pulse duration becomes shorter, and the peak intensity increases. This indicates that the pulse width in a mode-locked laser is mainly determined by the available gain bandwidth of the gain medium and the spectral filtering effects within the cavity.

Mode-locked pulses can be generated using either active or passive techniques, depending on how the phase relationship between the longitudinal modes is enforced. In active mode-locking, an external modulator—typically an acousto-optic modulator (AOM) or an electro-optic modulator (EOM)—is inserted into the laser cavity. This modulator periodically varies the intracavity loss in synchronization with the round-trip time of light in the resonator. The electronically driven modulation produces a sinusoidal pattern of loss variation, with a period equal to the cavity round-trip time T_r.

In steady-state operation, the saturated gain balances the losses mainly near the minimum of the loss-modulation curve. Consequently, only light that arrives at the cavity during these low-loss time windows is strongly amplified, while light arriving at other times is suppressed. This selective amplification forces the laser to emit a train of pulses that are much shorter than the cavity round-trip time. Active mode-locking therefore relies on precise electronic control and timing to maintain stable pulse generation.

In contrast, passive mode-locking does not require any external electronic modulator. Instead, a saturable absorber (SA) is placed inside the laser cavity to provide intensity-dependent loss. The SA introduces high loss at low light intensities and low loss at high intensities. As a result, weak continuous-wave (CW) components experience strong attenuation, while intense short pulses experience much lower loss and are preferentially amplified. For lasing to occur, the intracavity light must reach a sufficiently high intensity to saturate the absorber and reduce its loss.

This condition is naturally satisfied when the longitudinal modes lock in phase and form short pulses, since the peak power of a pulse is much higher than that of CW operation with the same average power. To suppress pure CW lasing, the small-signal gain of the cavity is typically adjusted slightly below the CW threshold. Under these conditions, CW light cannot build up because it experiences too much loss from the SA.

However, when a short pulse forms, its high peak intensity saturates the absorber, reduces the loss, and allows the gain to exceed the threshold during the pulse. After the pulse passes, the gain again falls below threshold, preventing continuous emission.

Efficient passive mode-locking therefore requires a saturable absorber with a fast recovery time, so that it can quickly return to its high-loss state after the pulse has passed. This rapid recovery ensures stable pulse shaping, suppresses noise, and supports the generation of clean, ultrashort pulses (Ahmed, & Latiff, 2016).

2.6 Description of laser pulses

Several key parameters are commonly used to characterize laser pulses. As illustrated in Figure 2.5, the pulse duration is defined as the full width at half maximum (FWHM) of the pulse intensity profile, which represents the temporal width of the pulse at half of its peak amplitude. Another fundamental parameter is the pulse repetition rate (PRR), which is the number of pulses emitted per second. The time interval between two successive pulses, known as the pulse period T, is simply the reciprocal of the repetition rate, $T = 1/\mathrm{PRR}$.

For ultrashort-pulse lasers, an especially important quantity is the peak power, P_{peak}, which represents the maximum instantaneous optical power reached during a pulse. For a laser pulse with a Gaussian temporal profile, the peak power can be approximated by

$$\mathrm{P_{peak}} \approx 0.94 \frac{\mathrm{E_L}}{\tau_{\mathrm{L}}} \tag{2.5}$$

where E_L is the pulse energy and τ_L is the pulse duration (FWHM). Because ultrashort pulses have durations in the picosecond or femtosecond range, even modest pulse energies can correspond to extremely high peak powers, often reaching the megawatt (MW) level.

In contrast to peak power, the average laser power, P_{ave}, describes the mean optical power delivered over time. It is given by the product of the pulse energy and the repetition rate:

$$\mathrm{P_{ave}} = \mathrm{E_L} \times \mathrm{PRR} \tag{2.6}$$

This parameter is important for applications where total energy delivery over time, thermal loading, or efficiency is a concern.

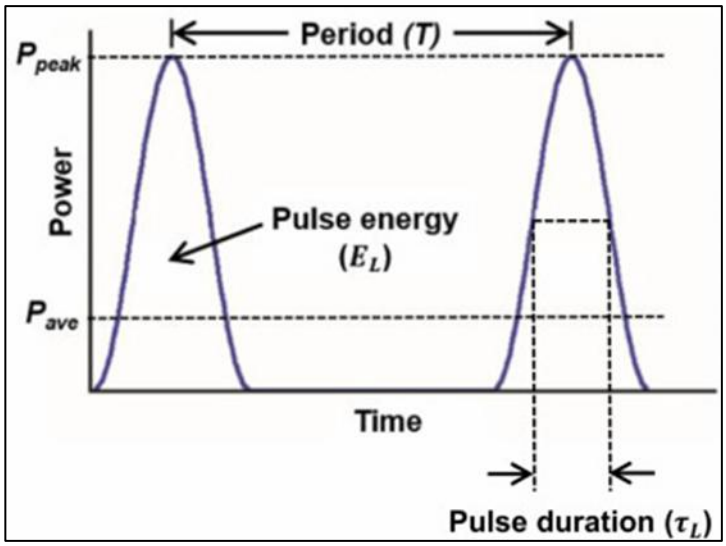


Figure 2.5 Illustration Of Pulse Duration (τ_L) Defined By The Full Width At Half Maximum (FWHM), And The Period T Between Two Successive Laser Pulses. The Pulse Energy (E_L) Corresponds To The Area Under The Power–Time Curve.

Another important quantity in laser–matter interaction is the fluence, which is defined as the incident optical energy per unit area. For a beam with a flat-top spatial profile, the fluence is uniform across the beam cross-section. However, most practical lasers produce beams with a Gaussian profile, where the fluence is highest at the beam center and decreases gradually toward the edges. Therefore, the peak fluence is often used, especially in laser ablation and micromachining studies. For a Gaussian beam, the peak fluence is given by

$$F_{peak}=\frac{2E_L}{\pi\omega_r^2} \tag{2.7}$$

where ω_r is the beam radius at which the intensity drops to $1/e^2$ (about 13.5%) of its maximum value at the beam center.

Similarly, the optical intensity is defined as the optical power per unit area. For a flat-top beam, the intensity is uniform, while for a Gaussian beam, the maximum intensity occurs on the beam axis. The peak intensity for a Gaussian beam is expressed as

$$I_{peak}=\frac{2P_{peak}}{\pi\omega_r^2} \tag{2.8}$$

These parameters—pulse duration, repetition rate, peak power, average power, fluence, and intensity—are essential for describing the temporal and spatial

characteristics of laser pulses and for understanding their interaction with materials in applications such as micromachining, medical treatment, and nonlinear optics.

2.7 Pulse Propagation in a Fiber

Light pulses propagate along an optical fiber mainly through the principle of total internal reflection. This occurs because the refractive index of the fiber core is intentionally made higher than that of the surrounding cladding. As a result, light entering the core at suitable angles is repeatedly reflected at the core–cladding interface and remains guided along the fiber. For efficient guidance, it is essential that the refractive index of the core is always greater than that of the cladding. During propagation, an optical pulse does not remain unchanged. Its shape, width, and spectrum can be affected by several physical mechanisms, including dispersion, nonlinear effects, and other wave–matter interactions. These effects become especially important in fiber lasers and long fiber links, where pulses travel over significant distances and often at high intensities. The following sections describe the main factors influencing pulse propagation in optical fibers.

2.7.1 Dispersion

Dispersion refers to the phenomenon in which different wavelengths of light travel at different velocities in a medium, causing an initially short pulse to spread in time as it propagates. In free space, all electromagnetic waves travel at the same speed, $c = 3 \times 10^8$m/s. However, inside a material medium such as optical fiber, the speed of light is reduced due to interactions between photons and the electrons of the material. This reduction is described by the refractive index n, and the velocity of light in the medium is given by

$$v_m = \frac{c}{n} \tag{2.9}$$

Because the refractive index depends on wavelength, different spectral components of a pulse travel at different speeds, leading to temporal broadening.

In multimode fibers, modal dispersion occurs because different modes propagate along different optical paths and therefore reach the fiber output at different times. The fundamental mode generally travels the fastest, while higher-order modes experience longer path lengths and lower effective velocities. The resulting time delay between

modes leads to significant pulse broadening at the fiber output. In single-mode fibers, modal dispersion is completely eliminated since only one propagation mode is supported. However, chromatic dispersion remains, as different wavelengths within the pulse still travel at different group velocities.

Chromatic dispersion, also known as group velocity dispersion (GVD), describes how the group velocity of light changes with wavelength or frequency. It is mathematically expressed as

$$\mathrm{GVD}=\frac{\partial}{\partial\omega}\left(\frac{1}{v_g}\right)=\frac{\partial}{\partial\omega}\left(\frac{\partial k}{\partial\omega}\right)=\frac{\partial^2 k}{\partial\omega^2} \tag{2.10}$$

where k is the wavenumber, v_g is the group velocity, and ω is the angular frequency. In fiber laser cavities, the total dispersion is obtained by summing the dispersion contributions of each fiber segment and optical component. In practice, dispersion is often described using the parameter β^2, which relates to wavelength rather than angular frequency:

$$\beta^2=-\frac{D_m(\lambda)\lambda^2}{2\pi c} \tag{2.11}$$

where $D_m(\lambda)$ is the wavelength-dependent dispersion coefficient of the fiber. Optical fibers typically have a zero-dispersion wavelength λ_D near 1310 nm. For wavelengths longer than λ_D, β^2 becomes negative, indicating anomalous dispersion. For wavelengths shorter than λ_D, β^2 is positive, corresponding to normal dispersion. The dispersion regime strongly influences pulse evolution and stability in fiber lasers.

2.7.2 Nonlinear Effect

Nonlinear effects become significant in optical fibers when light propagates at high intensity or over long distances. These conditions are easily achieved in fibers because of their small core size and low propagation loss. The dominant nonlinear response in silica fibers is the Kerr effect, which gives rise to phenomena such as self-phase modulation (SPM), cross-phase modulation (XPM), and four-wave mixing (FWM) (.Ahmeed, & Ahmad, 2025, 15. Al-Hiti, & Al-Masoodi, 2025). The Kerr effect causes the refractive index of the medium to depend on the optical intensity:

$$n_{eff}=n_1+n_2 I_{int} \tag{2.12}$$

where n_{eff} is the effective refractive index, n_1 is the linear refractive index, n_2 is the nonlinear refractive index coefficient, and I_{int} is the optical intensity. This intensity-dependent refractive index introduces an additional phase shift during propagation:

$$\phi_{nl} = \frac{2\pi}{\lambda} n_{eff} L \tag{2.13}$$

where $L$is the fiber length and $\lambda$is the operating wavelength. The nonlinear phase shift increases with fiber length, refractive index, and optical intensity, and is stronger at shorter wavelengths.

For optical pulses, intensity varies across time, so different parts of the pulse accumulate different nonlinear phase shifts. This leads to the formation of frequency chirp across the pulse, a process known as self-phase modulation. When the nonlinear length and dispersion length are comparable and the dispersion is anomalous, the effects of SPM and dispersion can balance each other. This balance results in the formation of optical solitons—pulses that propagate without changing shape in a dispersive and nonlinear medium. Such soliton dynamics play a crucial role in ultrafast fiber lasers. Cross-phase modulation and SPM are also key mechanisms in shaping picosecond and femtosecond pulses.

2.7.3 Formation of Kelly sidebands

When the nonlinear phase shift from the Kerr effect exactly balances dispersive broadening due to GVD, a stable soliton is formed. However, in real laser cavities, solitons experience periodic perturbations due to gain, loss, filtering, and cavity boundaries. These perturbations cause the soliton to shed small amounts of energy in the form of dispersive waves. Under resonant conditions, these dispersive waves interfere constructively with the soliton, leading to the appearance of symmetrical spectral sidebands around the central soliton peak. These features are known as Kelly sidebands (Aljunid,&, Ghafar, 2024,17. Alrebdi,& Sadiq, 2025). The spacing of the Kelly sidebands depends on the total cavity dispersion.

Kelly sidebands indicate strong interaction between dispersion and nonlinearity. However, their presence can also cause interaction between adjacent soliton pulses, leading to pulse timing jitter. This jitter reduces the stability of mode-locked fiber lasers and can introduce errors in long-distance optical communication systems.

2.8 Dark pulses

A soliton is a nonlinear wave packet that can propagate over long distances without changing its shape, maintaining its waveform through a process of dynamic self-stabilization. This phenomenon was first observed by Russell in 1844. Soliton formation occurs when the pulse broadening caused by dispersion is exactly balanced by the pulse compression induced by optical nonlinearity. Consequently, dispersion and nonlinearity are the two fundamental mechanisms governing soliton behavior. Dispersion is an inherent property of light propagation in a medium, where different frequency components of a pulse travel at different velocities, leading to a frequency-dependent phase velocity and temporal spreading of the pulse. In optical fibers, pulse evolution is mainly influenced by chromatic dispersion and polarization mode dispersion (PMD). PMD arises from birefringence in the fiber, causing different polarization components to propagate at different speeds. This effect can disturb the delicate balance required for soliton formation, leading to pulse distortion and instability. Therefore, in practical systems, PMD must be minimized or compensated, for example through adaptive compensation techniques (Apandi & Ahmad, 2017).

In laser systems where dispersive and nonlinear effects dominate pulse dynamics, soliton behavior is commonly described by the Nonlinear Schrödinger Equation (NLSE), as introduced by Hasegawa and Tappert (Barmenkov, Y. O., Kir'yanov, 2014). Under anomalous dispersion conditions, the NLSE predicts the formation of bright solitons, which appear as isolated intensity peaks. In contrast, under normal dispersion, dark solitons—characterized by intensity dips on a continuous background—can be formed. A dark soliton is a special type of nonlinear optical pulse that appears as a stable "dip" or notch in intensity on top of a continuous or quasi-continuous light background. Instead of being a bright, isolated peak like a bright soliton, a dark soliton is characterized by a localized reduction in intensity accompanied by a sharp phase change across the dip. Physically, a dark soliton forms when the natural pulse broadening caused by normal dispersion is exactly balanced by the nonlinear phase modulation (Kerr nonlinearity) of the medium. This balance allows the intensity dip to propagate without changing its shape or depth, even over long distances. In fiber lasers and optical fibers, dark solitons are important because they represent an alternative ultrafast pulse regime, useful for studying nonlinear dynamics, dispersion–nonlinearity balance, and advanced pulse shaping.

Dark solitons in optical fibers can be generated through several theoretical and experimental frameworks, mainly based on the Nonlinear Schrödinger Equation (NLSE), the Cubic–Quintic Nonlinear Schrödinger Equation (CQNLSE), and the Domain Wall (DW) model. Each mechanism relies on different physical conditions and cavity designs.

Pulse propagation in single-mode optical fibers is commonly described by the NLSE, which models the combined effects of GVD and Kerr nonlinearity. In this framework, solitons form when dispersive pulse broadening is exactly balanced by nonlinear self-phase modulation. Under anomalous dispersion, the NLSE predicts the formation of bright solitons, while under normal dispersion, dark solitons can be generated. Silica fibers naturally exhibit both dispersion regimes, with a zero-dispersion wavelength near 1330 nm. Below this wavelength, fibers operate in normal dispersion, which is favorable for NLSE dark soliton formation. Therefore, most NLSE-based dark soliton fiber lasers operate in the 1 μm band, typically using ytterbium-doped fiber lasers (YDFLs) with artificial saturable absorbers and polarization control (Becker, & Olsson,1999). In contrast, erbium-doped fiber lasers (EDFLs) operating near 1550 nm naturally lie in the anomalous dispersion regime and tend to support bright solitons unless special dispersion management is applied.

Standard NLSE considers only third-order (Kerr) nonlinearity. However, at very high optical intensities, higher-order nonlinear effects become significant, especially the fifth-order nonlinearity. In this case, the refractive index depends on both cubic and quintic terms, leading to the CQNLSE. By introducing highly nonlinear fiber (HNLF) into the laser cavity, the system nonlinearity can be strongly enhanced. Under such conditions, CQNLSE dark solitons can form regardless of whether the cavity operates in normal or anomalous dispersion. This makes CQNLSE-based dark solitons more flexible than NLSE dark solitons, which are limited to normal dispersion. Experimental studies have verified this mechanism. For example, dark solitons with nanosecond-scale pulse widths and MHz repetition rates have been demonstrated using nonlinear polarization rotation and long HNLF sections, showing stable propagation characteristics (Chavan, & Kim, 2023)

Domain wall (DW) dark solitons arise from a completely different physical mechanism. A domain wall is a topological boundary that connects two stable states of a system. In optics, domain wall solitons form through nonlinear interactions between two coexisting states, such as different wavelengths or orthogonal polarization modes. Unlike NLSE dark solitons, DW dark solitons do not require strict dispersion management.

Unlike CQNLSE solitons, they also do not rely on extremely strong nonlinearity. Instead, their formation is mainly governed by incoherent coupling between two optical states. As a result, DW dark solitons can be generated in both normal and anomalous dispersion regimes. DW dark pulse fiber lasers usually adopt interferometer-type cavity designs and often include nonlinear polarization rotation and sometimes saturable absorbers. Experimental studies have shown that DW dark solitons commonly appear during wavelength or polarization switching. For example, dual-wavelength operation in EDFLs has been shown to produce stable dark pulses at the transition point between two wavelengths [22]. These dark pulses are attributed not only to gain competition but also to incoherent coupling between orthogonal polarization modes in birefringent fibers.

2.9 Saturable Absorber (SA)

A saturable absorber (SA) is a material whose optical absorption decreases as the intensity of incident light increases. For a material to function effectively as a SA, it must exhibit a fast and reversible change in absorption with varying light intensity. After becoming saturated at high intensity, the material must quickly recover to its initial high-absorption state when the intensity drops. This rapid recovery is essential for repetitive pulse formation in lasers. In addition, an ideal SA must possess a high optical damage threshold so that it can withstand strong optical fields without physical degradation. Thermal stability is also critical, as the material should not deteriorate when exposed to elevated temperatures caused by intense laser operation. These properties are particularly important for short-pulse generation in passive Q-switching and mode-locking systems, where the absorber is repeatedly exposed to high peak powers.

The mechanism of saturable absorption is illustrated in Figure 2.6 using a simple two-level electronic model. In this model, the two energy levels are denoted as E_1 (ground state) and E_2 (excited state), with corresponding atomic or carrier populations N_1 and N_2. Under normal, low-intensity illumination, most electrons reside in the ground state, so N_1 is much larger than N_2. This means that many electrons are available to absorb incoming photons.

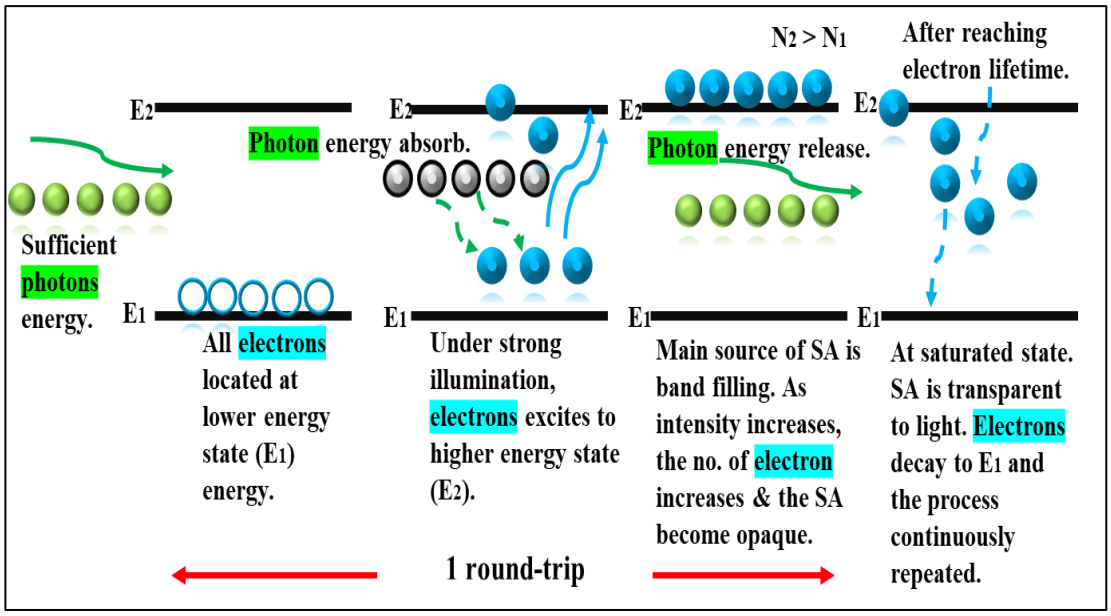


Figure 2.6 Schematic Representation of The Saturable Absorption Process Based On A Two-Level Electronic Model (Chen, H., Yin, 2017).

When light is incident on the material, electrons in the ground state E_1absorb photons and are promoted to the excited state E_2, provided that the photon energy matches the energy difference between the two levels. This energy difference is often referred to as the bandgap. At low optical intensities, only a small fraction of electrons are excited, so absorption remains strong and the material appears highly absorbing. As the incident light intensity increases, more electrons are driven into the excited state. Eventually, a significant portion of the available states in E_2 becomes occupied. When this happens, further absorption is reduced because fewer empty states remain for electrons to transition into. This phenomenon leads to saturation of absorption and a corresponding increase in optical transmittance. Thus, there is a direct relationship between the nonlinear absorption behavior of the material and the density of excited carriers.

At sufficiently high optical intensity, the population in the excited state can even exceed that in the ground state, a condition known as population inversion ($N_2 > N_1$). Although population inversion is more commonly discussed in gain media, in SAs the key effect is governed by the Pauli exclusion principle, which states that no two identical fermions can occupy the same quantum state simultaneously (Chen & Cheak,2024). Once most of the available excited states are filled, additional electrons cannot be promoted, and the material becomes increasingly transparent to incoming light. As a result, at high laser intensity the SA exhibits low loss and allows light to pass through with minimal

attenuation. When the excited electrons relax back to the ground state after a characteristic lifetime, the material recovers its initial high-absorption state. This cycle of excitation, saturation, recovery, and re-excitation repeats continuously during laser operation. In pulsed lasers, this mechanism enables intense portions of the optical field to experience less loss than weak portions, thereby favoring the formation of short, high-intensity pulses.

For a material to function effectively as a saturable absorber, it must exhibit sufficiently strong saturable absorption, a broad linear absorption band to support different wavelengths, and an appropriate recovery (relaxation) time. These properties ensure compatibility with various laser configurations and stable operation in passive Q-switching and mode-locking systems. In addition, an ideal SA must possess a high optical damage threshold so that it can withstand strong optical fields without physical degradation. Thermal stability is also critical, as the material should not deteriorate when exposed to elevated temperatures caused by intense laser operation.

2.10 SA materials

A wide range of functional materials has been explored as SAs for short-pulse laser generation. These include semiconductor saturable absorber mirrors (SESAMs) [25], carbon nanotubes (CNTs) (Dacey,(Dong & Samson,2016), topological insulators (TIs)(Du, & Yang, 2020), antimony films (Feng & Silverman, 2010), and various metal oxides (Fu & Hua, 2014) Among these, SESAMs are one of the most established and commercially available SAs for stable Q-switched and mode-locked pulses generation. Despite their effectiveness, SESAMs suffer from certain drawbacks, including limited operating bandwidth and high fabrication cost. These limitations have driven strong interest in two-dimensional (2D) materials, which are attractive due to their low-cost fabrication and broadband optical response. Common 2D materials used as saturable absorbers include graphene, black phosphorus (BP), topological insulators (TIs), and transition metal dichalcogenides (TMDs).

Graphene has been widely studied since 2009 for Q-switching and mode-locking at various wavelengths. It can exist as a single layer or in multiple layers and is typically obtained through mechanical exfoliation of graphite. Transition metal dichalcogenides (TMDs) are another important family of 2D materials. They have the chemical form MX_2, where M is a transition metal and X is a chalcogen element. Their structure consists of a

single layer of transition metal sandwiched between two chalcogen layers. Common examples include WS_2 and MoS_2 (Fu, & Sun, 2021, Ghafar, & Zulkipli.,2022) However, many of these materials possess relatively low optical damage thresholds—often bounded below 20 mJ/cm^2 to 50mJ/cm^2 for materials like black phosphorus, or intensities under 100MW/cm^2 for certain transition metal dichalcogenides—limiting their long-term laser performance and making them susceptible to photothermal degradation under intense intra-cavity fields (Hammadi, Y., Mansour, 2018, Haris, & Arof, 2019).

Topological insulators (TIs) form another class of 2D materials. They behave as insulators in the bulk but have conducting surface states. TIs are especially attractive as saturable absorbers because of their high modulation depth. Frequently reported TIs include bismuth telluride (Bi_2Te_3) and bismuth selenide (Bi_2Se_3). Black phosphorus (BP) is also notable due to its tunable bandgap, which lies between the zero bandgap of graphene and the relatively large bandgaps of TMDs. The bandgap of BP can be adjusted by changing the number of layers.

Tables 2.1 and 2.2 summarize previously reported Q-switched and mode-locked erbium-doped fiber lasers (EDFLs) that employ various 2D materials as saturable absorbers. These results demonstrate that 2D materials are highly versatile and effective for short-pulse generation across a wide range of operating conditions, making them strong alternatives to conventional SESAM-based systems.

Table 2.1

Q-Switched EDFL With 2D Materials As SA

SA	Operational Wavelength (nm)	Repetition Rate (kHz)	Pulse Width (µs)	SNR (dB)	Ref
WS_2	1558	7.7 – 35.2	19.3 - 2.6	7.06	(Dong & Samson, 2016).
MoS_2	1549.83	116 – 131	0.76 – 0. 66	-	(Haris, & Batumalay, 2022)
$TiSe_2$	1560.472	24.5 – 73.79	9.47 – 1.31	-	(Hasegawa, & Tappert, ,1973).
BP	1562.35	9.61 – 44.72	40.1 - 9.8	67	(Hecht &J. 2010).
Graphene	1557.43	14.49– 88.97	12.08 – 1.54	57	(Hisyam, & Rusdi, 2016)

Bi_2Te_3	1531	12.6– 177.7	9.33 – 1.32	49	(Du, & Lu,2020)
Bi_2Se_3	1560	23.5– 68.2	8.6 – 2.4	14.05	(Hong, & Liu, 2020)
$CaCO_3$	1563.5 / 1564.9	12.67 – 21.3	35.27-18.74	25	(Husaini, & Wadi,2024)

Table 2.2
Mode-Locked EDFL With 2D Materials As SA

SA	**Operational Wavelength (nm)**	**Repetition Rate (MHz)**	**Pulse Width**	**SNR (dB)**	**Ref**
WS_2	1558.6	523	711 fs	89	(Fu, & Sun,2021)
MoS_2	1573.7	27.1	630 fs	61	(Hammad& Mansour, 2019)
BP	1560.7	6.88	570 fs	59	(Huttner, & Geiser, 2002)
$PtSe_2$	1563	23.3	1.02 ps	61	(Ippen, E., Shank, 1972)
Bi_2Se_3	1562.4	22.6	0.63 ps	51.2	(Hong, & Liu, 2020)

2.11 Summary

This chapter presents a detailed description of the research literature review of this research employed in this experiment. examined the essential concepts and prior research pertinent to the advancement of pulsed erbium-doped fiber lasers (EDFLs) utilizing saturable absorbers, which started with an introduction to laser technology and

highlighted the evolution of lasers from the first ruby laser to contemporary fiber-based systems. The special characteristics of laser light, such as coherence, monochromaticity, and high directionality, have made widespread applications possible. It started with an overview of laser technology, emphasizing how lasers have changed throughout time, from the first ruby laser to contemporary fiber-based systems. Widespread uses have been made possible by the special qualities of laser light, such as coherence, monochromaticity, and great directionality.

The fundamental structure and operational principle of optical fibers were further examined. Optical fibers guide light through total internal reflection, enabling low-loss transmission over long distances. This technology forms the basis of fiber lasers, where rare-earth-doped optical fibers act as the gain medium. Of the different fiber laser systems, EDFLs are particularly significant because they operate near 1.55 μm, which corresponds to the low-loss transmission window of silica fibers. The excitation and stimulated emission processes of erbium ions under 980 nm pumping were described, demonstrating how optical gain and laser oscillation are accomplished. Through total internal reflection, optical fibers direct light, enabling low-loss transmission over extended distances. Fiber lasers, which use rare-earth-doped optical fibers as the gain medium, are based on this technique. Because EDFLs operate close to 1.55 μm, which corresponds to the low-loss transmission window of silica fibers, they are especially significant among other fiber laser systems. Optical gain and laser oscillation were demonstrated by the explanation of the excitation and stimulated emission processes of erbium ions under 980 nm pumping.

The chapter also examined pulse generation techniques in fiber lasers, namely Q-switching and mode-locking. Q-switching generates brief, high-energy pulses in the nanosecond to microsecond range by modulating cavity losses, whereas mode-locking synchronizes longitudinal cavity modes to produce ultrashort pulses in the picosecond or femtosecond range. Mode-locking synchronizes longitudinal cavity modes to generate ultrashort pulses in the picosecond or femtosecond regime. These pulsed regimes are highly valuable for applications requiring high peak power, precision material processing, nonlinear optics, and ultrafast photonics. The mode-lock sought after is soliton mode-lock can either dark pulse or bright pulse.

The propagation of pulses in optical fibers was reviewed with a focus on dispersion and nonlinear effects like self-phase modulation, cross-phase modulation, four-wave mixing, soliton formation, Kelly sidebands, and dark pulse generation, which

have a significant impact on pulse shaping, stability, and spectral behavior in fiber laser cavities. A number of pulse characterization parameters were recorded and examined, including pulse duration, repetition rate, pulse energy, peak power, average power, and pulse shape Additionally, dispersion and nonlinear phenomena such self-phase modulation, cross-phase modulation, four-wave mixing, soliton production, Kelly sidebands, and dark pulse generation were examined in relation to pulse propagation in optical fibers. In fiber laser cavities, these events have a significant impact on pulse shaping, stability, and spectrum behavior.

The chapter concluded with a review of various reported SA materials, such as SESAMs, carbon nanotubes, graphene, topological insulators, transition metal dichalcogenides, black phosphorus, antimony films, and metal oxides. Although these materials have shown promising results, limitations such as fabrication complexity, cost, environmental instability, or restricted performance remain. The nonlinear absorption mechanism, based on intensity-dependent transmission, was described along with the desirable properties of an ideal SA, including fast recovery time, thermal stability, and high damage threshold. The desired characteristics of an ideal SA, such as quick recovery time, wide working bandwidth, thermal stability, and high damage threshold, were explained along with the nonlinear absorption mechanism, which is based on intensity-dependent transmission. SESAMs, carbon nanotubes, graphene, topological insulators, transition metal dichalcogenides, black phosphorus, antimony films, and metal oxides were among the various SA materials that were evaluated. These materials have shown encouraging results, but they still have drawbacks such difficult manufacture, high cost, unstable environments, or limited performance.

The literature review indicates that $CuAlO_2$ and Cr_2GaC are promising candidates for further investigation as alternative saturable absorbers for generating stable Q-switched and mode-locked pulses in EDFLs. This provides the basis and rationale for the experimental work presented in the following chapters. As a result, there is ongoing motivation to investigate new SA materials with improved optical and physical properties. $CuAlO_2$ and Cr_2GaC are viable options for additional research as substitute saturable absorbers for producing stable Q-switched and mode-locked pulses in EDFLs, according to the examined literature. This serves as the basis and rationale for the experimental work described in the ensuing chapters.

Although extensive research has been carried out on pulsed erbium-doped fiber lasers (EDFLs) using various saturable absorbers such as graphene, carbon nanotubes,

topological insulators, transition metal dichalcogenides, black phosphorus, and metal oxides, several important gaps remain unresolved.In addition, most existing studies have focused heavily on well-known two-dimensional nanomaterials, while comparatively fewer investigations have explored alternative ceramic, oxide, and MAX-phase related materials with potentially superior thermal, mechanical, and nonlinear optical properties. Specifically, $CuAlO_2$ and Cr_2GaC remain underexplored as SAs in EDFL systems, particularly for passive Q-switching and mode-locking applications in the 1.55 μm wavelength region. While other rare-earth doped fiber work on different operating wavelength

This study fills the current research gap by examining $CuAlO_2$ and Cr_2GaC as novel saturable absorbers for EDFLs, evaluating their ability to generate stable Q-switched and mode-locked pulses, and analyzing key laser performance parameters. The results are anticipated to expand the range of available SA materials and contribute to the development of more efficient, robust, and cost-effective pulsed fiber laser systems. Additionally, there is limited comparative information regarding how these newer materials influence significant laser characteristics like pulse repetition rate, pulse width, signal-to-noise ratio, threshold power, and output efficiency. Additionally, it is yet unclear how their material characteristics relate to pulse generating performance.

Therefore, by examining $CuAlO_2$ and Cr_2GaC as innovative saturable absorbers for EDFLs, our study fills the current research gap. Key laser performance metrics will be examined, and their ability to produce steady Q-switched and mode-locked pulses will be assessed. The results are anticipated to increase the variety of SA materials accessible and aid in the creation of pulsed fiber laser systems that are more reliable, efficient, and affordable. In summary, while a vast body of literature has successfully demonstrated the use of 2D nanomaterials such as graphene, TMDs, and MXenes for pulse generation, a critical gap remains regarding their long-term structural and thermal stability under high-intensity optical fields. Many of these conventional saturable absorbers suffer from low damage thresholds or complex, high-cost fabrication techniques. This research carves out a specific niche by introducing and critically analyzing two distinct material families: Copper Aluminum Oxide $CuAlO_2$ and Cr_2GaC as innovative saturable absorbers for EDFLs, our study fills the current, a structurally stable p-type delafossite oxide, and Chromium Gallium Carbide, an exceptionally robust, oxidation-resistant MAX-phase compound. By embedding these materials into a cost-effective PVA host polymer matrix, this study bridges the gap between high damage threshold requirements and inexpensive

fabrication, providing a stable, alternative pathway for both bright and dark pulse laser architectures in the 1.55 μm window.

CHAPTER 3
RESEARCH METHODOLOGY

3.1 Introduction

This chapter presents the systematic research methodology employed in this study. It provides a comprehensive description of each experimental stage, beginning with the fabrication and characterization of the saturable absorber (SA) materials, followed by the laser cavity configuration, pulse formation, and data acquisition for Q-switched and mode-locked erbium-doped fiber laser (EDFL) operation. Detailed explanations are given on the characterization mechanisms used to evaluate the optical and physical properties of the fabricated SAs. The procedures and calculations for both linear and nonlinear absorption measurements are described to elucidate the saturable absorption behavior. This study focuses on two SA materials, namely Chromium Gallium Carbide (Cr_2GaC) and Copper Aluminium Oxide ($CuAlO_2$). Field-emission scanning electron microscopy (FESEM) was employed to investigate the surface morphology of the SA films, while energy-dispersive X-ray spectroscopy (EDX) was used to determine their elemental composition.

The methodology further encompasses the operational characterization of the laser system under different pulsed regimes, including Q-switching and mode-locking. Advanced diagnostic instruments—such as an oscilloscope, optical spectrum analyzer (OSA), radio frequency (RF) spectrum analyzer, and autocorrelator—were utilized for temporal and spectral pulse analysis. Data logging, processing, and documentation were carried out using Microsoft Excel and Microsoft Word. The overall research workflow is summarized in a flowchart, as illustrated in Figure 3.1.

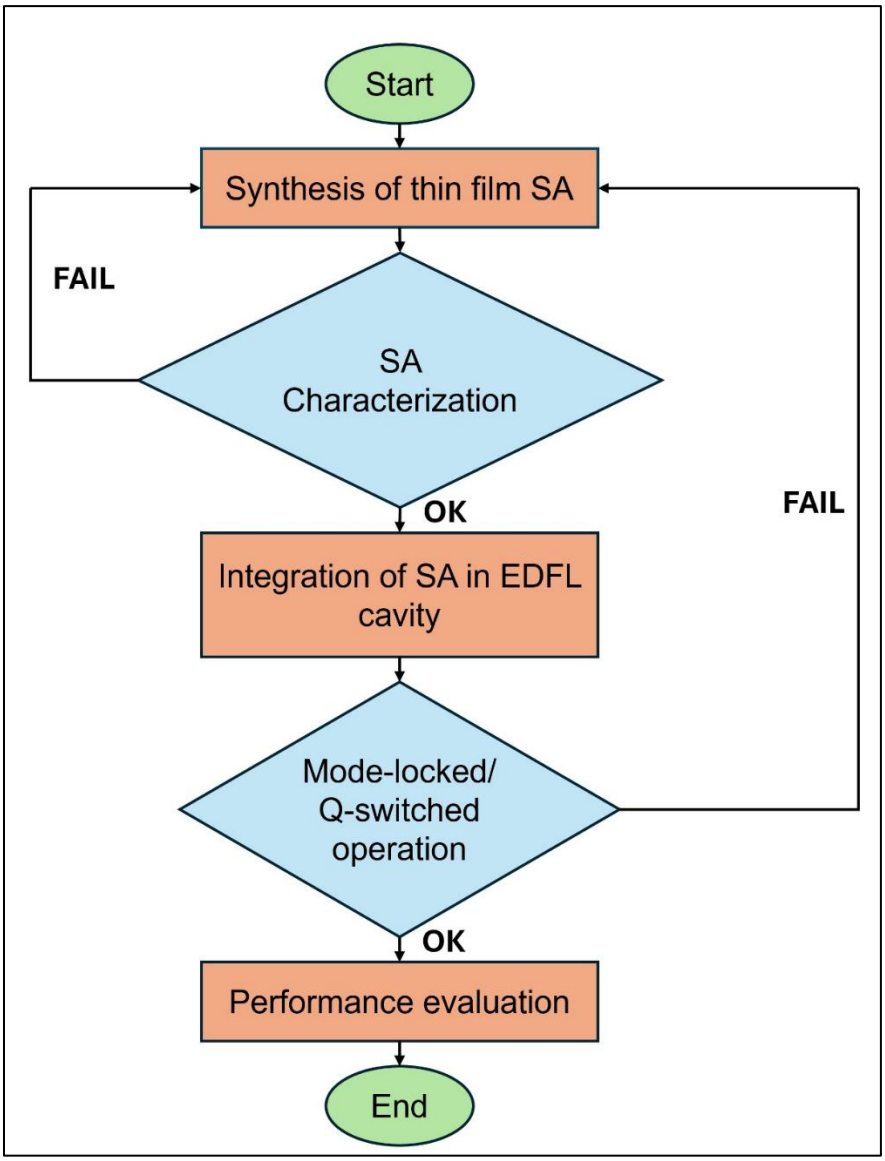


Figure 3.1 Basic Process Flowchart Of The Research Methodology Adopted In This Study

3.2 Material

3.2.1 Polyvinyl Alcohol

Polyvinyl alcohol (PVA) has become one of the most widely used host matrix materials for dispersing nanomaterials and fabricating flexible saturable absorber (SA) films through a simple and cost-effective process. PVA is a synthetic, water-soluble polymer that exhibits high optical transparency in the near-infrared (NIR) region, which corresponds to the operating wavelength range of erbium-doped fiber lasers. It offers excellent film-forming capability, ease of handling, good compatibility with a wide range

of nanomaterials, and flexibility in controlling the volume and composition of the SA material, making it highly suitable for SA device fabrication.

In a typical preparation process, the nanomaterial is first dispersed in deionized water. Separately, a PVA solution is prepared by dissolving PVA powder in water and stirring until a clear and homogeneous solution suitable for SA fabrication is obtained. The nanomaterial is then introduced into the PVA solution in an appropriate mass ratio to achieve the desired saturation characteristics and is thoroughly mixed to ensure uniform dispersion. The resulting composite solution is subsequently poured onto a Petri dish or glass substrate and allowed to dry under ambient or controlled conditions to form a thin film. After drying, a small section of the film is cut to the desired size and sandwiched between two fiber ferrules using a small amount of index-matching gel, enabling proper integration of the SA into the laser cavity.

Despite its advantages, PVA-based SA fabrication presents certain limitations. The water solubility of PVA can compromise long-term stability in humid environments, non-uniform nanomaterial dispersion may lead to inconsistent laser performance, and the damage threshold of PVA is generally lower than that of inorganic host materials.



Figure 3.2 PVA Powder Used In This Study

3.2.2 Copper Aluminum Oxide ($CuAlO_2$)

A transparent conducting oxide (TCO) is a class of materials that simultaneously exhibit electrical conductivity and high optical transparency, particularly in the visible and near-infrared (NIR) spectral regions. Common examples include indium tin oxide

(ITO), aluminum-doped zinc oxide (AZO), and fluorine-doped tin oxide (FTO). Owing to these unique properties, TCOs are widely employed in touchscreens and display technologies, solar cells, light-emitting diodes (LEDs), and optical modulators. In laser and photonics research, TCOs are especially attractive because they combine optical transparency with efficient charge transport, enabling the development of multifunctional and integrated photonic components.

Copper aluminum oxide ($CuAlO_2$) refers to a family of mixed metal oxides composed of copper (Cu), aluminum (Al), and oxygen (O), among which $CuAlO_2$ is the most extensively studied. $CuAlO_2$ crystallizes in the delafossite structure and is notable as one of the few p-type transparent conducting oxides, making it highly valuable for electronic and photonic applications. Copper-based oxides have also been reported to exhibit nonlinear optical absorption and show good compatibility with polymer host matrices such as polyvinyl alcohol (PVA). These characteristics make them promising candidates for use as saturable absorbers in fiber laser systems, enabling Q-switching and mode-locking operations.

Figure 3.3 illustrates the crystal structure of delafossite $CuAlO_2$. As shown, Cu^+ ions are linearly coordinated by two oxygen atoms (O–Cu–O), forming vertical chains along the c-axis, while Al^{3+} ions are octahedrally coordinated by oxygen, forming AlO_6 octahedra. These AlO_6 octahedra share edges within the ab-plane, resulting in a layered hexagonal (rhombohedral) crystal structure. This layered oxide configuration gives rise to a wide optical bandgap, enabling high transparency in the visible and near-infrared (NIR) spectral regions. Moreover, the anisotropic nature of the layered structure contributes to intensity-dependent optical absorption, which is advantageous for nonlinear optical applications. In this study, these properties enable the effective use of $CuAlO_2$ as a saturable absorber for Q-switching and mode-locking operations in fiber laser systems.

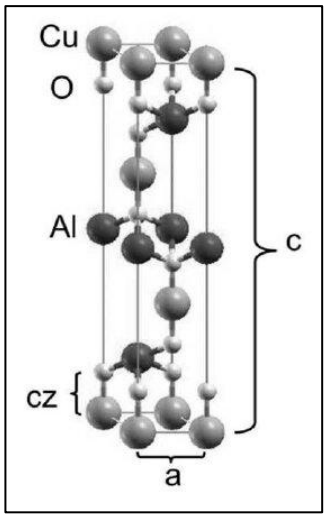


Figure 3.3 Crystal Structure of Delafossite $CuAlO_2$. The Lattice parameter a represents the Basal (Horizontal) Plane, c denotes the Lattice Parameter Along The Vertical Stacking Direction, and cz Corresponds To The Height of One Structural Block, typically associated with a Single Cu–O Layer.

3.2.3 Chromium gallium carbide (Cr2GaC)

Chromium gallium carbide (Cr_2GaC) belongs to the MAX-phase family of layered ternary carbides with the general chemical formula M_2AX, where M represents a transition metal, A is an A-group element, and X denotes carbon. Cr_2GaC exhibits a unique nanolaminated hexagonal crystal structure composed of alternating Cr–C octahedral layers and Ga atomic layers. This layered architecture endows Cr_2GaC with a combination of metallic-like electrical conductivity and ceramic-like thermal and chemical stability. Owing to its anisotropic electronic structure and strong light–matter interaction, Cr_2GaC demonstrates nonlinear optical absorption behavior, including intensity-dependent transmission, which is a fundamental requirement for saturable absorber operation. In addition, Cr_2GaC offers broadband optical response, fast carrier recovery dynamics, and a relatively high damage threshold, making it suitable for high-power and ultrafast laser applications. When incorporated into a polymer host matrix such as polyvinyl alcohol (PVA), Cr_2GaC can be conveniently processed into flexible thin-film saturable absorbers with good mechanical integrity and optical uniformity. These advantageous properties enable the effective utilization of Cr_2GaC as a saturable absorber for passive Q-switching and mode-locking in erbium-doped fiber laser systems, facilitating the generation of stable pulsed laser outputs.

Figure 3.4 shows the crystal structure of a MAX-phase material with the general formula M_2AX, which is the structural family to which Cr_2GaC belongs. The layered nanolaminated architecture gives rise to strong anisotropy and underpins the unique metallic–ceramic hybrid properties and nonlinear optical response of Cr_2GaC.

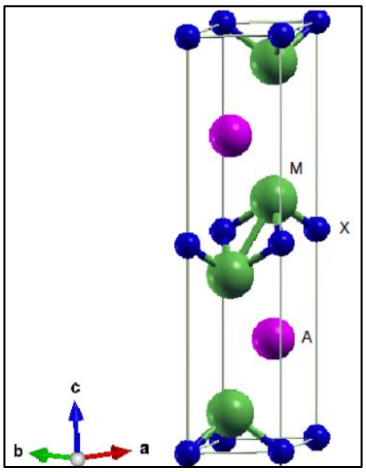


Figure 3.4 Crystal Structure of a MAX-Phase Material With The General Formula M_2AX (illustrated for Cr_2GaC). The structure consists of alternating M–X Octahedral Layers (Green: M = Cr; Blue: X = C) and A-Element Atomic Layers (Purple: A = Ga) Stacked Along the C-Axis.

3.3 Fabrication of SA

Saturable absorbers (SAs) are conventionally fabricated using techniques such as electrochemical exfoliation, evanescent-field coupling structures, and mechanical exfoliation. However, these approaches often suffer from inherent limitations that may adversely affect pulsed laser performance, including structural fragility, polarization sensitivity, and limited interaction length. To address these challenges, the embedding method was adopted in this work to fabricate the SA films, as it offers advantages such as polarization-insensitive operation, enhanced light–matter interaction, and precise control over the SA concentration. This section presents a step-by-step description of the thin-film SA preparation process. Owing to its simplicity, low cost, and scalability, the solution casting technique was employed for SA film fabrication. In this approach, $CuAlO_2$ (or Cr_2GaC) powder was dispersed within a PVA matrix to form a composite thin film. PVA serves as an effective host polymer for high-performance SA fabrication due to its excellent film uniformity, good mechanical stability and tensile strength, ease of emulsification, high water solubility, and low material cost, which are advantageous

for large-scale SA production. Further details on the fabrication procedures of both $CuAlO_2$ and Cr_2GaC SAs are provided in the following subsections.

3.3.1 Preparation of the $CuAlO_2$ film

Polycrystalline $CuAlO_2$ samples were synthesized via solid-state reaction. Copper oxide (Cu_2O) and aluminum oxide (Al_2O_3) were weighed according to the stoichiometric ratio and combined in a molar ratio of 1:1.1. The mixture was mechanically ground for 30 minutes using an agate mortar and pestle. The resulting blend was placed in a ceramic tube, which was sealed with ceramic paste. The tube was then heated in an oven at 1000°C for 10 hours. The produced nano-powder was used to fabricate a $CuAlO_2$ thin film. First, a $CuAlO_2$ liquid solution was prepared by ultrasonicating 300 mg of $CuAlO_2$ nano-powder in 10 ml of deionized (DI) water to achieve a 3 wt.% solution concentration. Next, 10 ml of the $CuAlO_2$ liquid was mixed with PVA, and the mixture was continuously stirred at 60°C until the volume was reduced to 5 ml. The $CuAlO_2$-PVA mixture was then transferred into a glass Petri dish and placed in an oven at 60°C for 3 hours to form a thin $CuAlO_2$-PVA film. Figure 3.5 presents a step-by-step procedure for preparing the $CuAlO_2$ film. It was fabricated using a solution-casting approach under controlled concentration and drying conditions, ensuring reproducible nonlinear absorption characteristics across multiple batches. The inset shows an image of the film after it has been carefully detached from the Petri dish. To minimize environmental effects, the films were encapsulated in the ferrule–ferrule connector setup and stored under ambient laboratory conditions, where no degradation was observed during several weeks of testing. For long-term applications, protective encapsulation methods (e.g., epoxy or hermetic sealing) may be employed to further enhance environmental stability. The film thickness, measured using an optical micrometre, is approximately 80 μm.

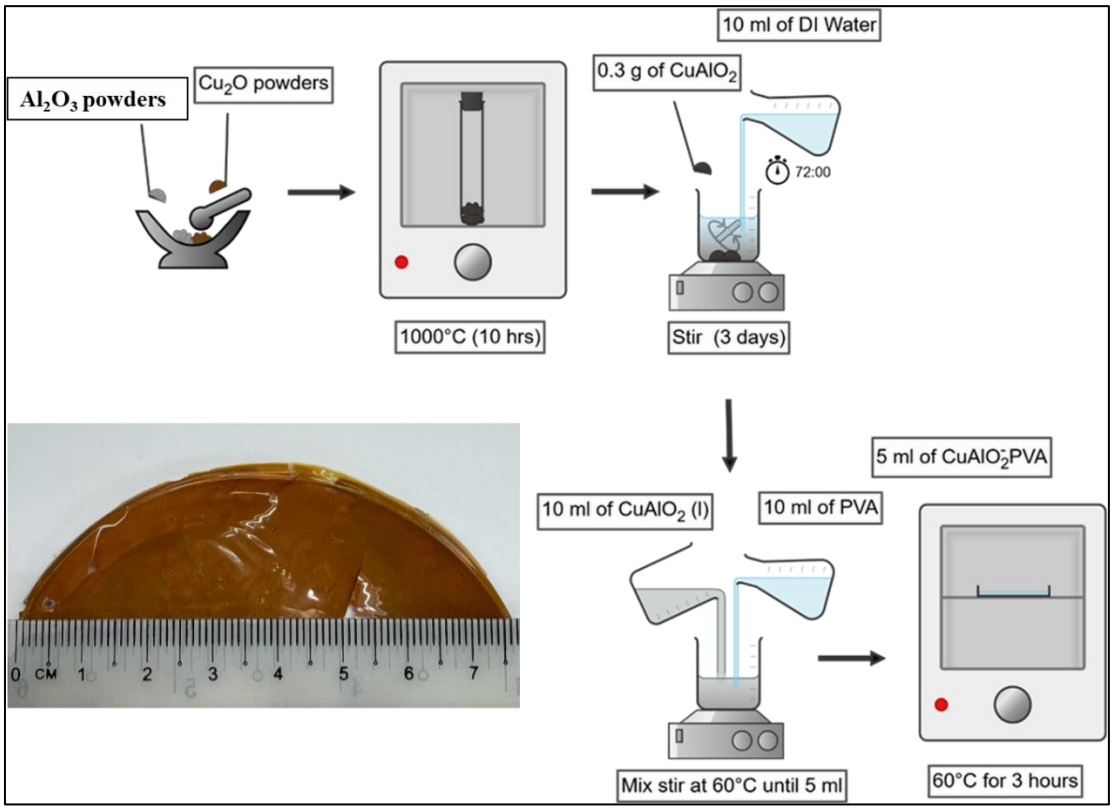


Figure 3.5 The Procedure for Preparing The $CuAlO_2$-PVA Film. The Inset Figure Displays an Image of the Produced Film.

3.3.2 Preparation of the Cr_2GaC film

The Cr_2GaC film SA was fabricated through a solution-casting method where the Cr_2GaC MAX phase powder was mixed into a PVA solution. The complete fabrication process is illustrated in Figure 3.6. Initially, PVA solution was prepared in a 1:1 ratio by diluting 1 g of PVA powder (Sigma Aldrich, CAS: 9002-89-5) into 100 ml of deionized water and undergoing stirring for about 2 hrs at 400 rpm to ensure complete dissolution. Then, 2.5 mg of Cr_2GaC powder was mixed with 5 ml of the PVA solution and stirred for 48 hrs at 400 rpm until uniformly combined. The homogeneous solution was then transferred into a petri dish for drying. The mixture took about 72 hours to dry at room temperature. The final product forms a Cr_2GaC film SA with a thickness of approximately 50 micrometres as shown in the inset figure. To verify the physical uniformity and thickness profile of the cast $CuAlO_2$-PVA and Cr_2GaC-PVA thin films, non-contact cross-sectional dimensional profiling was conducted using a high-precision optical micrometer [Keyence LS-9000 series]. Unlike mechanical micrometers which can physically compress, distort, or pierce the fragile polymer-matrix film, the optical

micrometer utilizes a non-contact laser scan or green LED shadow-casting method. The thin film sample is placed in the measurement zone where an optical receiver tracks the exact boundary lines of the film's physical obstruction profile. This non-contact technique guarantees sub-micron resolution measurements of the final 80µm thick saturable absorber arrays without altering their structural integrity.

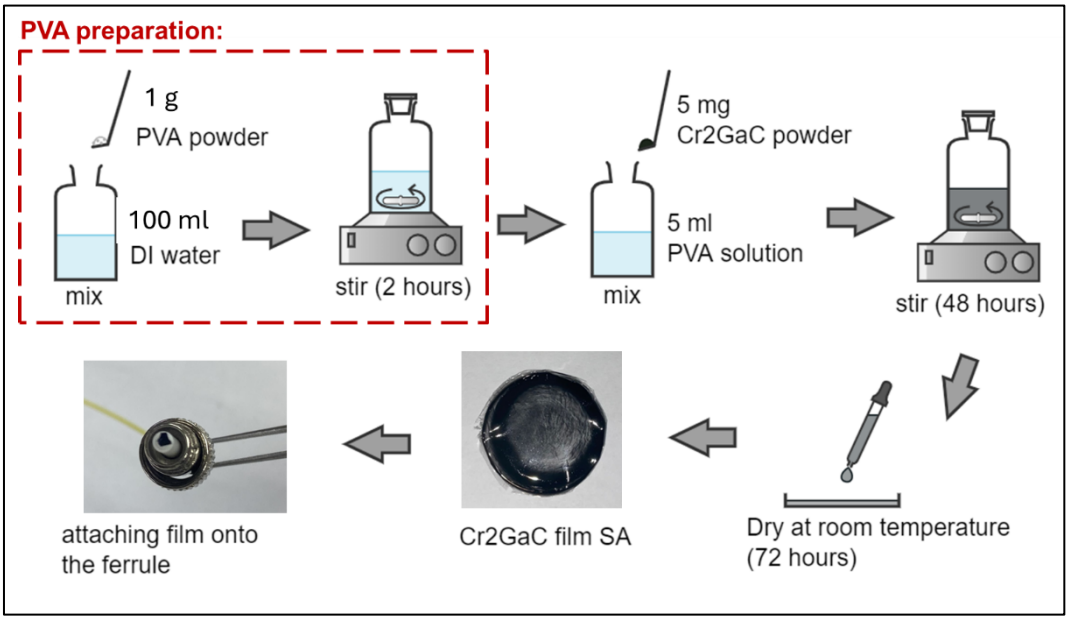


Figure 3.6 Complete Fabrication Flow for Cr_2GaC Film SA.

3.4 Characterization of the prepared thin film SA

The characterization process evaluates the suitability of the fabricated SA's thin films for both Q-switching and mode-locking operations. The elemental composition of the SA films was analysed using energy-dispersive X-ray spectroscopy (EDS), while their surface morphology and microstructural features were examined using field-emission scanning electron microscopy (FESEM). This section also presents a brief discussion of the linear absorption profiles and nonlinear optical properties of the SAs, which are essential for understanding their absorption behaviour across a broad near-infrared (NIR) spectral region.

$CuAlO_2$ and Cr_2GaC thin-film SAs were fabricated using the solution-casting method with PVA as the host polymer as described in the previous section. The physical characteristics of the fabricated SAs were investigated using FESEM and EDS to provide detailed insight into the film morphology and to confirm the elemental composition of the SA layers. Prior to incorporation into the laser cavity, the optical properties of the SA

thin films were also examined using homemade linear and nonlinear absorption measurement setups. The linear absorption setup, illustrated in Figure 3.7 (a), consists of a white-light source coupled to an optical spectrum analyser (OSA). Linear absorption over a wide wavelength range from approximately 600 to 1700 nm was determined by comparing the output spectra of a reference single-mode fiber (without SA) and the system with the SA inserted. These measurements were conducted at low input power levels to evaluate the intrinsic linear absorption characteristics of the fabricated SAs across the broad operating wavelength range.

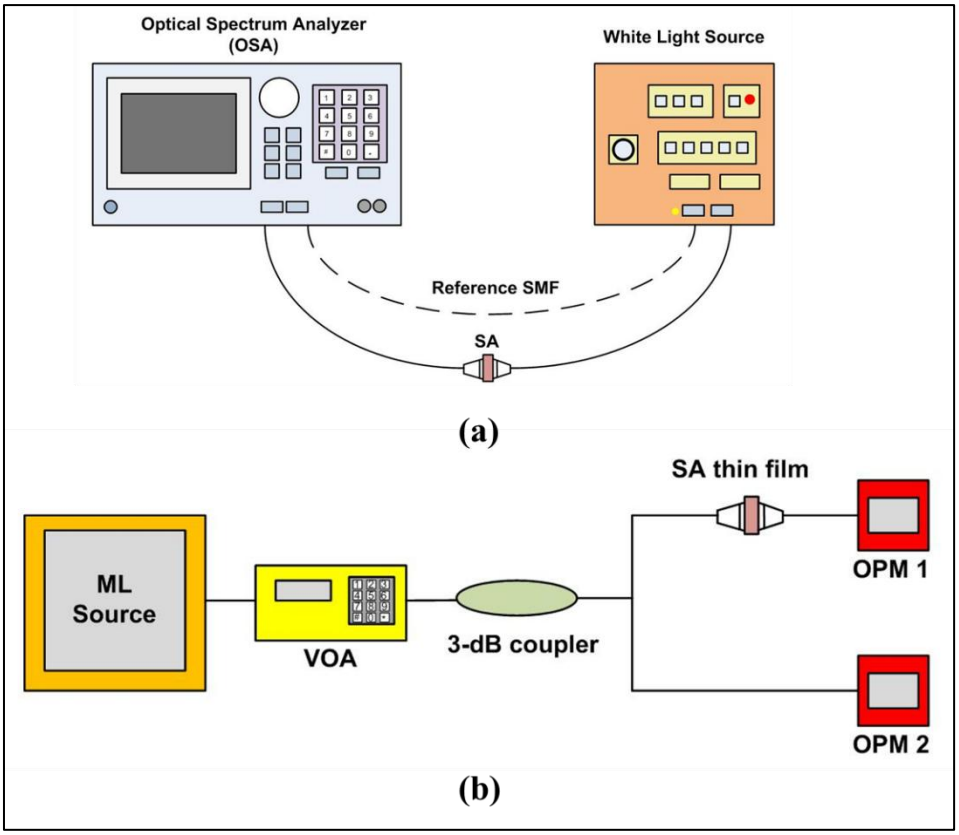


Figure 3.7 Experimental Setups For (a) Linear Absorption, and (b) Nonlinear Absorption Characterization.

Nonlinear absorption measurements were carried out using the twin balanced detector technique, and the corresponding experimental setup is illustrated in Figure 3.7 (b). To evaluate the nonlinear optical absorption characteristics of the fabricated SAs, a homemade measurement system was employed. A stable mode-locked pulse source was first established and used as the excitation signal. The output pulses were subsequently amplified using an erbium-doped fiber amplifier (EDFA) and then passed through a

variable optical attenuator to precisely control the incident optical intensity. The attenuated signal was directed into a 3 dB optical coupler, which split the optical power equally (50:50). One output arm was routed through the SA under test for nonlinear absorption assessment, while the other arm propagated through a length of SMF patch cord to serve as the reference signal.

The intensity-dependent absorption of the fabricated SAs was analysed using Eq. (3.1) to extract the key nonlinear optical parameters, namely the modulation depth (saturable absorption), non-saturable absorption, and saturation intensity.

$$\alpha(I) = \frac{\alpha_s}{\left(1 + \frac{I}{I_{sat}}\right)} + \alpha_{ns} \tag{3.1}$$

where $\alpha(I)$ denotes the intensity-dependent absorption, α_s is the saturable absorption (modulation depth), α_{ns} represents the non-saturable absorption, I is the incident optical intensity, and I_{sat} is the saturation intensity. These nonlinear optical parameters were evaluated for all fabricated SAs to assess their suitability for passive Q-switching and mode-locking operations. SAs with adequate modulation depth and appropriate linear absorption are essential for achieving stable Q-switched and mode-locked laser performance.

3.5 Laser Configuration

The laser configuration implemented for Q-switching and mode-locking operation is shown in Figure 3.8. The system operates in the 1.5 μm wavelength region, employing erbium-doped fiber (EDF) as the gain medium. A 980 nm laser diode (LD) serves as the pump source and is coupled into the EDF through a 980/1550 nm wavelength-division multiplexer (WDM). An optical isolator is incorporated to enforce unidirectional light propagation within the ring cavity, thereby protecting the resonator from unwanted back reflections and instability.

A small section of the fabricated SA film, with an approximate size of 1 mm × 1 mm, was cut and sandwiched between two clean FC/PC fiber ferrules to form a fiber-compatible SA device. A small amount of index-matching gel was applied at the fiber–film interfaces to secure the thin film and suppress parasitic reflections. The SA device was then integrated into the laser cavity by splicing it into the fiber ring. An output coupler was used to extract a fraction of the laser output while allowing the majority of the optical power to continue oscillating within the cavity.

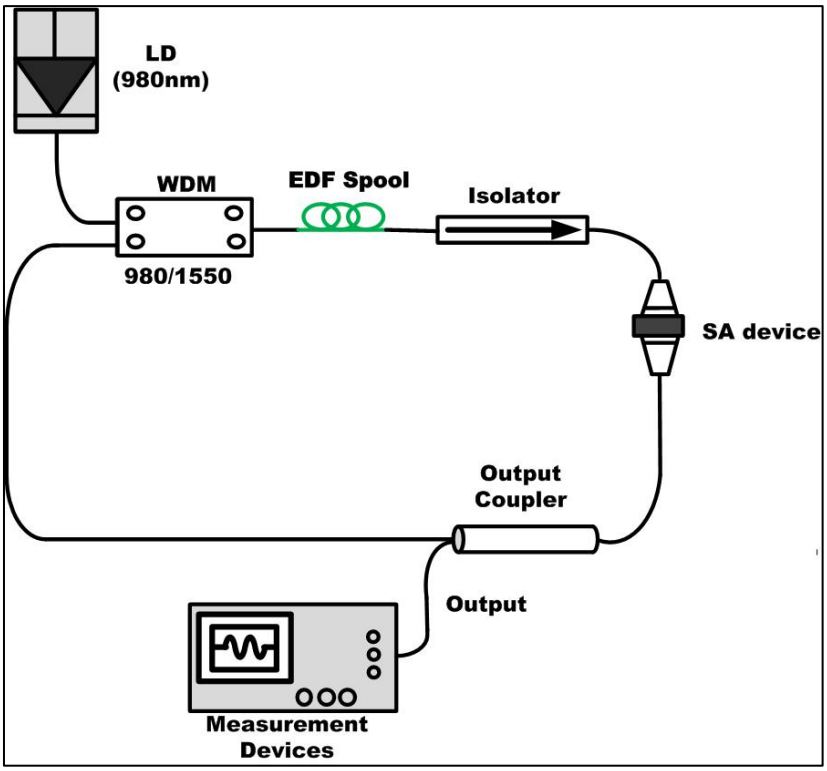


Figure 3.8 Schematic of the Erbium-Doped Fiber Laser (EDFL) Cavity Employed In This Study for the Generation of Q-Switched and Mode-Locked Pulses Using A Passive Modulation Technique Based on a Thin-Film SA.

The SA dynamically modulates the intracavity loss and quality factor (Q-factor), enabling optical energy to accumulate within the cavity before being rapidly released in the form of short laser pulses. No polarization controller (PC) was employed in the cavity to minimize insertion loss and simplify the laser configuration. All fiber connections were fusion-spliced, except for the SA device, which utilized fiber ferrules for film integration.

Spectral characteristics of the generated pulses were analyzed using an optical spectrum analyzer (OSA). The temporal behavior of the Q-switched and mode-locked pulses was monitored using a digital storage oscilloscope in conjunction with a radio-frequency (RF) spectrum analyzer equipped with an InGaAs photodetector. The average output power of the pulse train was measured using an optical power meter with an InGaAs power head. For the laser cavity characterization loop, the temporal pulse train was captured via a high-speed InGaAs Photodetector (Thorlabs, Model DET01CFC) paired with a 500MHz Digital Oscilloscope (Tektronix, Model TDS3054C). The corresponding spectral profile was monitored using an Optical Spectrum Analyzer (Yokogawa, Model AQ6370D). Frequency domain metrics and

radio-frequency purity were validated utilizing a RF Spectrum Analyzer (Anritsu, Model MS2692A), while average output capacities were quantified using an Optical Power Meter (Thorlabs, Model PM100D). Ultra-short pulse durations in the picosecond regime were confirmed via a commercial Optical Autocorrelator (APE, Model PulseCheck).

For mode-locking operation, the cavity length was extended by incorporating an additional spool of single-mode fiber (SMF). Increasing the cavity length enhances the balance between dispersion and nonlinear effects, thereby facilitating stable mode-locked pulse generation. The ultrafast pulse duration, in the picosecond or femtosecond regime, was characterized using an autocorrelator. While the p-type delafossite oxide CuAlO2 thin film demonstrated excellent high-energy extraction capabilities in the Q-switched regime, exploring alternative robust crystalline structures is vital to expanding cavity versatility. Consequently, the next section evaluates the implementation of a ternary MAX-phase compound, Chromium Gallium Carbide Cr2GaC, to investigate its potential in driving both bright and dark pulse mode-locked architectures.

3.6 Summary

This chapter presents a detailed description of the research methodology employed in this study. The fabrication procedures of both $CuAlO_2$- and Cr_2GaC-based SAs, using polyvinyl alcohol as the host polymer, are systematically explained. The preparation processes and characterization objectives are also outlined. Physical characterization was conducted on all fabricated SAs, where FESEM was used to obtain high-resolution images of the surface morphology, enabling detailed analysis of particle distribution within the films. In addition, energy-dispersive X-ray spectroscopy (EDS) was employed to confirm the elemental composition of the SA films.

While the transition from bulky organic dyes to low-dimensional nanomaterials (such as graphene, TMDs, and topological insulators) has significantly advanced ultrafast laser physics, a critical evaluation of the current state-of-the-art reveals two distinct Research Gaps: The Material Resilience vs. Performance Trade-off: Conventional 2D saturable absorbers are structurally fragile. Materials with high modulation depths (e.g., black phosphorus) undergo rapid ambient oxidation and possess low optical damage thresholds, leading to device ablation under high-power intra-cavity dynamics. Conversely, structurally rugged materials often suffer from low optical nonlinearity or high non-saturable insertion losses. There is a critical gap in the literature for an SA

material that simultaneously delivers extreme atmospheric stability, a high thermal damage threshold, and giant optical non-linearities. Secondly, Cavity Architecture Limitations: Most stable mode-locked operations documented in recent scholarship require complex, specialized cavity layouts or active polarization management to survive the physical degradation of the SA. There is a clear lack of systematic studies validating materials that can drive both bright soliton and highly demanding dark pulse regimes within a simple, uncompensated, standard traveling-wave fiber ring configuration.

The linear and nonlinear optical absorption characteristics of the SAs are further discussed, as these parameters are critical in determining their suitability for passive Q-switching and mode-locking operations. To function effectively in an EDFL cavity, the SAs must exhibit adequate linear absorption and sufficient modulation depth. Finally, the laser cavity configurations designed for Q-switched and mode-locked pulse generation operating in the 1.5 μm wavelength region are described.

CHAPTER 4
RESULTS AND DISCUSSION I: COPPER ALUMINUM OXIDE–BASED Q-SWITCHING AND MODE-LOCKING

4.1 Introduction

As a key representative of third-generation laser technology, fiber lasers are extensively utilized in both industrial and scientific applications, accounting for a substantial share of the commercial laser market (Ahmad, H., & Harun, S. ,2016) , Nizamani, B., & Harun, S. W.,2020),. They can operate in either continuous-wave or pulsed modes. Pulsed fiber lasers, with their short pulse widths and high pulse energy, are particularly valuable for nonlinear and ultrafast optics applications like communications (H. H., & Jalal Abdulrazzaq, M., 2023), optical sensing (Jasem, & Abdullah, 2023), and laser processing (Kadir, & Ismail,2017). Q-switching (QS) and mode-locking (ML) are two key techniques for generating pulses. QS works by modulating the laser cavity's quality factor (Q), releasing stored energy in microsecond-duration pulses with kilohertz repetition rates(Keller, U.,2003). . Mode-locking, on the other hand, synchronizes the laser cavity modes, producing shorter pulses with higher peak power but lower pulse energy compared to QS. These techniques can be realized actively or passively, with passive methods gaining popularity due to their compactness, flexibility, simplicity, and lower cost. Unlike active methods, passive techniques utilize a saturable absorber (SA) placed in the resonator to generate laser pulses without the need for complex optical modulators or electronic drivers. As such, SA materials are crucial to the development of passive pulsed lasers (Latiff, & Kadir, 2017).

Semiconductor SA mirrors (SESAMs) were extensively studied in the past and are considered a mature technology as a pulse transducer with widespread use in commercial laser systems, particularly in solid-state lasers (Lau, & Latif, , 2017). However, they are costly to manufacture and have a limited operational bandwidth (typically a few tens of nanometers), restricting their use in fiber laser systems. As a result, research has shifted toward low-dimensional carbon nanostructures, such as graphene, as promising SAs due to their advantages, including low saturation intensity, fast recovery time, and low cost (Chung, H., & Lee, J. H.,2016). . For example, Fu et al. demonstrated broadband ultrafast pulse generation at 1035, 1564, and 1908 nm using

a graphene SA device (Otto, A., & Schmidt, M. (2011).). This success has driven further investigation into other graphene-like 2D materials, including black phosphorus (Sun, Z., & Zhang, L.2019), topological insulators (Chen, Z., & Wang, J. ,2018), MAX phase materials (Zhao, Q., & Liu, W,2024). , and transition metal dichalcogenides (Liu, H., & Chow, K. ,2014. , Liu, H. H., & Chow, K. K. 2014).). Additionally, significant research efforts have focused on developing new SAs based on emerging materials such as organic and polymer compounds (Liu, X., Wang, 2020,Xu, & Chen, 2024 ,61. Liu, & Zhang, 2011). A practical SA device should be robust, cost-effective, and suitable for mass production. The choice of an SA for a specific application depends on factors such as modulation depth, response time, and saturation intensity. The pursuit of new and high-performance SAs remains an active research area, particularly for applications in ultrafast photonics and nonlinear optics.

Recently, there has been rising interest in transparent-conducting oxides (TCOs) owing to their various potential applications. These materials are electrically conductive and exhibit relatively small absorption of electromagnetic waves in the visible spectrum. Typically fabricated using thin film technologies, TCOs are commonly deployed in opto-electrical devices such as opto-electrical interfaces, solar cells, light-emitting diodes, displays, and semiconductor lasers (Maiman,1960). Copper-based delafossite oxides are particularly promising candidates for p-type TCOs, which are crucial for enabling transparent semiconductor applications. In the previous work, Salah et al. reported the low-energy electronic structure of Copper Aluminum Oxide ($CuAlO_2$) using angle-resolved photoemission spectroscopy (Malik, & Rohrer,2023). It was also reported bandgap size of $CuAlO_2$ range 1.9 eV to 13 eV.

This chapter presents a novel laser application of a $CuAlO_2$-based device, demonstrating its effectiveness as a SA for generating stable passive Q-switched and mode-locked pulses on EDFA. The preparation and fabrication of the SA device were described in the preceding chapter. Based on the research methodology outlined therein, lasing experiments were carried out to experimentally validate copper aluminum oxide ($CuAlO_2$) as an SA for both Q-switched and ultrafast mode-locked pulse generation in an erbium-doped fiber laser (EDFL) cavity. The performance characteristics of the resulting pulsed laser operations are systematically investigated and discussed in this chapter.

4.2 Characteristics of the $CuAlO_2$ film.

The fabricated $CuAlO_2$-PVA film was analyzed using advanced techniques including Energy Dispersive X-ray Spectroscopy (EDX), Field Emission Electron Microscopy (FESEM), and X-ray diffraction (XRD). The EDX analysis shown in Figure 4.1 (a) examined the elemental composition of the film, identifying a dominant presence of carbon (C), oxygen (O), copper (Cu), and aluminum (Al). The carbon content mainly comes from the PVA matrix. The inset of Figure 4.1 shows the FESEM image of the prepared $CuAlO_2$–PVA film, revealing a uniform surface morphology that confirms the homogeneous dispersion of $CuAlO_2$ particles within the PVA matrix. Such homogeneity significantly enhances the film's effectiveness as a saturable absorber material. The film thickness, measured using an optical micrometer, is approximately 80 μm.FESEM analysis on 0.3 g/ 10ml CuAlO2 SA carbon at 56% of weight with 0.7 omega, Oxygen 42.4% of weight with 0.7 omega, copper 42.4% of weight with 0.3 omega, aluminium 42.4% of weight with 0.1 omega. It even undergoes XRD analysis.

XRD data were obtained using a Bruker D4 Endeavor Advance diffractometer across the angular range of 10°–80° with CuKa radiation ($\lambda = 0.154178$ nm), a counting time of 2s per step and a step size of 0.02°. The resulting patterns were matched with the JCPDS Cards using the Bruker Eva program to confirm the reaction's completion. The XRD pattern of the synthesized $CuAlO_2$ sample is displayed in Figure 4.1 (b). The observed peaks correspond to the delafossite structure of $CuAlO_2$, with a pronounced orientation observed along multiple planes, including (006), (101), and (012). These peaks are consistent with the characteristics of pure delafossite $CuAlO_2$, as indicated by JCPDS Card No. 35-1401. $CuAlO_2$ crystallizes in a hexagonal close-packed lattice with the 3R polytype, where Al^{3+} ions occupy the centres of trigonally distorted octahedra, which are linked by edge-sharing to form infinite AlO_2 sheets in the (001) planes.

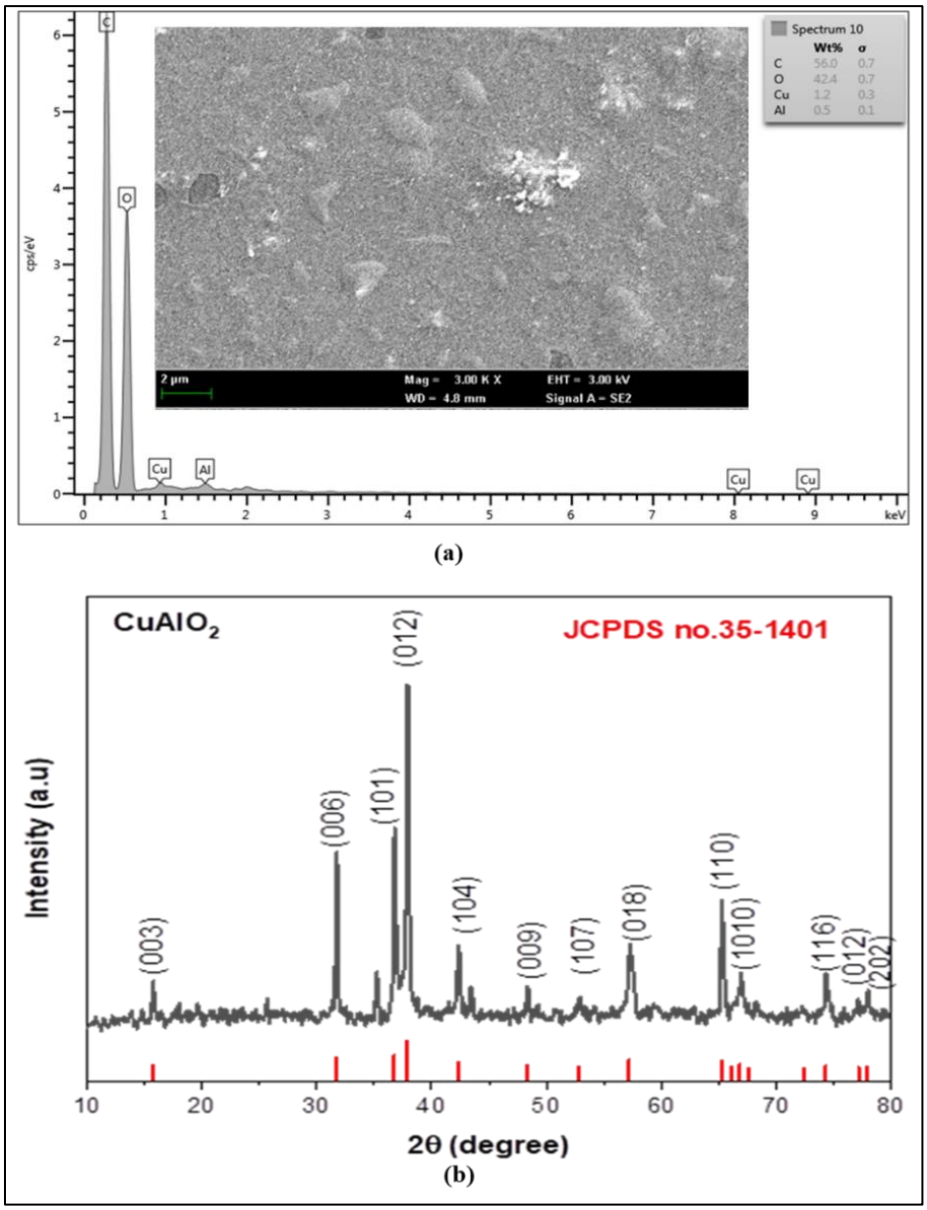


Figure 4.1 (a) EDX Analysis Results, with an Inset Showing the FESEM Image at 3000x Magnification. (b) XRD Pattern of $CuAlO_2$.

The linear absorption properties of the $CuAlO_2$-PVA film were evaluated by passing photons from a white light source through the SA film and measuring the output utilizing an optical spectrum analyzer (OSA, MS97010C Anritsu) as described in the previous chapter. The results are shown in Figure 4.2 (a), where an absorption of 2.11 dB is observed at a wavelength of approximately 1560 nm. To assess the nonlinear absorption of the $CuAlO_2$ film, a balanced twin-detector system was employed. Achieving accurate modulation depth measurements required the light incident on the $CuAlO_2$ film to reach the material's saturation point, necessitating high peak power. For

this, an ultrafast fiber laser with 1.5 ps pulse duration was used as the light source. The laser operated at wavelength of 1562 nm.

To evaluate the nonlinear optical properties of the $CuAlO_2$ film, the laser output was passed through an optical amplifier and a variable optical attenuator (VOA), which controlled the incident beam power. A 3 dB coupler split the beam equally, with one path directed to a power meter as a reference and the other passing through the $CuAlO_2$ film before reaching a second power meter. The resulting nonlinear absorption curve was fitted using the standard saturable absorption model as described in Eq. (3.1) in the previous chapter (Mansor, & Zainol Abidin,2022).

The fitting results, shown in Figure 4.2 (b), revealed a modulation depth of 4.1%, a saturation intensity of 4 kW/cm², and a non-saturable loss of 33.5%. These findings confirm that the $CuAlO_2$ film exhibits intensity-dependent absorption—transmitting more light at low intensities and saturating at higher intensities. This behavior enables its use for modulating intra-cavity losses in Q-switching and mode-locking applications. The saturable absorption in $CuAlO_2$ is likely associated with intrinsic defect levels and carrier dynamics, such as oxygen vacancies and mixed Cu^{1+}/Cu^{2+} states, which enable bleaching under high optical intensities.

The modulation depth and non-saturable absorption of the candidate's saturable absorber are typically determined using a nonlinear optical transmission measurement, commonly performed with the balanced twin-detector method or a power-dependent transmission setup. In this method, ultrashort laser pulses are directed onto the saturable absorber while the incident intensity is gradually increased. The transmitted power is then recorded as a function of input intensity.

The experimental data are fitted using the standard saturable absorption equation:

$$\alpha(I)=\frac{\alpha_0}{(1+\frac{I}{I_{sat}})}+\alpha_{ns} \tag{4.1}$$

where ΔT is the modulation depth, I_sat is the saturation intensity, and T_ns is the non-saturable absorption loss.

Modulation depth represents the maximum change in absorption between low and high optical intensity. It indicates how effectively the material can modulate intracavity loss for pulse generation. Non-saturable absorption refers to the residual loss

that does not decrease even at high intensity, usually caused by scattering, defects, imperfect film formation, or intrinsic linear losses. Therefore, the candidate likely measured these parameters by fitting the measured transmission curve from the nonlinear absorption experiment.

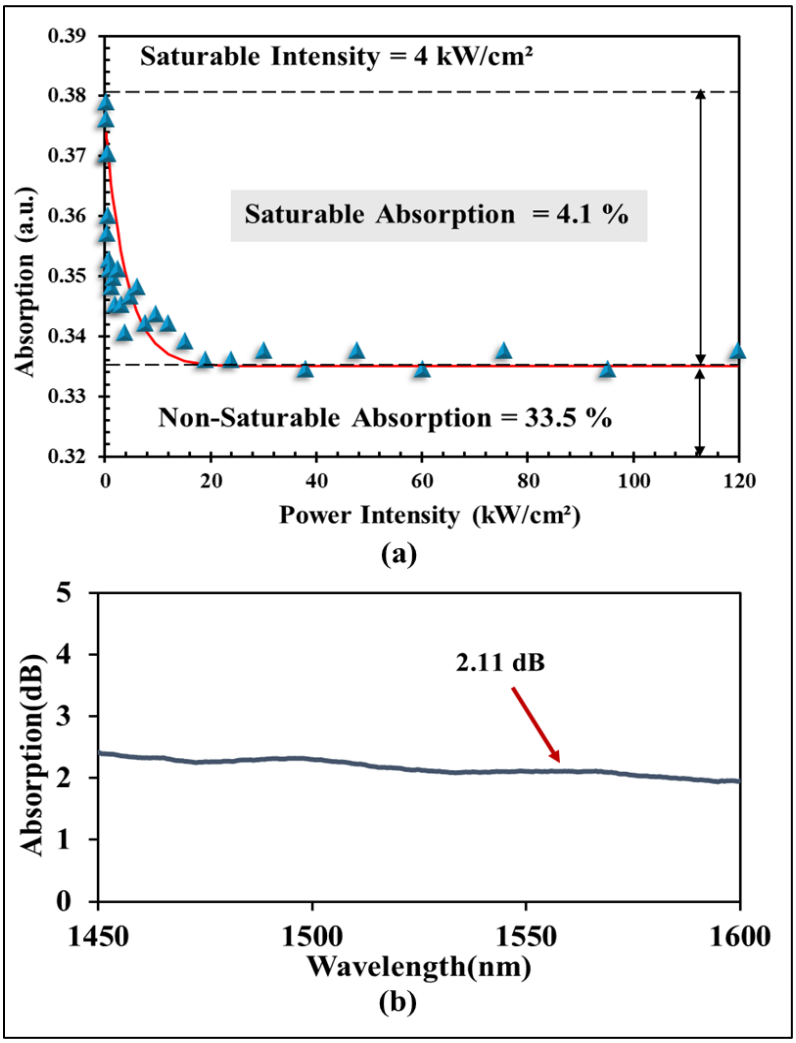


Figure 4.2 (a) Linear, and (b) Non-Linear Absorption Characteristics

4.3 Laser configuration

To evaluate the $CuAlO_2$ film's effectiveness as both a Q-switcher and mode-locker, an erbium-doped fiber laser (EDFL) cavity was constructed, as shown in Figure 4.3. A 980/1550 nm wavelength-division multiplexer (WDM) coupled a 980 nm pump laser diode (LD) into the cavity, with a maximum output power of 280.12 mW. The gain medium comprised 0.7 m of erbium-doped fiber (EDF), featuring an absorption coefficient of 68 dB/m at 980 nm and a group velocity dispersion (GVD) of –22.7

ps^2/km. A polarization-independent isolator ensured unidirectional light propagation, and laser output was extracted via the 10% port of a 10 dB coupler. For mode-locking operation, 100 m of single-mode silica fiber (GVD: –21.9 ps^2/km) was added, extending the total cavity length to approximately 102.7 m. The ring cavity consisted of 0.7 m EDF, 2 m of WDM fiber, and 100 m of single-mode fiber, operating in the anomalous dispersion regime with a total group delay dispersion of –2.28 ps^2. Pulse characteristics—including temporal profile, optical spectrum, and frequency spectrum—were analyzed using an autocorrelator, optical spectrum analyzer (OSA), and radiofrequency (RF) spectrum analyzer, respectively. A 350 MHz oscilloscope coupled with a 5 GHz photodetector (PD) was also used to monitor the pulse train.Although the measured saturation intensity (Isat) was obtained, no clear correlation between Isat and the pulse performance was observed. This suggests that other parameters such as modulation depth and non-saturable absorption may play a more significant role in determining the laser operation stability.

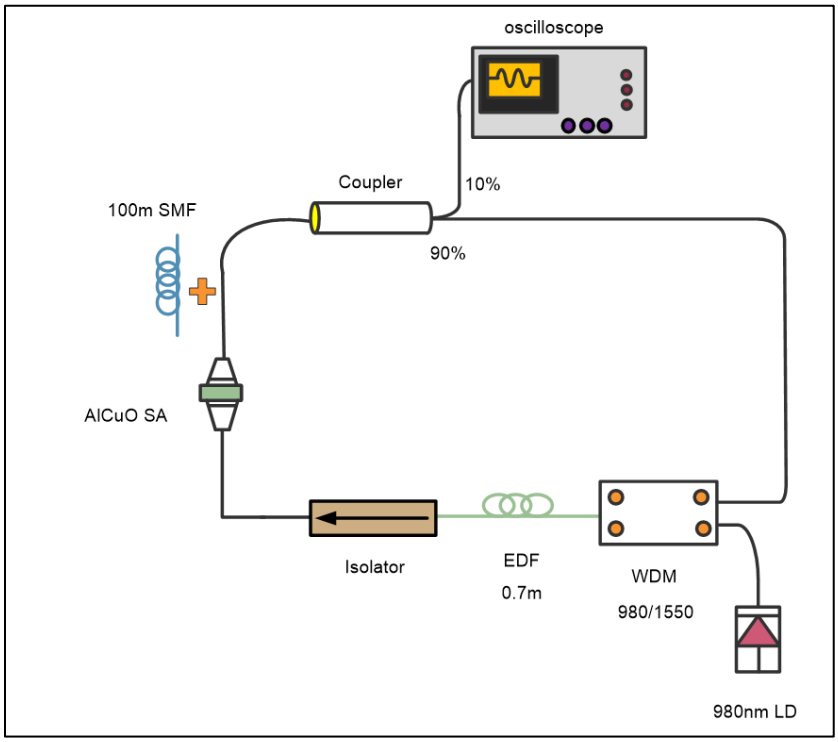


Figure 4.3 Schematic of the Proposed EDFL Incorporating A $CuAlO_2$ Film as a SA. an Additional 100 m Spool of Single-Mode Fiber was Included To Enable Mode-Locking Operation.

4.4 Q-switching performance

To evaluate the cavity's ability to generate pulses without the $CuAlO_2$-based SA, the film was initially removed. Across a wide range of pump powers, only continuous-wave operation was observed, with no indication of self-pulsing. Continuous-wave lasing commenced at a pump power of 72.14 mW. Upon reinserting the $CuAlO_2$-PVA film using a sandwich-structured ferrule platform, stable Q-switched pulses were achieved once the pump power reached 132.15 mW, and the Q-switching regime remained stable up to 210.62 mW. At 210.62 mW, the Q-switched laser produced a consistent pulse train with a 11.8 μs interval, corresponding to a repetition rate of 84.96 kHz, as shown in Figure 4.4 (a). The corresponding RF spectrum in Figure 4.4 (b) exhibits multiple harmonics, with a fundamental frequency at 84.96 kHz and a signal-to-noise ratio (SNR) of 57.8 dB, confirming the pulse stability. The discrepancy happens because of a classic rounding limitation on digital storage oscilloscopes. When the oscilloscope cursor measures a pulse interval of 11.8 μs, it is rounding the raw internal value to 3 significant figures. However, the internal hardware counter calculates the frequency directly from the unrounded time period.

The optical spectrum, displayed in Figure 4.4 (c), shows a central wavelength of 1563.3 nm. To further verify the stability of the $CuAlO_2$-based Q-switched EDFL, the output spectra were recorded over a 100-minute interval at 10-minute steps, as shown in Figure 4.4 (d). All spectra were consistent, maintaining a central wavelength of 1563.3 nm with a full-width half-maximum (FWHM) of 1.5 nm, confirming stable Q-switching performance. Notably, the setup operated without a polarization controller, as polarization adjustments had minimal influence on both the pulse train and spectral characteristics.

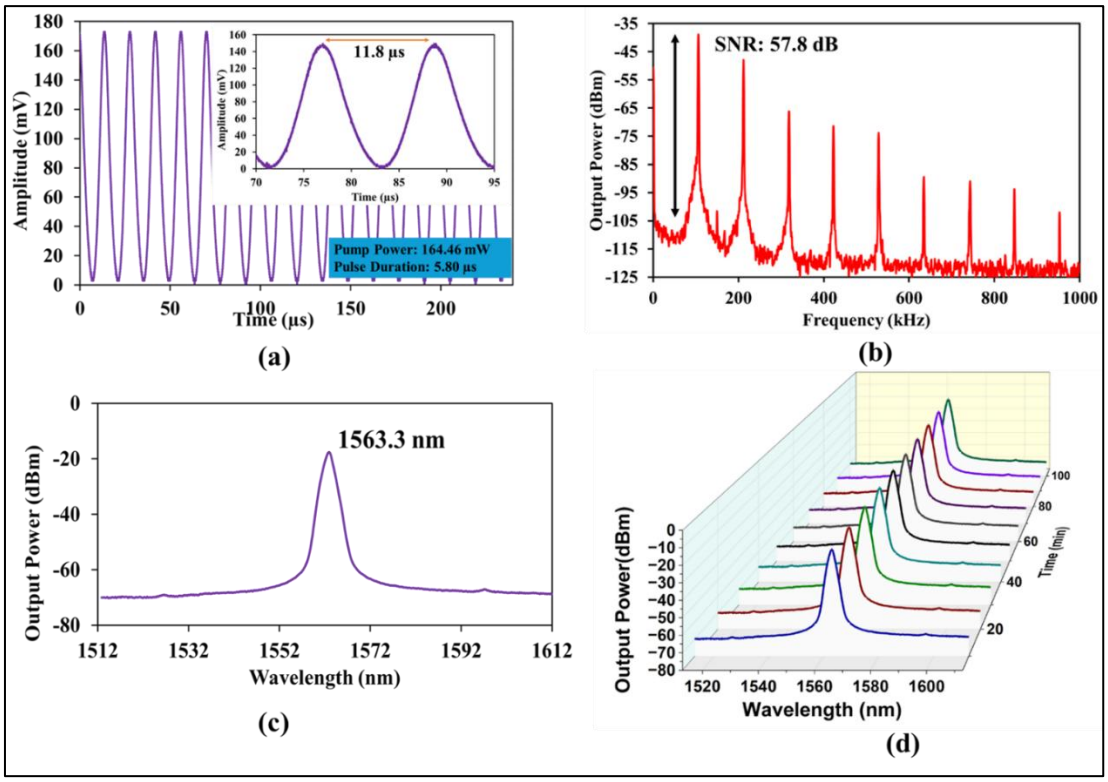


Figure 4.4 (a) Oscilloscope Trace, (b) RF Spectrum with a span of 1000 kHz, (c) Output Spectrum, and (d) Output Spectrum Measured Over Time.

Figure 4.5 summarizes the variation of laser performance with the change of pump power. Figure 4.5 (a) shows the average output power, and single-pulse energy against pump power. The Q-switching operation stayed stable as the pump power escalated from 132.15 mW to 210.62 mW, with the average output power rising nearly linearly from 1.94 mW to 3.7 mW. Higher pump power resulted in greater gain, leading to increased pulse energy due to faster accumulation of Q-switched pulses. The maximum single-pulse energy achieved was 43.55 nJ. Figure 4.5 (b) depicts the dependence of the pulse repetition rate and width on pumping strength. Unlike mode-locked fiber lasers, where the repetition rate is fixed by the cavity length, the repetition rate of Q-switched pulses varies with the saturation level of the SA. As a result, the repetition rate increased from 66.09 kHz to 84.96 kHz as the pump power rose from 132.15 mW to 210.62 mW. This increase in repetition rate is attributed to the SA's faster saturation under higher pump power. In addition to the measured slope efficiency of 1.95%, the rise in pump power enhanced the photon density growth rate, which governs the energy storage duration. This led to the formation of faster pulses and a corresponding increase in repetition rate. To comprehensively analyze the temporal

features of the Q-switched laser cavity, the evolution of pulse width and repetition rate was scrutinized as a function of incident pump power. Quantitatively, as the pump power escalated from 132.15 mW to 210.62 mW, a sharp contraction in the time-domain profile was observed, where the pulse width shrank from 6.31 μs down to 5.03 μs. This systematic reduction provides a compelling, textbook confirmation of a strict inversely proportional relationship dictated by passive Q-switching governing theory.

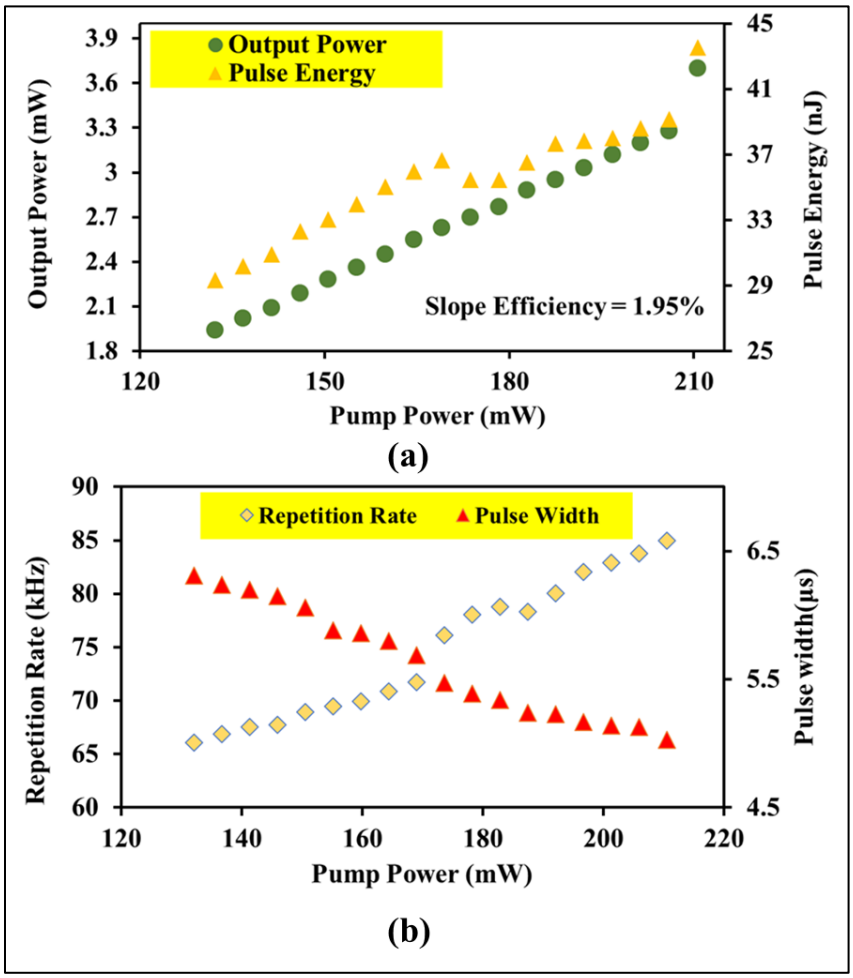


Figure 4.5 Q-Switched Laser Performance Showing (a) Output Power and Pulse Energy as Functions of Pump Power, and (b) Repetition Rate and Pulse Width Versus Pump Power.

A key metric dictating the operational efficiency of the passive Q-switched laser is its slope efficiency, which was graphically and mathematically evaluated to be 1.95% for the $CuAlO_2$-PVA saturable absorber configuration. While this value appears modest, it strictly reflects the complex, multi-variable interplay and balance between the total intra-cavity insertion losses introduced by the polymer film and the designated output

coupling ratio (90:10). The inclusion of a host matrix film inherently brings about non-saturable scattering losses, scattering at the fiber ferrule interfaces, and localized material absorption. Despite these loss channels, a steady slope efficiency of 1.95% indicates that the 10% output coupler successfully extracts a stable portion of coherent light without over-damping the cavity gain. This demonstrates that the insertion loss of the fabricated $CuAlO_2$ transducer is sufficiently optimized, preventing the laser from dropping below the threshold or suffering from severe thermal lensing, thereby preserving the structural integrity of the pulse-shaping mechanism during prolonged optical extraction.

The performance of the proposed $CuAlO_2$-based Q-switched fiber laser was benchmarked against recently reported passively Q-switched EDFLs employing various SA materials, as summarized in Table 4.1. The results show that the $CuAlO_2$-based SA delivers comparable performance to other reported materials, with a notably higher maximum repetition rate than most. Further optimization of the fiber cavity design and SA parameters is expected to yield even better Q-switching characteristics. Compared to alternative SAs such as graphene and other emerging 2D materials, $CuAlO_2$ offers several advantages, including ease of fabrication and robustness. Nonetheless, its optical damage threshold may be lower than that of ceramic-based materials such as MAX phases and MXenes.

Table 4.1
Performance Comparison Of Proposed $CuAlO_2$-Based Q-Switched EDFL With Other Works.

SA materials	**Mod. depth (%)**	**Wave-length (nm)**	**Max. Freq. (kHz)**	**Min. Pulse Width (µs)**	**Max. Pulse Energy (nJ)**	**Ref.**
Nano-diamond	15	1558	127.2	1.565	NA	[65]
Bi_2Te_3	4.1	1558.1	47.1	1.58	17.8	[66]
PAN	11.4	1572	66.1	2.43	52	[59]

SA materials	Mod. depth (%)	Wave-length (nm)	Max. Freq. (kHz)	Min. Pulse Width (µs)	Max. Pulse Energy (nJ)	Ref.
Graphene	NA	1522~1555	103	2	40	(Naidu, & Ahmad, 2025)
WS_2	2.1	1560	39.37	3.71	126.96	(Naidu, & Masruroh, 2025)
Bi_2Se_3	39.8	1560	68.2	2.4	47.1	(Hong, & Liu, 2020)
V_2AlC	NA	1559	53.55	2.54	57.14	(Omar, & Rosol, 2021)
MoAIB	10.4	1559	82.92	2.14	27.49	(70. Pang, &

						Jiang, 2025)
$CuAlO_2$	4.1	1563.3	84.96	5.03	43.55	This work

4.5 Mode-locking performance

The mode-locking mechanism, achieved by integrating 100 meters of SMF into the cavity, generates ultra-short optical pulses through the synchronization of longitudinal mode peaks via constructive interference. This approach not only ensures stable pulse generation but also results in high repetition rates and ultra-short pulse durations, leading to significantly higher peak power compared to other operating regimes, such as continuous-wave (CW) and Q-switching. The $CuAlO_2$ inserted into the EDFL cavity serves as a mode-locker, enabling the generation of picosecond pulses. In this experimental setup, a self-starting pulse sequence was observed at a threshold pump power of 141.38 mW, with stable mode-locking maintained up to the maximum pump power of 233.7 mW. Removing the $CuAlO_2$ SA from the cavity caused the system to transition from mode-locked operation back to CW emission.

Figure 4.6 (a) displays the relationship between average output power, pulse energy, and pump power. As the pump power was increased from 141.38 mW to 233.7 mW, the output power rose linearly from 1.11 mW to 2.42 mW, with a slope efficiency of 1.44%. Meanwhile, the pulse energy increased from 0.62 nJ to 1.35 nJ, as shown in Figure 4.6 (a). Both pulse energy and output power exhibited a consistent and proportional increase with rising pump power. The maximum achievable output power is limited by the available pump power. Employing higher pump powers is expected to result in greater output power and higher pulse energy. Pulse energy can also be further enhanced through several optimization strategies, such as tailoring the gain medium, extending the cavity length, and minimizing intracavity losses. The pulse energy is calculated by dividing the average output power by the corresponding repetition rate. Extending the optical cavity length lowers the repetition rate of the mode-locked laser, which in turn increases the pulse energy. Additionally, the output power can be improved by adjusting the output coupler ratio to enable more efficient extraction of intracavity energy.

Figure 4.6 (b) presents the autocorrelation trace of the mode-locked pulses, revealing a pulse width of 3.17 ps, determined using the sech² fitting method. The time-bandwidth product (TBP) is approximately 0.39, slightly exceeding the theoretical transform limit of 0.315, indicating minimal chirping in the output pulses. Figure 4.6 (c) displays the optical spectrum of the $CuAlO_2$-based mode-locked laser at a pump power of 141.38 mW. The mode-locked spectrum has a 3 dB bandwidth of 1 nm and a center wavelength of 1560 nm. In comparison to the Q-switched laser, the operating wavelength shifts to a shorter wavelength due to the longer cavity length. Finally, Fig. 7 (d) shows the mode-locked pulse train, which exhibits uniform pulse intensities and a consistent pulse interval of 555 ns over a time span of 12,000 µs. These results highlight the effectiveness of the $CuAlO_2$-based SA in achieving stable, high-performance mode-locked operation in the EDFL cavity.

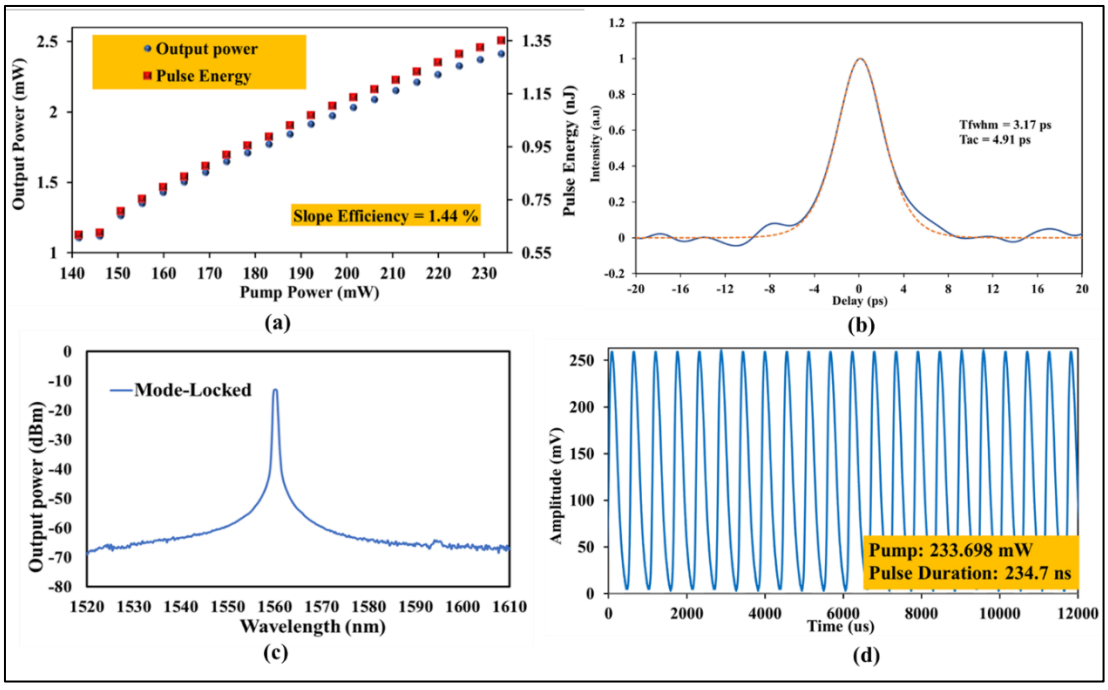


Figure 4.6 Analysis of Mode-Locked Laser Parameters (a) Output Power And Pulse Energy Versus Pump Power, (b) Autocorrelation Trace, (c) Output Spectrum, (d) Typical Oscilloscope Trace.

The correlation between peak power and pump power is illustrated in Figure 4.7 (a). The peak power reaches a maximum value of 5.07 kW at a 233.7 mW pumping, demonstrating the efficient energy conversion and high peak power capabilities of the mode-locked laser. The significance of achieving high peak power is particularly

relevant for applications such as dermatology and fiber laser-based cutting processes, where intense and precise energy delivery is critical. Figure 4.7 (b) displays the RF spectrum, measured over an 85 MHz span with a resolution bandwidth of 3 kHz. The fundamental repetition rate of 1.792 MHz corresponds precisely to the 555 ns temporal separation between consecutive pulses, highlighting the precise synchronization inherent to the mode-locking process. The signal-to-noise ratio (SNR) of the fundamental mode is measured at 71.75 dB, further confirming the exceptional stability of the mode-locked operation. To evaluate the stability of the mode-locked operation, the optical spectrum was recorded at 10-minute intervals over a 100-minute duration, as shown in Figure 4.7 (c). The spectral shape, intensity, and bandwidth remained unchanged throughout the measurement, confirming excellent long-term stability. Moreover, consistent results were reproduced in repeated experiments over a two-week period, indicating that the proposed $CuAlO_2$-based mode-locked EDFL offers high repeatability and durability. The long-term operating stability and amplitude consistency of the pulse train were verified via radio-frequency (RF) spectral analysis. The laser exhibited a remarkably pristine fundamental frequency peak with a record-high Signal-to-Noise Ratio (SNR) of 71.75 dB (and 71.70 dB for the Cr_2GaC configuration). To contextualize this value mathematically, an SNR of ~72 dB signifies that any parasitic pulse fluctuations, amplitude modulations, or background electronic noise are strictly suppressed by a factor of over 10^7 (ten million times) relative to the fundamental carrier peak power.

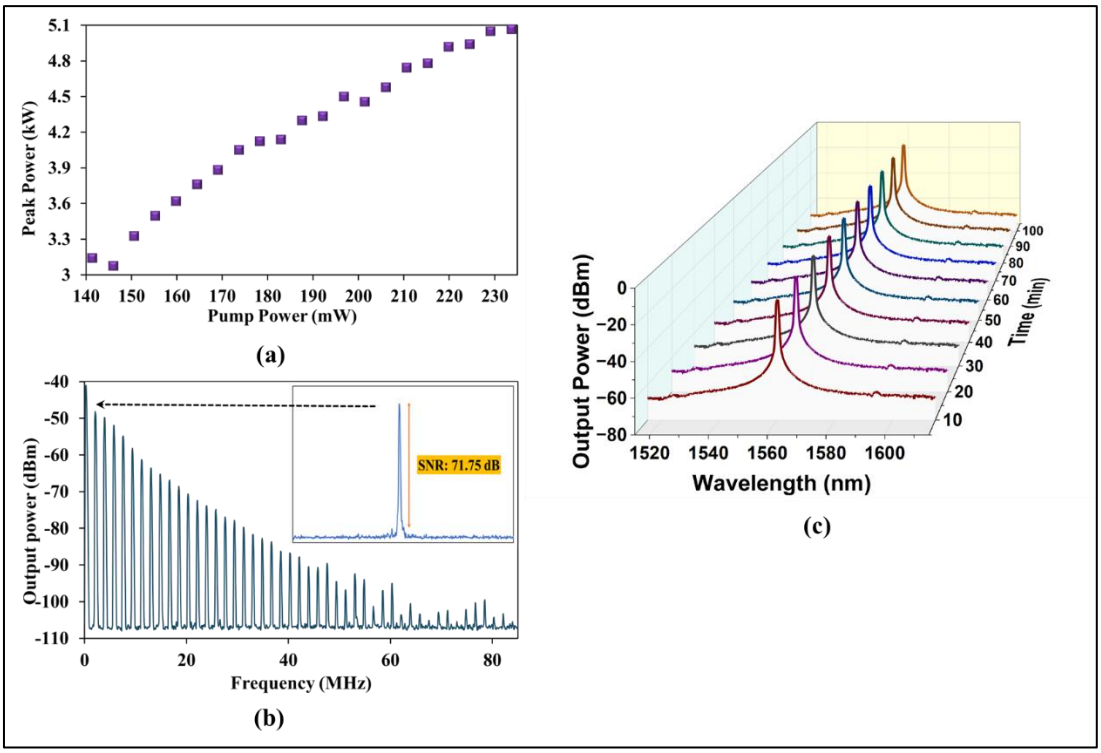


Figure 4.7 (a) Variation of Peak Power With Pump Power, (b) Corresponding RF Spectrum at 233.7 mW. Inset Highlights The Fundamental Mode Featuring an SNR of 71.75 dB, and (c) Stability Test Result.

Table 4.2 presents the key parameters obtained in this study, offering a comparative overview of mode-locked operations using different SAs. The $CuAlO_2$-based SA shows performance on par with others, particularly in terms of pump duration and SNR. These results underscore the reliability and effectiveness of the $CuAlO_2$-based SA in achieving stable and high-performance mode-locked operation in the EDFL cavity.

Table 4.2
Performance Comparison of Proposed $CuAlO_2$-Based Mode-Locked Lasers With Other Works.

Materials	**Pump Power (mW)**	**Wave-length (nm)**	**Rep. Rate (MHz)**	**Pulse width**	**OPM (mW)**	**SNR (dB)**	**Ref**
SESAM	302	1561.0	5 GHz	3.86 ps	1.37	62.1	**(Czyzyk. 2018).**
Graphene	45-83	1559.2	15.96	0.589 ps	NA	74	**(Paschotta, R. ,2008).**
Carbon Nanotubes	280	1563.2	26.79	73 ps	NA	62	**(Popa, D., Sun, 2011)**
PANI	113 - 155	1530.8	0.962	228 ns	2.1 – 3.1	66.3	**(Liu, & Xu, 2024)**
PAN	87.2 – 254.1	1568.4	1.781	3.46 ps	0.75 – 3.63	78.89	**(Razak & Abdul Latiff, 2017)**
FePc	118.5 – 149.8	1531.2	0.9681	2.1 ps	2.75 – 3.53	66.17	**(Liu, & Zhang, 2011)**
Ta_2AlC	95.2 – 210.62	1561.7	1.866	3.80 ps	9.38 – 21.01	70	**(**Ren, & Wang, 2015)

$CuAlO_2$	141.38 – 233.7	1560	1.792	3.17 ps	1.11 – 2.42	71.75	**This work**

4.6 Chapter summary

By integrating a developed CuAlO2-based SA into an EDFL cavity, stable Q-switched and mode-locked pulse generation was successfully demonstrated. The SA, fabricated by integrating a conductive oxide material with a polymer matrix to form a composite film, was positioned between two fiber ferrules, seamlessly integrating into the laser cavity. In the Q-switched regime, stable pulse generation was achieved at a wavelength of 1563.3 nm, with pump powers ranging from 132.15 mW to 210.62 mW. The maximum repetition rate reached 43.55 kHz, with a minimum pulse width of 5.03 µs and a SNR of 57.8 dB. In the mode-locked regime, the CuAlO2-based SA facilitated the production of ultrashort pulses at a central wavelength of 1560 nm, with a repetition rate of 1.792 MHz. The pump power ranged from 141.38 mW to a maximum of 233.7 mW, yielding pulses with a width of 3.17 ps and an SNR of 71.75 dB. At the maximum pump power of 233.7 mW, the laser delivered pulses with an energy of 1.35 nJ and a peak power of 5.07 kW. These results highlight the exceptional performance and versatility of the $CuAlO_2$-based SA, demonstrating its potential as a robust pulse transducer in in fiber laser systems.

$CuAlO_2$-based SA has relatively high minimum pulse width and high pulse energy in Q-switch experiment. $CuAlO_2$-based SA has much lower pulse width second only to FePc on bright pulse mode-locking experiment suggesting that CuAlO2-based SA good for generating pulse laser for scientific application.

CHAPTER 5
RESULTS AND DISCUSSION II: CHROMIUM GALIUM CARBIDE–BASED Q-SWITCHING AND MODE-LOCKING

5.1 Introduction

In recent years, MXenes have attracted considerable attention due to their outstanding optical and electronic properties [75]. Owing to their high electrical conductivity and tunable electro-optical characteristics, MXenes have been reported to exhibit strong nonlinear optical absorption, making them promising candidates for ultrafast pulse generation. For instance, a stable mode-locked laser was demonstrated using a MXene-based saturable absorber (SA) fabricated via optical deposition of $Ti_3C_2T_x$ onto a microfiber [76]. The reported device exhibited a modulation depth of 11.3% and generated 597.8 fs pulses in an erbium-doped fiber laser (EDFL) oscillator.

Inspired by the success of MXenes, increasing research attention has been directed toward MAX-phase materials, which act as the parent compounds of MXenes. MAX-phase materials are generally described by the chemical formula $M_{n+1}AX_n$, where M represents a transition metal (e.g., Mo, Cr, Ta, Nb, V, Hf, Zr, Ti, Sc), X denotes carbon and/or nitrogen (with n = 1, 2, or 3), and A corresponds to a group III–VI element such as Al, Ga, Si, Ge, Sn, P, or As (Shakaty, A. A., Hmood, 2022). These materials possess a distinctive layered atomic structure characterized by a combination of metallic–covalent and ionic bonding. As a result, MAX phases exhibit a unique synergy of metallic and ceramic properties, including high electrical and thermal conductivity, good damage tolerance, and high-temperature and oxidation resistance [78]. Such attributes are particularly advantageous for laser and photonic applications. Notably, MAX-phase Ti_3AlC_2 has recently been reported as an effective saturable absorber for mode-locked pulse generation (Shiner, B. 2016).

In this chapter, Q-switched and mode-locked pulse generations in an erbium-doped fiber laser (EDFL) cavity are demonstrated using a novel saturable absorber (SA) based on chromium gallium carbide (Cr_2GaC). As described in Chapter 3, the SA thin film was fabricated by embedding Cr_2GaC within a polyvinyl alcohol (PVA) host matrix. Upon integration into the laser cavity, stable Q-switched pulses were generated while stable mode-locking was achieved by incorporating an extended length of single-

mode fiber (SMF) to establish an appropriate balance between dispersion and nonlinear effects. The performance characteristics of the generated Q-switched and mode-locked pulses are systematically analyzed and discussed in this chapter.

5.2 Characteristics of the Cr_2GaC film.

As described in Chapter 3, the Cr_2GaC-based SA film was synthesized using a wet chemical approach, with film formation achieved via the solution-casting method. This fabrication technique offers advantages such as simplicity, cost-effectiveness, versatility, and precise control over the nonlinear optical properties of the material, making it well suited for laser and photonic research applications. In addition, the resulting SA film can be readily integrated into fiber laser cavities. An actual photograph of the Cr_2GaC film transducer, with an approximate thickness of 50 μm, is shown in Figure 5.1(a). A small section of the film, measuring approximately 1 mm × 1 mm, was cut and placed onto the end face of a fiber ferrule, as illustrated in Figure 5.1(b). The SA device was then completed by coupling it with a second clean ferrule, forming a fiber-compatible transducer as depicted in Figure 5.1(c).

The Cr_2GaC film SA was examined for its surface morphology through field emission scanning electron microscopy (FESEM) (ZEISS, Model: MERLIN). Figure 5.1 (d) exhibits the FESEM image at 10-k magnification, revealing the random dispersion of Cr_2GaC compounds within the host polymer composite. Subsequently, Figure 5.1 (e) introduces its elemental composition after identification through energy-dispersive X-ray spectroscopy (EDS) where it shows the presence of carbon (C), chromium (Cr), and gallium (Ga), which coincides with the element proportion in Cr_2GaC with the acquired spectrum of 32.81 weight %, 32.20 weight % and 25.22 weight % respectively. The presence of oxygen (O) at 9.76 weight % comes from the PVA polymer.The Cr2GaC film SA was could not undergo XRD analysis as the equipment were broke down during that time.

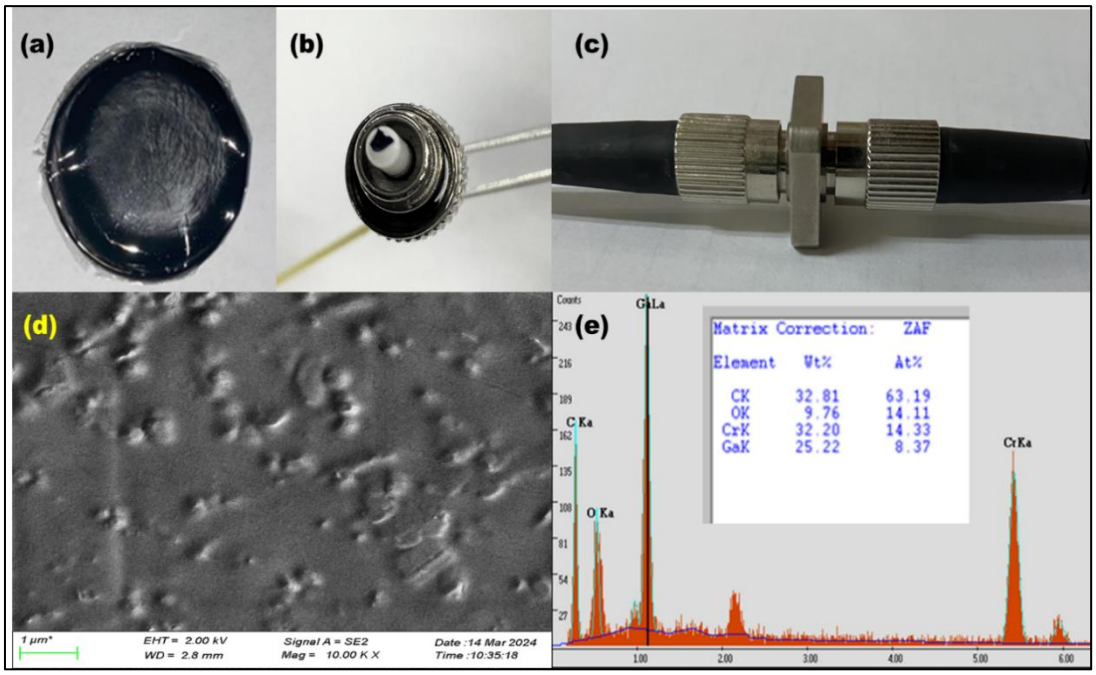


Figure 5.1 (a) Real Image of Cr_2GaC Film Transducer, (b) The Integration of Cr_2GaC Film Onto The Tip of Fiber Ferrule, (c) Cr_2GaC Transducer Mechanism, (d) Its Corresponding FESEM Image, and (e) EDX Analysis Results

The Cr_2GaC film transducer was further investigated for its optical characteristics with linear and nonlinear absorption analysis. The linear absorption setup consists of a white light source connected to an optical spectrum analyzer (OSA). This setup measures absorption over a wide wavelength range, approximately 600 to 1700 nm. By comparing the output of a reference single-mode fiber (SMF) without the Cr_2GaC film to the output with the film inserted, the difference is measured to determine the linear absorption. Figure 5.2 (a) illustrates that the Cr_2GaC SA demonstrated a nearly uniform linear absorption of 5.75 dB at an operating wavelength from 1529.6 nm to 1531.6 nm. Conversely, the nonlinear characteristics were assessed through the balanced twin detector method, utilizing a custom-built mode-locked fiber laser as the pump source. This laser operated at a wavelength of 1568 nm, with a frequency of 1.778 MHz and a pulse width of 4.32 ps. The acquired power-dependent absorption measurements were analyzed using the saturation model formula (Eq. 3.1). From the fitted data, key parameters such as modulation depth (5.7%), non-saturable absorption (60.4%), and saturation intensity (100 MW/cm²) of Cr_2GaC transducer were determined. Figure 5.2 (b) provides a graphical representation of its absorption profile.

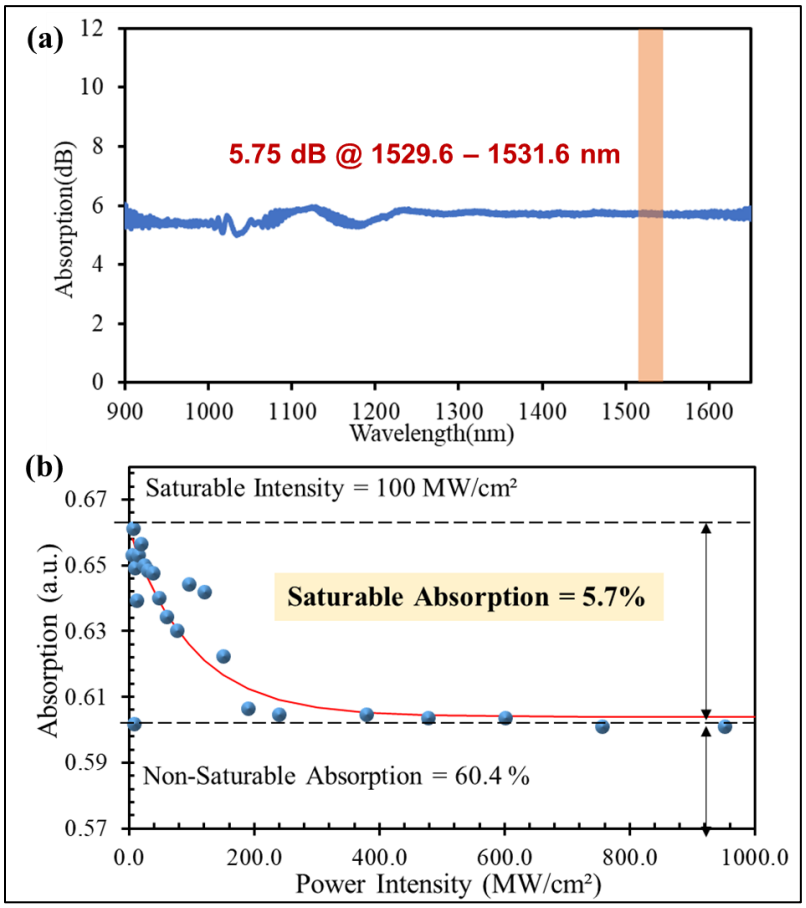


Figure 5.2 Optical Characterization of Cr_2GaC Film Transducer (a) Linear Absorption, (b) Nonlinear Absorption.

5.3 Laser configuration.

Based on the nonlinear absorption measurement, the Cr_2GaC SA has a sufficient modulation depth to introduce a self-amplitude modulation in the EDFL cavity at 1560 nm region. This intensity-dependent loss modulation is exploited in this study to generate a stable pulse train in this spectral region through passive Q-switching and mode-locking mechanisms. Accordingly, the fabricated Cr_2GaC SA was incorporated into a ring-shaped EDFL cavity to function as a Q-switcher or mode-locker, as illustrated in Figure 5.3. The EDFL cavity was constructed entirely from single-mode fiber components, resulting in a compact, robust, and alignment-free laser system.

The cavity gain mechanism in this system is facilitated by a fiber amplifier comprising a 1.8-meter-long Erbium-doped fiber (EDF), co-pumped by a 980 nm pump laser diode. Lasing initiation is achieved by directing 980 nm photons into the EDF through a wavelength division multiplexer (WDM). The EDF used in this setup features a numerical aperture of 0.16, a core diameter of 4 μm, and exhibits Erbium ion

absorption of 23 dB/m at 980 nm. To ensure unidirectional propagation, a polarization-independent optical isolator is integrated into the cavity configuration.

To tap out the oscillating laser, an 80:20 coupler was integrated between the SA device and WDM coupler. This configuration ensures that 20% of the signal is directed towards the output, while 80% serves as feedback within the EDFL cavity. For spectral performance analysis, an optical spectrum analyzer (OSA) with high precision (ANRITSU: MS9710C) was employed, operating with a resolution of 0.05 nm. Temporal analysis was conducted using a digital storage oscilloscope boasting a bandwidth of 350 MHz (GWINSTEK: GDS-3352), complemented by a fast photodetector featuring a bandwidth of 1.2 GHz (THORLABS: DET01CFC). The photodetector was further interfaced with an electrical spectrum analyzer (ANRITSU: MS2683A) to monitor the frequency spectrum. To measure the average output power accurately, an optical power meter was employed.

With the current configuration, the laser operates in the Q-switching regime with a cavity length of 5.3 m. For mode-locking operation, a 100 m spool of single-mode fiber (SMF) was incorporated into the cavity to extend the cavity length, manage dispersion, and enhance nonlinear effects. The SMF spool was inserted between the SA device and the output coupler. As a result, the complete mode-locked laser cavity has a total length of 105.3 m, consisting of 0.5 m of WDM fiber, 1.8 m of erbium-doped fiber (EDF), and 103 m of SMF. The net cavity dispersion was calculated to be approximately $-2.2\ ps^2$, ensuring that the EDFL operates in the anomalous dispersion regime. Furthermore, an autocorrelator was employed in the experimental setup to enable detailed characterization of the pulse width.

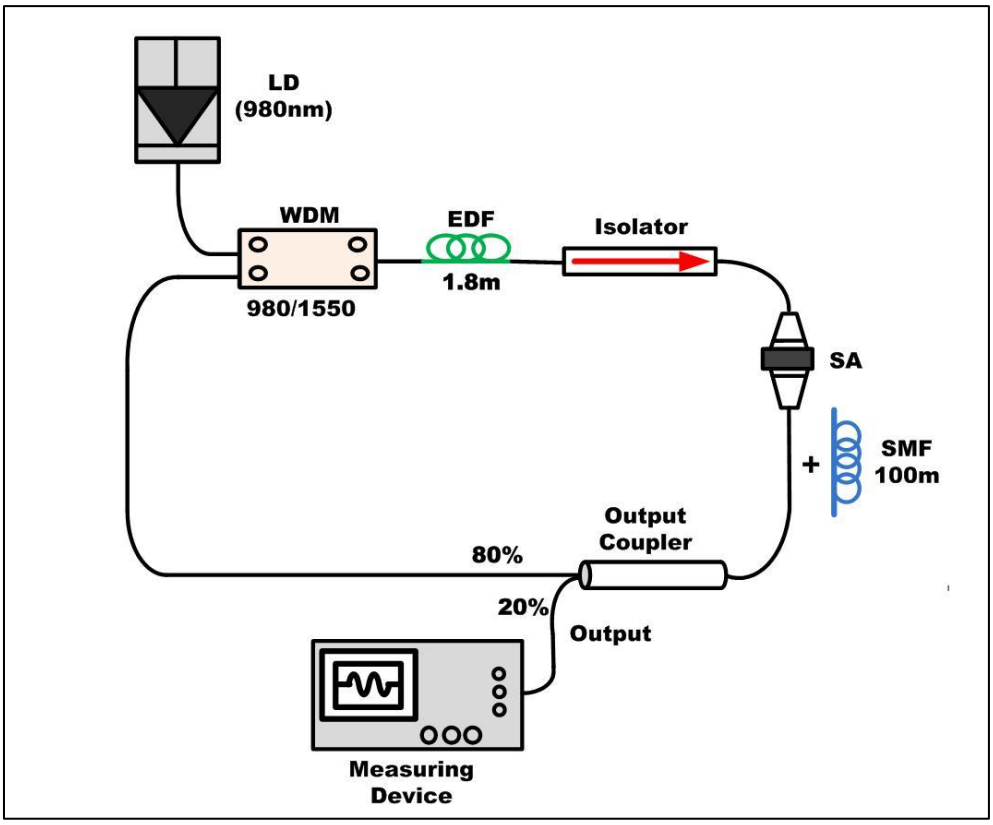


Figure 5.3 Schematic Representation of the EDFL Employing a Cr_2GaC SA. A 100-Meter-Long SMF is also Inserted Between the SA and Coupler To Effectively Manage Dispersion and Enhance Nonlinear Effects, Crucial for Achieving Mode-Locking.

5.4 Q-switching performance with Cr_2GaC SA

This section reports the generation of Q-switched pulses from an EDFL employing a newly developed Cr_2GaC–based SA. As described in Chapter 3, the SA film was fabricated by embedding Cr_2GaC within a PVA host matrix. Upon integration into the EDFL cavity, stable Q-switched operation was successfully achieved over a pump power range of 25.98 to 53.67 mW.

Q-switched laser emission commenced once the pump power exceeded 49.06 mW, marking the threshold for stable pulsed operation. At this threshold, the average output power was measured to be 0.83 mW. As the pump power was gradually increased to 53.67 mW, the Q-switched regime remained highly stable. Figures 5.4(a–c) illustrate the temporal pulse trains obtained at pump powers of 49.06, 62.91, and 72.14 mW. The measured pulse intervals are 15.3, 13.5, and 12.9 µs, corresponding to repetition rates of 65.1, 74.0, and 76.9 kHz, respectively. At the same time, the pulse duration exhibits a monotonic reduction, decreasing from 4.82 µs to 4.12 µs and further to 3.75 µs with

increasing pump power. This trend indicates that higher pump powers facilitate greater energy accumulation in the gain medium, resulting in increased repetition rates and shorter pulse durations. The uniform pulse amplitudes observed across the investigated pump powers further confirm the efficiency and stability of the Q-switching mechanism.

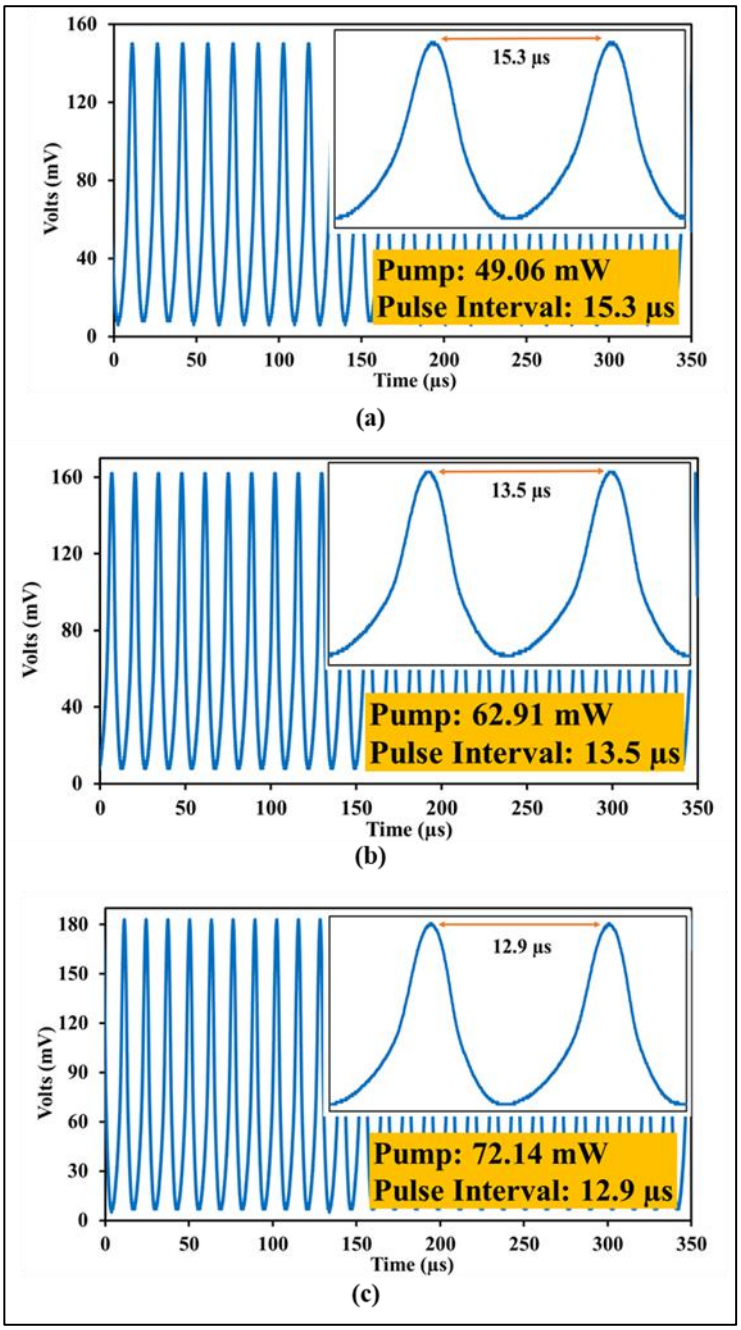
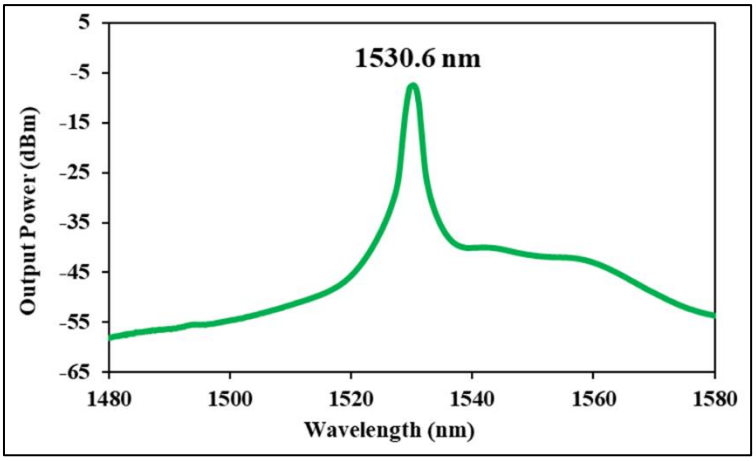
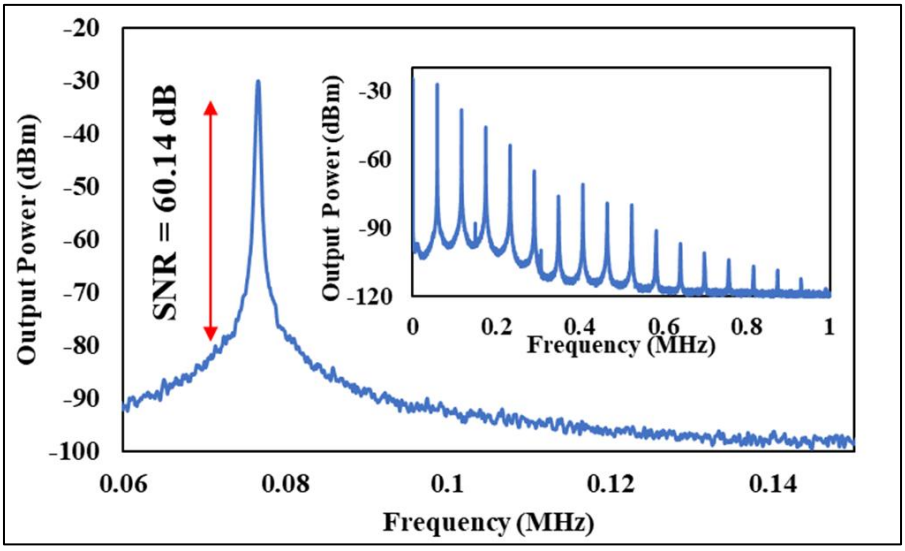


Figure 5.4 Q-Switched Pulse Trains Recorded at Pump Powers of (a) 49.06 mW, (b) 62.91 mW, and (c) 72.14 mW.

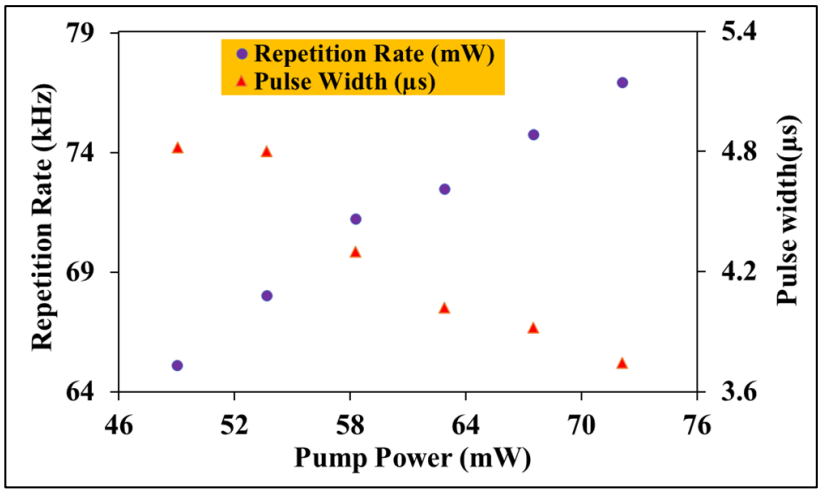
The spectral characteristics of the Q-switched pulses are shown in Figure 5.5(a). The laser operated at a central wavelength of 1530.6 nm with a 3-dB bandwidth of 1.8 nm. The absence of noticeable chirping within the spectral profile suggests effective suppression of intracavity disturbances. Temporal stability was further evaluated through radio frequency (RF) spectral analysis at a pump power of 72.14 mW, as depicted in Figure 5.5(b). A fundamental repetition frequency of 76.9 kHz was observed with a signal-to-noise ratio (SNR) exceeding 60 dB, confirming the excellent stability of the Q-switched operation.



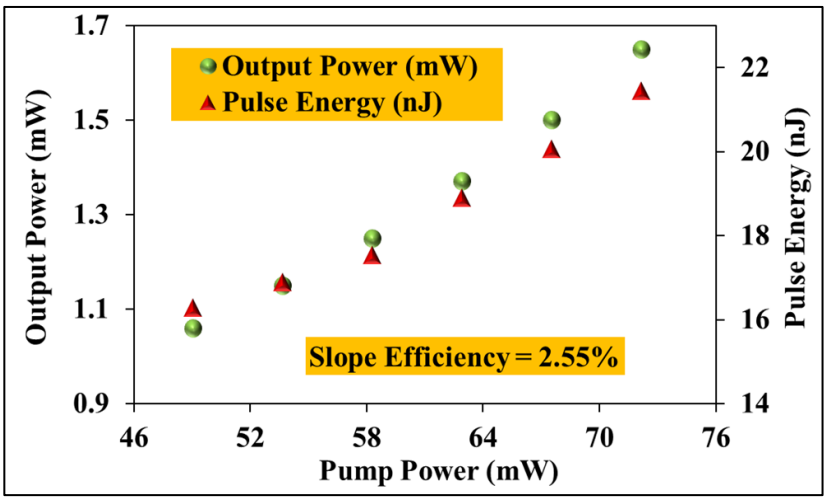
(a)



(b)



(c)



(d)

Figure 5.5 Performance Characteristics of the Q-switched EDFL: (a) Optical Spectrum, (b) RF Spectrum, (c) Dependence of Pulse Width and Repetition Rate on Pump Power, and (d) Output Power and Pulse Energy as Functions of Pump Power.

Figure 5.5(c) illustrates the evolution of pulse width and repetition rate as functions of pump power. As the pump power increased from 49.06 to 72.14 mW, the pulse width steadily decreased from 4.82 to 3.75 μs, while the repetition rate increased linearly from 65.1 to 76.9 kHz. This inverse relationship between pulse duration and repetition rate is a characteristic feature of Q-switched laser behavior. Additionally, Figure 5.5(d) shows the corresponding variations in average output power and pulse energy. The output power increased linearly from 1.06 to 1.65 mW, yielding a slope efficiency of approximately 2.55%, while the pulse energy rose from 16.28 to 21.45 nJ.

When the pump power exceeded 72.14 mW, the Q-switched regime transitioned into continuous-wave (CW) operation. This behavior is attributed to the Cr_2GaC-based SA reaching a fully saturated state, where it becomes transparent to the circulating intracavity light and can no longer support pulse modulation. Notably, reducing the pump power back to 72.14 mW immediately restored stable Q-switching, indicating that the SA suffered no permanent damage. This observation suggests that the damage threshold of the Cr_2GaC SA exceeds the maximum available pump power of 210 mW. Furthermore, the laser emission spectrum remained stable over a continuous 2-hour monitoring period, demonstrating the robustness and reliability of the Q-switched EDFL under laboratory operating conditions.

Figure 5.6 illustrates the stability of the output spectrum as it was measured within 60 minutes, with the central wavelength remaining fixed at 1530.6 nm. The spectral profile was consistently preserved as the pump power increased from 49.06 to 72.14 mW. Such spectral stability is essential for applications requiring high pulse precision, such as spectroscopy. Notably, the 3 dB bandwidth of the output spectrum remained constant at 1.8 nm across all investigated pump power levels, further confirming the robustness of the laser operation.

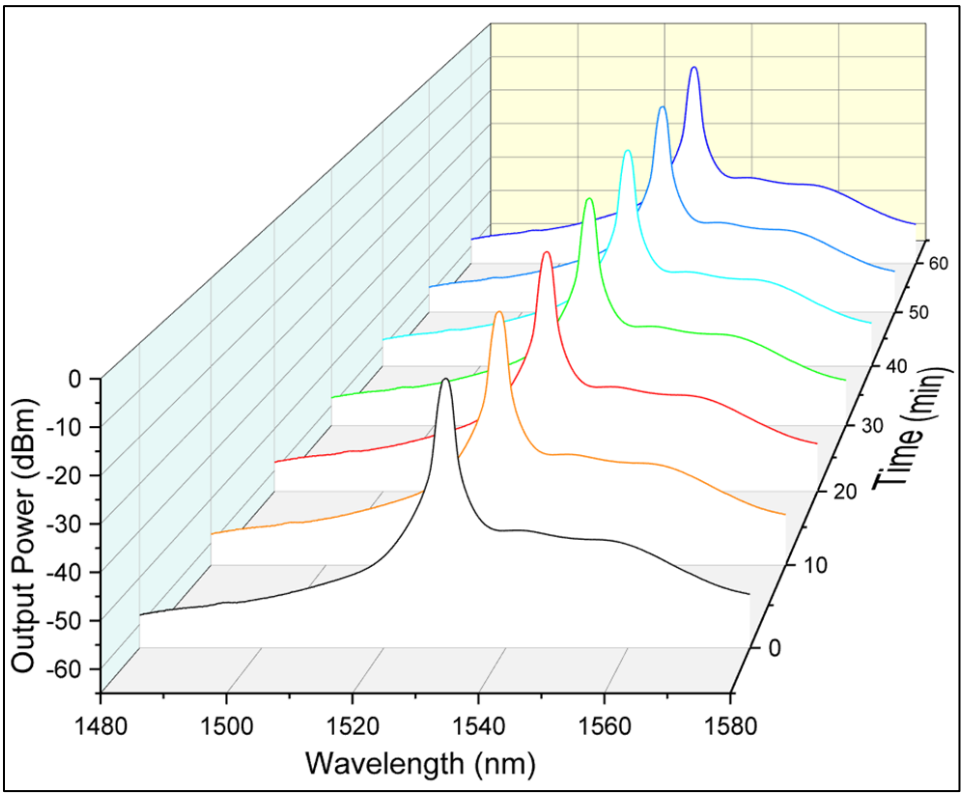


Figure 5.6 Output Spectrum Stability Monitored Over A 60-Minute Duration.

Table 5.1 summarizes the key performance metrics of various SAs employed for Q-switched pulse generation. These parameters are essential for evaluating the efficiency and suitability of each SA for specific applications. The Q-switched EDFL incorporating the Cr_2GaC SA demonstrates performance that is comparable to other SA-based systems reported in the literature. Notably, the Cr_2GaC-based Q-switched laser operates in the shorter wavelength region of around 1530 nm compared with the other materials listed in Table 5.1. When compared with a previously reported $CuAlO_2$-based Q-switched fiber laser, the present system exhibits operation at a shorter wavelength, along with a lower Q-switching threshold and a shorter pulse duration. However, the earlier work achieved a higher pulse energy, which can be attributed to the larger cavity loss introduced by the Cr_2GaC film in the current configuration.

Table 5.1
Comparison Of Q-Switched Laser Performance Using The Cr_2GaC SA With Other Reported SAs.

Material	Pump Power (mW)	Wave-length (nm)	Rep. Rate (kHz)	Pulse Width (μs)	Output Power (mW)	SNR (dB)	Ref.
Nano diamond	59–187	1558	77.84–127.2	4.24–1.565	–	73	(Milani, 2015)
PAN-PVA	113.3–175.9	1572	50–66.1	4.04–2.43	0.7–3.47	66.1	(Liu, &., Wang, 2018)
$CaCO_3$	180–270	1561	12.67–21.3	35.27–18.74	–	25	(Silvestroni, & Melandri, 2021)
PAN powder	61.1–155.0	1560	33.39–45.35	8.55–6.42	3.6–10.9	66.06	(S. P., & Singh, 2007)
$MnMoO_4$	28–312.5	1559.14	24.98–88.11	15.22–2.35	0.128–2.95	–	(Song, X., Diblawe, 2024)
Cr_2GaC	49.06 – 72.14	1530.6	65.1 – 76.92	4.82 – 3.75	1.06 – 1.65	60.14	This work

5.5 Mode-locking performance with Cr_2GaC SA

Mode-locking is a well-established technique for generating ultrashort laser pulses and has been widely applied in areas such as biochemistry, material micro-processing, optical communications, and metrology, owing to its excellent stability, high peak power, and ultrashort pulse duration. Mode-locking can be implemented through either active or passive approaches. Compared with conventional active mode-locking, the passive technique is generally preferred due to its self-starting capability, simpler cavity design, and enhanced environmental stability, with the SA serving as the key

enabling component. Passive mode-locking using an SA allows the generation of significantly shorter pulses, as the ultrafast recovery time of the SA induces rapid intracavity loss modulation.

In the previous chapter, passive mode-locked laser operation has been demonstrated using a conductive oxide–based SA composed of $CuAlO_2$. In this section, we employ a MAX-phase material, Cr_2GaC—where Cr is the transition metal, Ga is the group element, and carbon acts as the non-metallic component—as a SA to achieve mode-locking in an EDFL. Commercial Cr_2GaC powder was dispersed into a polymer solution to fabricate a thin-film SA via a solution-casting method. The resulting film was subsequently integrated into a ring EDFL cavity to function as the mode-locker. To the best of our knowledge, this work represents the first demonstration of passive mode-locking in an EDFL using a MAX-phase Cr_2GaC SA.

Initially, the Cr_2GaC SA was temporarily removed from the laser cavity configured with additional 100 m long SMF and replaced with a pure PVA film of comparable thickness. Under pump power exceeding 32 mW, the laser generated a continuous wave (CW) output at 1561.1 nm, as illustrated in Figure 5.7 (a). Despite extensive adjustments to the pump power levels, no pulse operation occurred with the PVA film. The absence of self-mode-locking or Q-switched phenomena indicated the PVA film's inability to induce such effects. Subsequently, upon reintroducing the Cr_2GaC thin film into the laser cavity, stable mode-locked operation was achieved with a threshold power of 53.7 mW. This unequivocally demonstrated that the mode-locking effect was solely attributed to the presence of the Cr_2GaC material. The unique properties of Cr_2GaC, including a substantial modulation depth, underscored its effectiveness as a mode-locker. The Cr_2GaC film exhibited selective transmission characteristics, allowing high-intensity modes to pass through while effectively filtering out low-intensity modes. Through successive rounds of light propagation, low-intensity modes were efficiently filtered, while high-intensity modes became phase-locked, culminating in the formation of picosecond pulses within the cavity. Remarkably, mode-locked operation persisted as the pump power was increased up to 95.2 mW. However, an intriguing observation emerged as the pumping strength surpassed this threshold: the mode-locked pulses ceased to manifest.

The output spectrum of the pulses at a pump power of 95.2 mW is depicted in Figure 5.7 (a). Operating at a center wavelength of 1558.2 nm, the spectrum exhibits a blue shift compared to the CW laser operating under similar pump power conditions.

This shift is attributed to increased thin film loss resulting from the doping of Cr_2GaC compounds. As a consequence, the laser's operation shifts to a shorter wavelength, where higher gain compensates for the increased loss. Furthermore, the optical spectrum reveals characteristics of soliton pulses, including Kelly sidebands. This observation indicates the generation of solitons within the anomalous dispersion cavity. The formation of soliton pulses arises from the intricate interplay among various factors, including the total laser gain and loss, nonlinear optical effects, cavity dispersion, and the saturable absorption effect induced by the SA. Moreover, pulse broadening is observed with the SA film due to the self-phase modulation effect within the laser resonator. This effect contributes to the temporal evolution of the pulses, influencing their duration and spectral characteristics.

The pulse train captured in Figure 5.7 (b) reveals a distinct pulse interval of 540 ns, which can be translated to a pulse rate of 1.82 MHz. This recorded pulse interval matches well with the cavity length highlights the laser's stable mode-locked state, a crucial aspect of its operational reliability. Figure 5.7 (c) offers a glimpse into the frequency spectrum of the laser, obtained across a 100 MHz span with a spatial resolution of 3 kHz. The high signal-to-noise ratio (SNR) of 71.7 dB recorded for the fundamental frequency serves as compelling evidence of the robust stability inherent in the mode-locked operation. The pulse durations depicted in Figure 5.7 (b) appear to exceed hundred nanoseconds, attributed to the resolution limitations of the oscilloscope. Consequently, an autocorrelator was employed to accurately measure the actual pulse duration.

Figure 5.7 (d) presents the measured autocorrelation trace of the generated soliton pulses, revealing a pulse duration of 3.04 ps. The corresponding time–bandwidth product (TBP) was evaluated using:

$$\mathrm{TBP}=\frac{\tau_{\mathrm{FWHM}}\times\lambda_{3\mathrm{dB}}}{\lambda^2}\mathrm{c} \tag{5.1}$$

where τ_{FWHM} denotes the pulse width, λ_{3dB} is the 3 dB spectral bandwidth, c is the speed of light in vacuum, and λ represents the central operating wavelength. The calculated TBP is 0.902, which is considerably larger than the transform-limited value of 0.315 for a sech² pulse, indicating that the output pulses are chirped—a behavior commonly encountered in mode-locked laser systems.

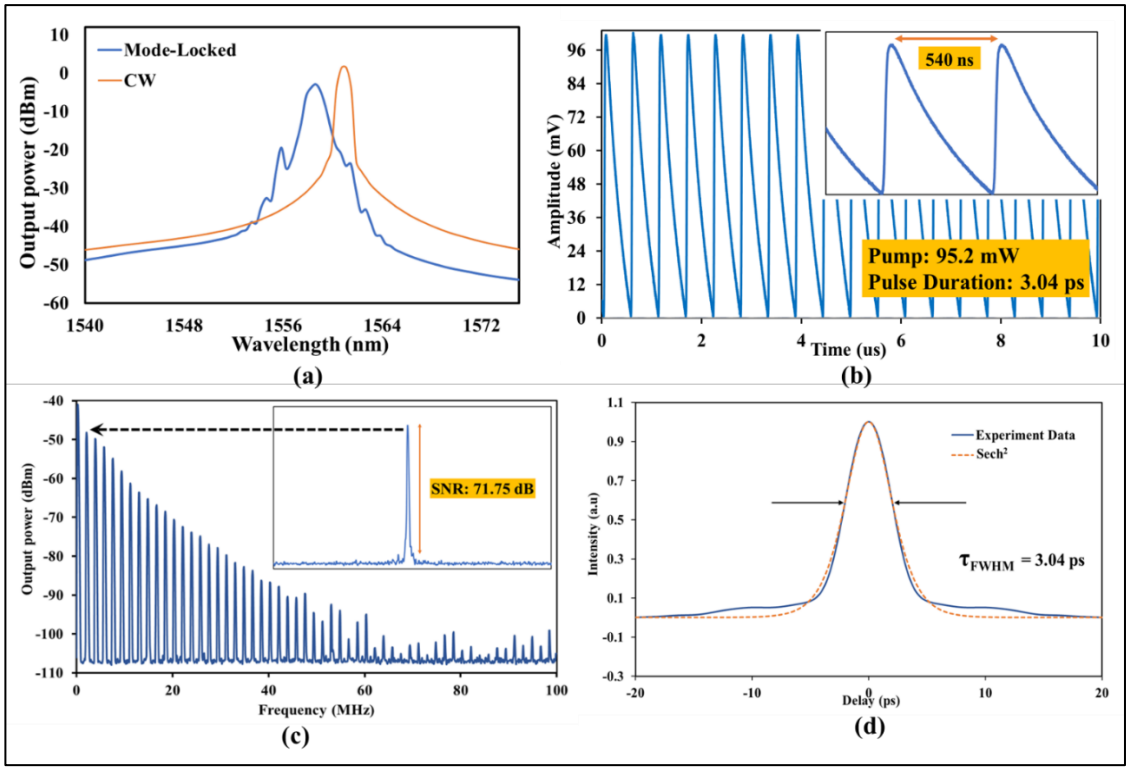


Figure 5.7 (a) Output Spectrum, (b) Typical Pulse Train. Inset shows the Envelope of Two-Pulse. (c) RF Spectrum. Inset displays the Fundamental Frequency, and (d) Autocorrelator Trace.

By increasing the pumping strength from 53.7 to 95.2 mW, the laser consistently generates stable pulses, with the repetition rate fixed at 1.82 MHz, confirming passive mode-locking operation. In Figure 5.8 (a), the variation in average output power and pulse energy with respect to pump power is illustrated. The pulse power shows a linear increase from 3.67 mW to 6.81 mW, indicating a slope efficiency of 7.85% as the pump power rises from the threshold of 53.7 to 95.2 mW. Pulse energy, on the other hand, also increases from 2.01 nJ to 3.74 nJ as the pump power is varied within this range. The pulse energy was calculated by dividing the average power with the repetition frequency. Figure 5.8 (b) demonstrates the relationship between peak power and pump power, revealing a linear increase from 0.58 W to 1.08 W, as the pump power escalates from 53.7 to 95.2 mW.

To further confirm the stability of the mode-locked EDFL operation, the laser's output spectra were monitored over successive 110-minute periods, with each period consisting of 10-minute intervals, as illustrated in Figure 5.9. Notably, all output samples were obtained under identical conditions. The consistent spectral

characteristics observed throughout the observation period, with a central wavelength of 1558.2 nm, underscore the robust stability of the mode-locking operation. Moreover, peak intensity fluctuations remained within a narrow margin of ± 0.1 dB, further confirming the stability of laser operation. Additionally, extended observation through oscilloscope traces over a period of three days reaffirmed the sustained stability of the pulse trains. During this extended duration, uniformity persisted without any discernible fluctuations or noise, providing conclusive evidence of the laser's stable operation over an extended timeframe. Table 5.2 compares the Cr_2GaC based laser performance with the previous reports with other materials. The mode-locking operation utilizing Cr_2GaC SA exhibits performance comparable to most reported SAs, underscoring the potential of Cr_2GaC material for ultrafast laser applications.

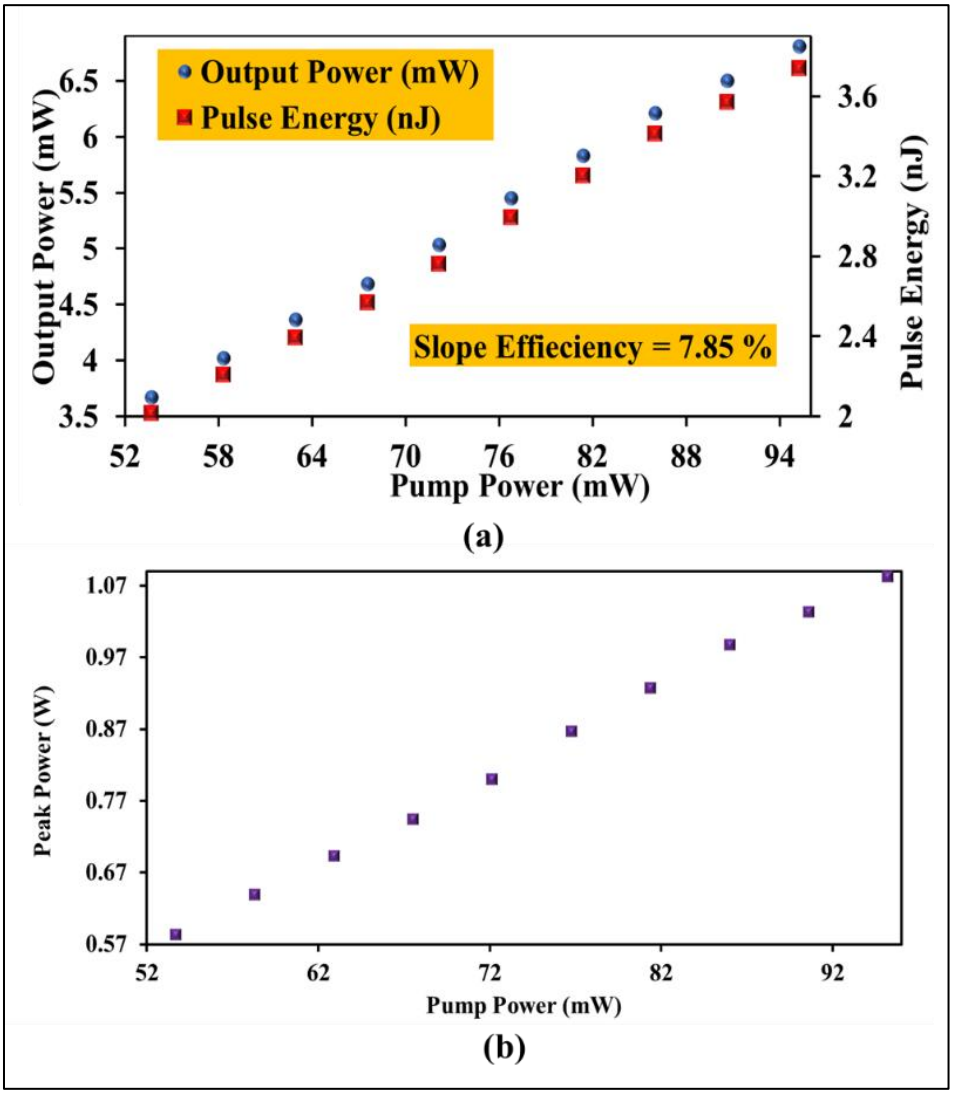


Figure 5.8 The Cr_2GaC SA Performance with Pump Power Variation (a) Average Output Power and Pulse Energy, and (b) Peak Power.

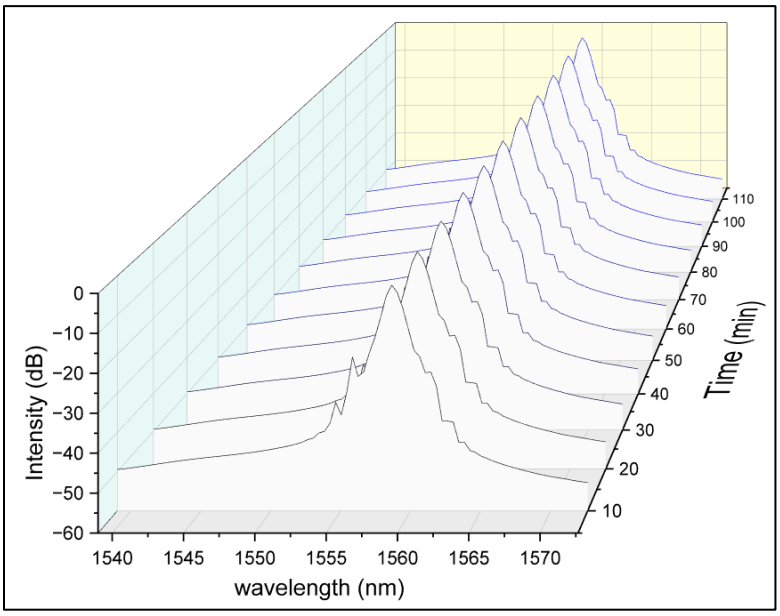


Figure 5.9 The Output Spectrum Evolution Over Time

Table 5.2
Mode-Locking Performance For Various SA Materials

SA	**Max pump power (mW)**	**Rep rate (MHz)**	**Pulse width (ps)**	**Pulse energy (nJ)**	**Output Power (mW)**	**λ (nm)**	**Ref**
Graphene	363	1.85	2.24	0.86	1.6	1562	(Tiu, & Suthaskumar, 2015)
WS_2	250	3.48	2.43	2.12	7.4	1566	(Travagnin, M. ,2001).

BP	250	1.0	2.66	7.35	7.38	1561	(Wadi & Ab Kadir, 2024)
Turmeric	305	3.4	0.9	1.67	5.67	1568.4	(Haris & Arof, 2019)
$Ti_3C_2T_x$	118.5	17.9	0.6	NA	0.3	1564.2	(Salah & Yoon, 2022)
Ti_3AlC_2	97.6	1.8	5.0	4.46	8.34	1559.7	(Shin 2016)
Nb_2AlC	439	6.5	2.8	1.5	9.6	1561.9	(Wadi & Kadir, 2024)
Cr_2GaC	95.2	1.82	3.04	3.74	6.81	1558.2	This work

5.6 Dark pulse generation in mode-locked EDFL using Cr_2GaC SA

Bright pulses, characterized by peaks in intensity, are commonly observed. However, dark pulses may also emerge in pulsed lasers under specific conditions, such as anomalous dispersion and nonlinear interactions. Unlike bright pulses, dark pulses

are identified by a localized dip in intensity against a continuous wave (CW) background, appearing as a "dark" area where the intensity drops before returning to its background level. Compared to bright pulses, dark pulses are less affected by propagation losses. Additionally, while bright pulses with high peak power can lead to undesirable nonlinear effects, dark pulses benefit from their lack of energy in the CW background, which minimizes pulse degradation during propagation [87]. The formation of dark pulses in fiber lasers with net anomalous dispersion is generally explained by domain-wall theory. According to this theory, dark pulses arise as boundaries between regions of differing intensity levels within the laser cavity. The dark pulse represents a low-intensity zone separating two high-intensity areas, and this contrast in phase and intensity supports the stable propagation of the dark pulse through the fiber [88].

In the previous section, a stable picosecond mode-locked EDFL with soliton pulse generation have been reported utilizing Cr_2GaC as a pulse transducer [89]. The study employed a 100 m SMF spool to manage dispersion and enhance nonlinear effects. On the other hand, further extension of cavity length by 50 m results in the generation of dark-pulsed due to strong nonlinearities in the cavity. This section will introduce dark pulse mode-locked generation with net anomalous dispersion by utilizing Cr_2GaC as transducer in EDFL. This is the first demonstration of dark soliton generation using Cr_2GaC SA. Compared to other SAs [90-92], Cr_2GaC offers a simpler synthesis process and a moderate modulation depth of 5.7%, making it suitable for mode-locking applications. It efficiently modulates cavity loss, facilitating the generation of short, intense pulses. Dark pulses, in contrast to bright pulses, offer benefits such as reduced nonlinear scattering, higher propagation speed, and improved noise resistance, making them ideal for long-distance transmission, precision measurement, and other advanced laser applications [20, 22].

The experimental configuration for the passively mode-locked EDFL incorporating the Cr_2GaC transducer was developed based on the setup shown in Figure 5.3, with the primary modification being the length of the SMF. To tailor the cavity dispersion and strengthen nonlinear interactions, the cavity was extended by adding 150 m of SMF, replacing the 100 m used in the earlier mode-locked arrangement. As a result, the total cavity length reached 157.3 m, comprising 0.5 m of WDM fiber, 1.8 m of EDF, and 155 m of SMF. This configuration yields operation in the anomalous dispersion regime, with an estimated net cavity dispersion of approximately −2.2 ps^2. Integrating

the Cr_2GaC film transducer into the lasing cavity enabled the generation of the dark-pulsed mode-locked laser as the pump power increased from 83.68 mW to 99.83 mW. Exceeding 99.83 mW, the pulse became unstable and gradually diminished, but it reappeared once the pump power returned within the specified range. The pulse was confirmed to be attributed to Cr_2GaC mode-locked, as initial testing without integrating the transducer only produced a CW laser.

Figure 5.10 shows the mode-locked laser performance at the maximum pump power of 99.82 mW. Figure 5.10 (a) displays a broad rectangular spectrum with a shifted spectral profile, both of which are characteristic of dark solitons. The sharp spectral edges and tail result from the soliton's localized nature, while the shifted spectrum arises from the intensity dip of the dark soliton, which corresponds to a shift in the frequency domain. In Figure 5.10 (a), a dissipative soliton is demonstrated with two distinct steep-edged spectra centred at wavelengths of 1529.6 nm and 1531.6 nm, respectively. This soliton represents a localized intensity dip within a continuous wave background, resulting from the balance of energy gain and loss in a nonlinear system. The interaction of dual wavelengths at 1529.6 nm and 1531.6 nm can induce topological defects in the temporal domain, leading to the generation of a domain-wall dark soliton train through a dissipative four-wave mixing process. In this process, the energy from the two dominant frequencies in the laser cavity is converted into higher-order harmonics via four-wave mixing. Dark pulses are produced as the phases of the longitudinal modes become locked owing to parametric wave mixing.

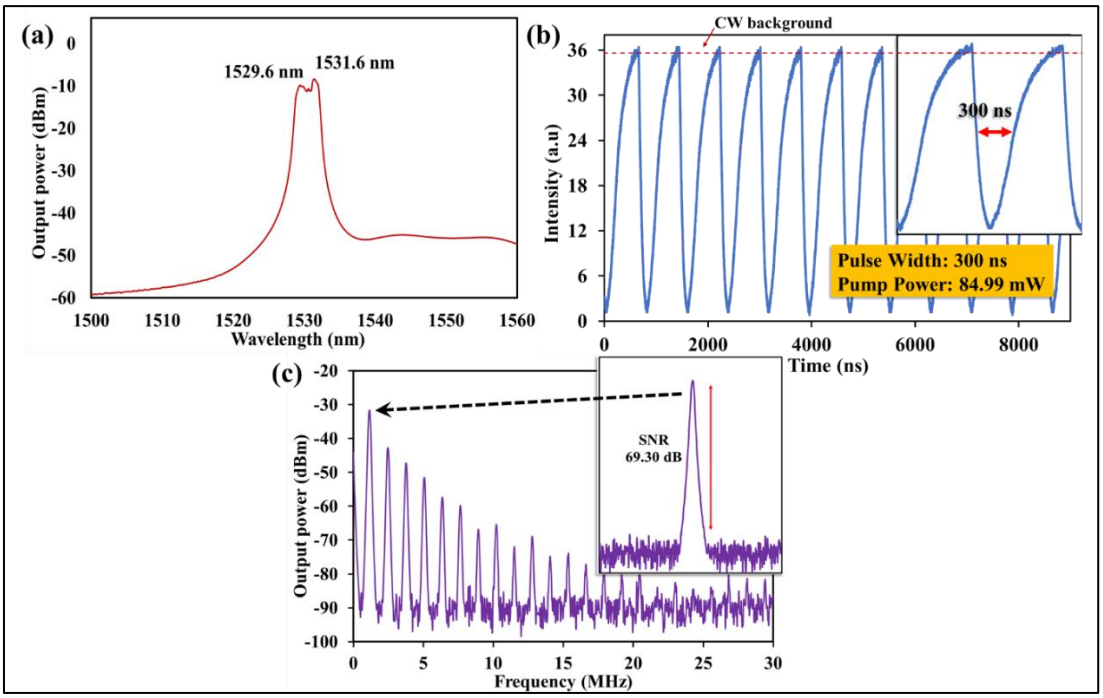


Figure 5.10 Performance of Cr_2GaC Dark Pulse Mode-Locked (a) OSA Spectrum (b) Pulse Train (c) RF Spectrum

Figure 5.10 (b) showcases the time-domain characteristics of the dark-pulsed mode-locked laser, displaying recurring dips against the CW noise background driven by the interplay between anomalous dispersion and nonlinear effects. The pulse width was measured at 300 ns, with a repetition rate of 1.27 MHz, consistent with the cavity length of approximately 157.3 meters. The RF spectrum was analyzed to assess the stability of the generated dark-pulsed mode-locked laser. Figure 5.10 (c) shows the frequency spectrum throughout 25 MHz, revealing a high signal-to-noise ratio (SNR) of 69.30 dB, strongly indicating the excellent stability of dark-pulsed mode-locked laser. As the pump power escalates from 83.68 mW to 99.83 mW, the laser continuously produces stable pulses, maintaining a constant repetition rate of 1.27 MHz, verifying stable mode-locked operation. Figure 5.11 displays the relationship between average output power with the pumping strength variation. The pulse power demonstrates a consistent and proportional rise from 3.73 mW to 4.56 mW, corresponding to a slope efficiency of 5.12%.

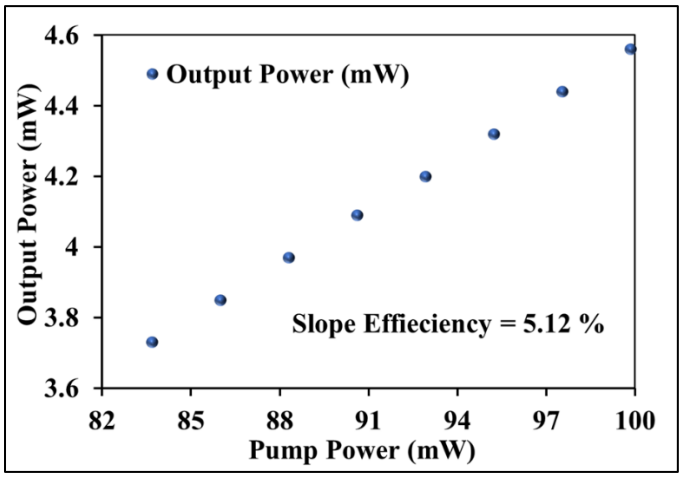


Figure 5.11 Average Output Power as a Function of Pumping Strength for the Cr_2GaC-Based Mode-Locked Laser

It is important to note that the dual-peak spectrum was achieved due to the enhanced birefringence effect inside the laser cavity after inserting the 150 m long SMF. The two lasers, operating at slightly different wavelengths, oscillate simultaneously in the cavity, leading to the formation of temporal topological defects. The strong birefringence within the cavity increased the gain bandwidth and facilitated cross-phase coupling between the two wavelengths, which, as the pump power increased, led to the formation of dark soliton pulses. The SA absorbed the high-intensity mode components in the cavity, creating competition among the lower-intensity modes. This mode competition further triggered dual-wavelength oscillation in the ring cavity. As a result, the interaction between the two wavelength oscillations gave rise to stable domain wall dark pulses within a pump power range of 83.68 mW to 99.83 mW. However, at pump powers exceeding 99.83 mW, the pulses became unstable and diminished due to reduced mode competition within the laser cavity, subsequently ceasing the dual-wavelength oscillation. It is worth noting that the mode-locked laser with dark pulse output can be reproduced with nearly identical performance, as the Cr_2GaC film was produced using the same procedure. Table 5.3 compares the performance of the dark pulse mode-locked EDFL with previous studies utilizing other SAs. Notably, the proposed EDFL operates at the shortest wavelength, approximately 1530 nm. Furthermore, the proposed laser achieved the highest SNR of 69.3 dB at the fundamental frequency. Based on the absorption characteristics of the fabricated film, we believe that Cr_2GaC SA can also be effective at wavelengths beyond the current configuration, including in the 1 μm and 2.0 μm regions. It is also worth noting that by manipulating the cavity design, both Q-

switched and bright pulse mode-locking can be achieved using similar SA devices. However, achieving femtosecond-level (fs) mode-locking remains challenging with the current saturable absorber. It is believed that femtosecond mode-locked pulses could be realized by optimizing the fabrication of Cr_2GaC to enhance its saturable absorption while also reducing insertion loss.

Table 5-3
Performance Comparison of the Dark Pulse Mode-Locked EDFL with other Reported Studies.

SA Material	**Wave-length (nm)**	**Rep. Rate (MHz)**	**Pulse width (ns)**	**SNR (dB)**	**Output power (mW)**	**Ref.**
CNT	1565.58	15.6	NA	NA	NA	(Yang, & Zhang, 2022)
Polyacrylonitrile	1561	0.99	306	67	13.37	(Zhang, & Pan, 2024)
$Mo_xW_{1-x}Te_2$	1563	5.7	NA	66.6	NA	(Zhang,& Feng, 2018)
Ti_2SnC	1559	1.78	261.2	45	3.08	(Zhang, & Feng, , 2014)
Sc_2O_3	1597.8	10.42	23	55.6	7.4	(Zhang, & Zhou, 2014)
Cr_2GaC	1530	1.27	300	69.3	4.56	This work

5.7 Chapter summary

By integrating a Cr_2GaC-based SA into an erbium-doped fiber laser (EDFL) cavity, stable Q-switched and mode-locked pulse generation was successfully

demonstrated. The SA was fabricated by embedding a MAX-phase Cr_2GaC material within a polymer matrix to form a composite thin film, which was then sandwiched between two fiber ferrules for seamless integration into the laser cavity. The Cr_2GaC SA exhibited a modulation depth of 2.1%, a non-saturable loss of 97.4%, and a saturation intensity of 180 MW cm^{-2}.

In the Q-switched regime, stable pulse operation was achieved at a central wavelength of 1530.6 nm with pump powers ranging from 49.06 to 72.14 mW. The maximum repetition rate reached 76.92 kHz, accompanied by a minimum pulse width of 5.03 μs and a signal-to-noise ratio (SNR) of 60.14 dB. For mode-locked operation, soliton pulses centered at 1558.2 nm were generated using the same Cr_2GaC thin-film SA. By extending the EDFL cavity with an additional 100 m of SMF, a long-cavity configuration was realized, producing a stable soliton pulse train at a repetition rate of 1.82 MHz, in good agreement with the calculated cavity length. Mode-locking was sustained over a pump-power range of 53.7–95.2 mW, yielding a pulse duration of 3.04 ps. A maximum pulse energy of 3.74 nJ was obtained at 95.2 mW, while the excellent stability of the mode-locked operation was confirmed by a high SNR of 71.7 dB at the fundamental frequency.

Furthermore, dark-pulse generation was successfully demonstrated in a mode-locked EDFL incorporating the Cr_2GaC SA under net anomalous dispersion by further extending the cavity length with 150 m of SMF. Dark-pulse formation arose from the combined effects of anomalous dispersion and cavity nonlinearities. A stable dark-pulse train was observed over a pump-power range of 83.68–99.83 mW. The laser operated at a constant repetition rate of 1.27 MHz, producing dissipative soliton pulses with a pulse width of approximately 300 ns and dual steep-edged spectra centered at 1529.6 nm and 1531.6 nm. At the maximum pump power of 99.83 mW, the average output power reached 4.56 mW with a high SNR of 69.30 dB.

To the best of our knowledge, this work represents the first demonstration of dark-pulse mode-locking in an EDFL using a Cr_2GaC transducer. Overall, the results highlight Cr_2GaC as a promising and versatile saturable absorber for generating Q-switched, bright-soliton, and dark-pulse regimes, offering significant potential for ultrafast laser applications in optical communications, biomedical diagnostics, and advanced material processing.

Cr_2GaC based SA has high minimum pulse width and low maximum pulse width compared to other based SA. For bright pulse mode-locking Cr2gac based SA has low

pulse width and high pulse energy compared to other based SA as shown in Table 5-4. For dark pulse mode-locking Cr2gac based SA has high pulse width.

Table 5.4
Performance Of Difference SA Materials.

SA Material	**Modulation Depth (%)**	**Pulse Width**	**Peak Power / Pulse Energy**	**Long-term Stability / Damage Threshold**	**Reference**
Graphene	Low (< 1%)	Femtosecond to Picosecond	Low	Prone to optical damage under high pump power	(Zhang, & Qi, 2021)
TMDs (MoS2 /WSe2)	Moderate (1 - 5%)	Picosecond to Microsecond	Moderate	Susceptible to environmental oxidation	(Zheng, & Li, 2023)
CuAlO2	High	3.17 ps (Mode-locked) / 5.03 µs (Q-switched)	43.55 nJ	High stability (SNR 71.75 dB); robust delafossite structure prevents degradation	This work
Cr2GaC	2.10%	3.04 ps (Bright) / ~300 ns (Dark)	3.74 nJ	Exceptional (SNR 71.7 dB); MAX-phase offers superior thermal/radiation tolerance	This work

It is worth noting that while alternative architectural geometries—such as linear (Fabry-Perot) cavities or figure-of-eight double-loop configurations—can be employed to achieve pulsed operation, a unidirectional fiber ring cavity configuration was

strategically selected for this work. Linear cavities utilize reflective fiber mirrors or fiber Bragg gratings (FBGs) which can induce severe spatial hole burning due to the formation of standing-wave patterns in the gain medium, often leading to multi-mode instabilities and localized thermal stresses. Figure-of-eight cavities offer high peak power handling but introduce extreme complexity in balancing the nonlinear optical loop mirror (NOLM) splitting ratios. In contrast, the unidirectional ring cavity design effectively completely suppresses spatial hole burning by ensuring traveling-wave propagation. This geometry maximizes the interaction length within the Erbium-doped fiber, offers flexible insertion of discrete polarization controllers, and minimizes total cavity insertion loss. Consequently, this configuration yields the most structurally stable and reproducible operating regimes for evaluating the fundamental, unperturbed nonlinear performance of the newly introduced $CuAlO_2$ and Cr_2GaC saturable absorbers.

CHAPTER 6
CONCLUSION

6.1 Research Outcome

Passive Q-switched and mode-locked fiber lasers that employ saturable absorbers (SAs) have become one of the most effective approaches for generating short and ultrashort optical pulses. This technique offers many advantages, including high beam quality, compact and alignment-free structure, low cost, and excellent compatibility with all-fiber systems. Early developments in SA technology mainly relied on organic dyes and semiconductor saturable absorber mirrors (SESAMs). Although these materials enabled stable pulse generation, they also introduced limitations such as narrow operating bandwidths, complex fabrication, and high cost. The rapid progress in graphene-based saturable absorbers has significantly accelerated research into new classes of SA materials. Since the successful fabrication and demonstration of graphene SAs, there has been growing interest in exploring other emerging materials with simpler fabrication routes, broader spectral response, and improved durability. In this context, transparent conducting oxides (TCOs) and MAX-phase materials have attracted increasing attention due to their unique electrical, optical, and structural properties. These materials offer the potential for broadband operation, high damage thresholds, and strong nonlinear absorption, making them promising candidates for next-generation saturable absorbers.

The exploration of TCOs and MAX-phase materials is expected to open new opportunities for advancing pulsed fiber laser technology, particularly in achieving stable and efficient Q-switched and mode-locked operation. As introduced in Chapter 1, the main aim of this research is to fabricate and develop novel SA devices based on transparent conducting oxides and MAX-phase materials, and to investigate their performance in improving Q-switched and mode-locked operation in an erbium-doped fiber laser (EDFL) cavity. To accomplish this aim, three specific research objectives have been formulated, which guide the material fabrication, device integration, and laser performance evaluation throughout this study.

The first objective of this study was to fabricate thin-film saturable absorbers based on Copper Aluminium Oxide ($CuAlO_2$) and Chromium Gallium Carbide (Cr_2GaC) using a simple solution-casting technique, with polyvinyl alcohol (PVA) serving as the host polymer matrix. PVA was selected because of its good film-forming ability, optical transparency, and compatibility with various functional materials. As detailed in Chapter 3, both SA films were successfully prepared by dispersing $CuAlO_2$ or Cr_2GaC powder into a PVA solution to form a uniform mixture. The solution was then drop-cast onto a flat substrate and left to dry under controlled conditions, allowing the solvent to evaporate and form a solid composite film. After drying, the resulting thin films exhibited good mechanical integrity and optical quality, making them suitable for integration into fiber laser systems as SAs.

The second objective of this research was to characterize the physical and optical properties of the fabricated SAs using field-emission scanning electron microscopy (FESEM), energy-dispersive X-ray spectroscopy (EDX), and the balanced twin-detector technique. These characterizations are essential to verify the structural quality, elemental composition, and nonlinear optical behavior of the SAs before their integration into laser cavities. An XRD analysis be able to perform on $CuAlO_2$ and not on Cr_2GaC due to hardware availability. As described in Chapter 3, physical characterization was first carried out for both $CuAlO_2$- and Cr_2GaC-based SAs. FESEM was used to obtain high-resolution images of the film surfaces, allowing detailed observation of surface morphology and particle distribution within the PVA matrix. The images confirmed that the functional particles were successfully embedded in the polymer host with reasonably uniform dispersion. In addition, energy-dispersive X-ray spectroscopy (EDX) analysis was performed to verify the elemental composition of the films, confirming the presence of the constituent elements corresponding to $CuAlO_2$ and Cr_2GaC.

The linear and nonlinear optical absorption characteristics of the SAs were then investigated, as these parameters are critical for evaluating their suitability for passive Q-switching and mode-locking. Using the balanced twin-detector technique, the nonlinear absorption response of each SA was measured. As reported in Chapter 4, the $CuAlO_2$-based SA exhibited a modulation depth of 4.1%, a saturation intensity of 4 kW/cm², and a non-saturable loss of 33.5%. Its linear absorption was measured to be 2.11 dB at approximately 1560 nm. In Chapter 5, the optical properties of the Cr_2GaC-based SA are presented. This SA showed nearly uniform linear absorption of 5.75 dB over the wavelength range from 1529.6 nm to 1531.6 nm. Its modulation depth, non-saturable

absorption, and saturation intensity were measured as 5.7%, 60.4%, and 100 MW/cm², respectively.

These results confirm that both $CuAlO_2$ and Cr_2GaC thin films exhibit clear intensity-dependent absorption behavior: they strongly absorb light at low intensities and become increasingly transparent at higher intensities. This saturable absorption characteristic enables effective modulation of intracavity losses, making both materials suitable for passive Q-switching and mode-locking in fiber laser systems.

The third and final objective of this study was to evaluate the performance of the fabricated saturable absorber films by demonstrating Q-switched and mode-locked pulse generation in an EDFL cavity. Using the $CuAlO_2$ thin-film SA, stable Q-switched operation was obtained over a pump-power range of 132.15 mW to 210.62 mW. With increasing pump power, the repetition rate increased from 66.09 kHz to 84.96 kHz, while the pulse width decreased from 6.31 μs to 5.03 μs. The laser operated at a central wavelength of 1563.3 nm, producing a maximum pulse energy of 43.55 nJ and a slope efficiency of 1.95%. For mode-locked operation, a 100 m single-mode fiber (SMF) spool was inserted to extend the cavity and enhance nonlinear effects. Self-starting mode-locking was achieved over a pump range of 141.38 mW to 233.7 mW. At the threshold pump power of 141.38 mW, pulses centered at 1560 nm were generated with a repetition rate of 1.792 MHz and a pulse duration of 3.17 ps.

The Cr_2GaC thin-film SA also successfully enabled both Q-switched and mode-locked operation. In the Q-switched regime, stable pulses were produced at 1530.6 nm with pump powers between 49.06 mW and 72.14 mW. The repetition rate reached 76.92 kHz, accompanied by a minimum pulse width of 5.03 μs and a signal-to-noise ratio (SNR) of 60.14 dB. For mode-locking using the Cr_2GaC SA, soliton pulses centered at 1558.2 nm were generated. By adding 100 m of SMF to form a long-cavity configuration, a stable pulse train with a repetition rate of 1.82 MHz was achieved, in good agreement with the calculated cavity length. Mode-locking was sustained over a pump-power range of 53.7 mW to 95.2 mW, producing pulses with a duration of 3.04 ps and a maximum pulse energy of 3.74 nJ. Excellent stability was confirmed by a high SNR of 71.7 dB.

In addition, dark-pulse generation was demonstrated using the Cr_2GaC SA by further extending the cavity with 150 m of SMF under net anomalous dispersion. A stable dark-pulse train was observed over a pump-power range of 83.68 mW to 99.83 mW. The laser operated at a constant repetition rate of 1.27 MHz, generating pulses with widths of approximately 300 ns and dual spectral peaks at 1529.6 nm and 1531.6 nm. At the highest

pump power of 99.83 mW, the average output power reached 4.56 mW with an SNR of 69.30 dB. These results clearly demonstrate that both $CuAlO_2$ and Cr_2GaC are effective SAs for Q-switching and mode-locking in EDFLs, highlighting their strong potential for applications in ultrafast lasers, nonlinear optics, and advanced photonic systems.

In summary, all three research objectives were successfully achieved. The findings confirm that $CuAlO_2$ and Cr_2GaC are promising materials for both short- and ultrashort-pulse generation. Moreover, the proposed fabrication and integration approach is simple and versatile and can be readily extended to fiber lasers operating at other wavelengths.

6.2 Recommendation & Limitation of Work

All of the objectives outlined in this study have been successfully achieved. However, there remains significant scope for further investigation of both $CuAlO_2$ and Cr_2GaC materials in Q-switched and mode-locked fiber laser systems. The present work is focused on operation in the 1.5-µm region, which corresponds to the emission band of erbium-doped fiber lasers (EDFLs) above 1530 nm. In future studies, these saturable absorbers could be extended to other rare-earth-doped fiber laser platforms, such as ytterbium-doped fiber lasers (YDFLs), neodymium-doped fiber lasers (NDFLs), and thulium-doped fiber lasers (TDFLs), which operate in the 1-µm and 2-µm wavelength regions. This would allow the broadband capability and versatility of $CuAlO_2$- and Cr_2GaC-based SAs to be more comprehensively evaluated.

Further work should also focus on enhancing the output performance of the developed fiber lasers. Key performance targets include shortening the pulse duration, increasing the repetition rate, boosting the average output power, and improving the pulse energy. Achieving these improvements may require optimization of several aspects of the system, including the choice and length of the gain medium, refinement of the SA fabrication process, and careful redesign of the laser cavity to better manage dispersion and nonlinearity.

In this study, thin-film SAs fabricated using the PVA host polymer demonstrated effective pulse generation. However, previous work has shown that using polydimethylsiloxane (PDMS) as a host matrix can lead to superior performance. For example, a CeO_2/PDMS-based SA was reported to produce mode-locked pulses as short as 800 fs (Zheng & Zhao,2023). Therefore, future research on $CuAlO_2$ and Cr_2GaC SAs

could explore PDMS as an alternative host polymer to replace PVA. This may improve film uniformity, optical damage threshold, and recovery dynamics, potentially enabling even shorter pulses and higher-performance pulsed fiber laser operation. While the fabricated $CuAlO_2$-PVA and Cr_2GaC-PVA thin-film saturable absorbers demonstrated excellent, high-purity pulse generation with record-high SNR values, certain operational limitations must be acknowledged. First, the optical damage threshold of the SAs is fundamentally bounded by the thermal degradation temperature of the Polyvinyl Alcohol (PVA) host polymer matrix under high intra-cavity average powers. Second, the solution-casting fabrication method can introduce minor variations in film thickness, which slightly influences local non-saturable losses. To overcome these limitations, future research could explore embedding these novel transducers into more thermally resilient host materials, such as polyimide, or directly depositing the $CuAlO_2$ and Cr_2GaC materials onto fiber ferrules via optical deposition or sputtering methods to achieve completely polymer-free, high-power laser operation.

REFERENCES

Abbas, M., Shehab, A. A.-M., Hassan, N., & Al-Samuraee, A. (2011). Effect of temperature and deposition time on the optical properties of chemically deposited nanostructure PbS thin films. Thin Solid Films, 519(15), 4917-4922.

Abbasi, F., Ghorashi, S. M. B., Eskandarian, P., & Zabolian, H. (2022). Investigating the effect of copper phthalocyanine-emitting dopant on the production of near-infrared organic light-emitting diodes. Journal of Materials Science: Materials in Electronics, 33(13), 10494–10503.

Ahmad, A. D., Elseman, A., Masruroh, M., Fouad, O. A., Geioushy, R. A., Moussa, M. E., & Harun, S. W. (2026). Saturable absorption in $Mg_2Sn_{1-x}Sb_x$ alloy for Q-switched and mode-locked erbium-doped fiber lasers. Applied Optics.

Ahmad, A. D., Mokhtar, N., Arof, H., Badruddin, I. A., Kamangar, S., & Harun, S. W. (2025). Q-switched and Mode-Locked pulse generation in fiber laser with micro particles polyacrylonitrile absorber. Optical Fiber Technology, 93, 104208.

Ahmad, A. D., Mokhtar, N., Rosol, A. H. A., Arof, H., Apsari, R., & Harun, S. W. (2024). Nanosecond-pulse fiber laser mode-locked with polyaniline saturable absorber. Journal of Physics: Conference Series, 301.

Ahmad, A. D., Mokhtar, N., Salam, S., Anjum Badruddin, I., Kamangar, S., Apsari, R., & Harun, S. W. (2024). Polyacrylonitrile enabled soliton mode-locked fiber laser. Infrared Physics & Technology, 140.

Ahmad, A. D., Salam, S., Mokhtar, N., Arof, H., Apsari, R., Hamida, B. A., & Harun, S. W. W. (2024). Q-Switched Pulse Generation in L-Band Region with Polyacrylonitrile Saturable Absorber. Physica Scripta.

Ahmad, H., Rusni, N., & Samion, M. (2025). Rhodamine 6G fluorescent dye as a saturable absorber for harmonic mode-locked pulses generation in thulium-holmium doped fiber lasers. Optical Fiber Technology, 95, 104438.

Ahmad, H., Samion, M. Z., Sharbirin, A. S., Norizan, S. F., Aidit, S. N., & Ismail, M. F. (2018). Graphene-PVA saturable absorber for generation of a wavelength-tunable passively Q-switched thulium-doped fiber laser in 2.0μm. Laser Physics, 28(5).

Ahmed, M., Ali, N., Salleh, Z., Rahman, A. A., Harun, S. W., Manaf, M., & Arof, H. (2015). Q-switched erbium doped fiber laser based on single and multiple

walled carbon nanotubes embedded in polyethylene oxide film as saturable absorber. Optics & Laser Technology, 65, 25–28.

Ahmed, M. H. M., Latiff, A. A., Arof, H., Ahmad, H., & Harun, S. W. (2016a). Femtosecond mode-locked erbium-doped fiber laser based on MoS2–PVA

Ahmed, M. H. M., Latiff, A. A., Arof, H., Ahmad, H., & Harun, S. W. (2016b). Soliton mode-locked erbium-doped fibre laser with mechanically exfoliated molybdenum disulphide saturable absorber. Iet Optoelectronics, 10(5), 169–173.

Ahmed, M. H. M., Latiff, A. A., Arof, H., & Harun, S. W. (2016). Ultrafast erbium-doped fiber laser mode-locked with a black phosphorus saturable absorber. Laser Physics Letters, 13(9). https://doi.org/10.1088/1612-2011/13/9/095104

Ahmeed, M. M., Ahmad, B., Supian, L. S., Diblawe, A. M., & Harun, S. W. (2025). Generation of Dark Pulses in Mode-Locked Erbium-Doped Fiber Ring Laser Operating in L-Band Region Using Sc2O3 Absorber. Microwave and Optical Technology Letters, 67(1), e70103.

Al-Hiti, A. S., Al-Masoodi, A. H., Yasin, M., Harun, S. J. I. P., & Technology. (2020). Femtosecond mode-locked laser at 1.5 μm region using Turmeric-based saturable absorber. 103548.

Aljunid, S. Z. Z., Ghafar, N. A. M. A., Ahmad, B. A., Apsari, R., & Harun, S. W. (2024). Q-switched and mode-locked pulse generations with Ti3AlC2 absorber. Nanosystems: Physics, Chemistry, Mathematics, 15(2), 184–191.

Alrebdi, T. A., Sadiq, S., Tian, S.-C., Asghar, M., Saghir, I., & Asghar, H. (2025). Applications of Prepared MnMoO4 Nanoparticles as Saturable Absorbers for Q-Switched Erbium-Doped Fiber Lasers: Experimental and Theoretical Analysis. Photonics,

Apandi, N. H. M., Ahmad, F., Ambran, S., Yamada, M., & Harun, S. W. (2017). Bismuth (III) Telluride (Bi2Te3) Based Topological Insulator Embedded in PVA as Passive Saturable Absorber in Erbium-Doped Fiber Laser. IOP Conference Series: Materials Science and Engineering, 210.

Barmenkov, Y. O., Kir'yanov, A. V., Cruz, J. L., & Andres, M. V. (2014). Pulsed Regimes of Erbium-Doped Fiber Laser Q-Switched Using Acousto-Optical Modulator. IEEE Journal of Selected Topics in Quantum Electronics, 20(5), 337–344.

Becker, P. M., Olsson, A. A., & Simpson, J. R. (1999). Erbium-doped fiber amplifiers: fundamentals and technology. Elsevier.

Chavan, G. T., Kim, Y., Khokhar, M. Q., Hussain, S. Q., Cho, E.-C., Yi, J., Ahmad, Z., Rosaiah, P., & Jeon, C.-W. (2023). A brief review of transparent conducting oxides (TCO): the influence of different deposition techniques on the efficiency of solar cells. Nanomaterials, 13(7), 1226.

Chen, H.-R., Tsai, C.-Y., Cheng, H.-M., Lin, K.-H., & Hsieh, W.-F. (2014). Passive mode locking of ytterbium-and erbium-doped all-fiber lasers using graphene oxide saturable absorbers. Optics express, 22(11), 12880–12889.

Chen, H., Yin, J., Yang, J., Zhang, X., Liu, M., Jiang, Z., Wang, J., Sun, Z., Guo, T., & Liu, W. (2017). Transition-metal dichalcogenides heterostructure saturable absorbers for ultrafast photonics. Optics letters, 42(21), 4279–4282.

Chen, Y., Cheak, T. Z., Jin, T. S., Vinitha, G., Dimyati, K., & Harun, S. W. (2024). Domain-wall dark pulse generation with SMF-GIMF-SMF structure as artificial saturable absorber. Scientific reports, 14(1), 2141.

Dacey, G. (1962). Optical Masers in Science and Technology: Advances in the control of light waves give promise of important applications in science and technology. Science, 135(3498), 71–74.

Diblawe, A. M., Ahmad, B. A., Dimyati, K., Rosol, A. H. A., Zulkipli, N. F., Apsari, R., & Harun, S. W. (2023). Molybdenum Aluminum Boride as the Q-Switcher and Mode-Locker in the Erbium-Doped Fiber Laser Configuration. Journal of Russian Laser Research, 44(1), 68–76.

Dong, L., & Samson, B. (2016). Fiber lasers: basics, technology, and applications. CRC press.

Du, L., Lu, D., Li, J., Yang, L., Yang, K., Huang, B., Miao, L., Qi, X., Zhao, C., & Zhong, J. (2020). Antimony thin film as a robust broadband saturable absorber. IEEE Journal of Selected Topics in Quantum Electronics, 27(2), 1–7.

Feng, M., Silverman, K. L., Mirin, R. P., & Cundiff, S. T. (2010). Dark pulse quantum dot diode laser. Optics Express, 18(13), 13385–13395.

Fu, B., Hua, Y., Xiao, X., Zhu, H., Sun, Z., & Yang, C. (2014). Broadband graphene saturable absorber for pulsed fiber lasers at 1, 1.5, and 2 μm. IEEE Journal of Selected Topics in Quantum Electronics, 20(5), 411–415.

Fu, B., Sun, J., Wang, C., Shang, C., Xu, L., Li, J., & Zhang, H. (2021). MXenes: Synthesis, optical properties, and applications in ultrafast photonics. Small, 17(11), 2006054.

Ghafar, N. A. M., Zulkipli, N. F., Omar, S., Markom, A. M., Yasin, M., & Harun, S. W. (2022). Q-Switched Pulse Generation in Erbium-Doped Fiber Laser Cavity with Vanadium Aluminum Carbide Absorber. Journal of Russian Laser Research, 43(6), 702–707.

Hammadi, Y., Mansour, T., Alani, I., Ahmed, M., Al-Masoodi, A., Jusoh, Z., & Harun, S. (2018). Graphene based soliton mode-locked erbium doped fiber laser for supercontinuum generation. Digest Journal of Nanomaterials and Biostructures, 13(3), 777–784.

Haris, H., Arof, H., Muhammad, A. R., Anyi, C. L., Tan, S. J., Kasim, N., & Harun, S. W. (2019). Passively Q-switched and mode-locked Erbium-doped fiber laser with topological insulator Bismuth Selenide (Bi2Se3) as saturable absorber at C-band region. Optical Fiber Technology, 48, 117–122.

Haris, H., Batumalay, M., Tan, S. J., Markom, A. M., Muhammad, A. R., Harun, S. W., Megat Hasnan, M. M. I., & Saad, I. (2022). Mode-Locked YDFL Using Topological Insulator Bismuth Selenide Nanosheets as the Saturable Absorber. Crystals, 12(4), 489.

Hasegawa, A., & Tappert, F. (1973). Transmission of stationary nonlinear optical pulses in dispersive dielectric fibers. I. Anomalous dispersion. Applied Physics Letters, 23(3), 142–144.

Hecht, J. (2010). Short history of laser development. Optical Engineering, 49(9), 091002–091002–091023.

Hisyam, M. B., Rusdi, M. F. M., Latiff, A. A., & Harun, S. W. (2016). Generation of mode-locked ytterbium doped fiber ring laser using few-layer black phosphorus as a saturable absorber. IEEE Journal of Selected Topics in Quantum Electronics, 23(1), 39–43.

Hong, Z., Liu, Y., Yang, F., Liu, X., Zhang, H., Guo, L., & Ge, X. (2020). Passively Q-Switched Erbium-Doped Fiber Laser with TiSe₂ as Saturable Absorber. Optics and Photonics Journal, 10(11), 251–263.

Husaini, M. N. A. H. M., Wadi, N. I. S., Markom, A. M., Dimyati, K., Apsari, R., & Jusoh, Z. (2024). Mode-locked erbium-doped fiber laser based on Cr2GaC saturable absorber. Optik, 311, 171902.

Huttner, B., Geiser, C., & Gisin, N. (2002). Polarization-induced distortions in optical fiber networks with polarization-mode dispersion and polarization-dependent losses. IEEE Journal of Selected Topics in Quantum Electronics, 6(2), 317–329.

Ippen, E., Shank, C., & Dienes, A. (1972). Passive mode locking of the cw dye laser. Applied Physics Letters, 21(8), 348–350.

Ismail, E., Kadir, N., Latiff, A., Ahmad, H., & Harun, S. (2016). Black phosphorus crystal as a saturable absorber for both a Q-switched and mode-locked erbium-doped fiber laser. RSC Advances, 6(76), 72692–72697.

Jafry, A. A. A., Kasim, N., Rusdi, M. F. M., Rosol, A. H. A., Yusoff, R. A. M., Muhammad, A. R., Nizamani, B., & Harun, S. W. (2020). MAX phase based saturable absorber for mode-locked erbium-doped fiber laser. Optics and Laser Technology, 127, Article 106186.

Jasem, I. N., Abdullah, H. H., & Jalal Abdulrazzaq, M. (2023). Dual-Wavelength Passively Q-Switched Erbium-Doped Fiber Laser Incorporating Calcium Carbonate Nanoparticles as Saturable Absorber. Journal of Nanotechnology, 2023(1), 8858582.

Jasem, I. N., Abdullah, H. H., Jalal Abdulrazzaq, M., & Manavalan, R. K. (2023). Dual-Wavelength Passively Q-Switched Erbium-Doped Fiber Laser Incorporating Calcium Carbonate Nanoparticles as Saturable Absorber. Journal of Nanotechnology, 2023, 1–11

Kadir, N., Ismail, E. I., Latiff, A. A., Ahmad, H., Arof, H., & Harun, S. W. (2017). Transition metal dichalcogenides (WS2 and MoS2) saturable absorbers for mode-locked erbium-doped fiber lasers. Chinese Physics Letters, 34(1), 014202.

Keller, U. (2003). Recent developments in compact ultrafast lasers. nature, 424(6950), 831–838.

Latiff, A. A., Kadir, N. A., Ismail, E. I., Shamsuddin, H., Ahmad, H., & Harun, S. W. (2017). All-fiber dual-wavelength Q-switched and mode-locked EDFL by SMF-THDF-SMF structure as a saturable absorber. Optics Communications, 389, 29–34

Lau, K. Y., Latif, A. A., Abu Bakar, M. H., Muhammad, F. D., Omar, M. F., & Mahdi, M. A. (2017). Mechanically deposited tungsten disulfide saturable absorber for low-threshold Q-switched erbium-doped fiber laser. Applied Physics B, 123(8).

Lee, J., Lee, J., Koo, J., Chung, H., & Lee, J. H. (2016). Linearly polarized, Q-switched, erbium-doped fiber laser incorporating a bulk-structured bismuth

telluride/polyvinyl alcohol saturable absorber. Optical Engineering, 55(7), 076109.

Leitz, K.-H., Redlingshöfer, B., Reg, Y., Otto, A., & Schmidt, M. (2011). Metal ablation with short and ultrashort laser pulses. Physics Procedia, 12, 230–238.

Li, J., Wang, Y., Luo, H., Liu, Y., Yan, Z., Sun, Z., & Zhang, L. (2019). Kelly sideband suppression and wavelength tuning of a conventional soliton in a Tm-doped hybrid mode-locked fiber laser with an all-fiber Lyot filter. Photonics Research, 7(2).

Li, L., Lv, R., Liu, S., Wang, X., Wang, Y., Chen, Z., & Wang, J. (2018). Transition metal dichalcogenide (WS2 and MoS2) saturable absorbers for Q-switched Er-doped fiber lasers. Laser physics, 28(5), 055106.

Li, L., Xue, Z., Pang, L., Xiao, X., Yang, H., Zhang, J., Zhang, Y., Zhao, Q., & Liu, W. (2024). Saturable absorption properties and ultrafast photonics applications of HfS 3. Optics letters, 49(5), 1293–1296.

Liu, H., & Chow, K. (2014). Dark pulse generation in fiber lasers incorporating carbon nanotubes. Optics express, 22(24), 29708–29713.

Liu, H. H., & Chow, K. K. (2014). Dark pulse generation in fiber lasers incorporating carbon nanotubes. Optics Express, 22(24), 29708–29713.

Liu, W., Liu, M., Liu, X., Wang, X., Deng, H. X., Lei, M., Wei, Z., & Wei, Z. (2020). Recent advances of 2D materials in nonlinear photonics and fiber lasers. Advanced Optical Materials, 8(8), 1901631.

Liu, Y., Xu, Y., Xu, C., Chen, J., Liu, H., Zhang, H., Jin, L., Fan, J., Zou, Y., & Ma, X. (2024). Interface charge transfer in MXenes/graphene heterostructures for ultrafast photonics. Advanced Optical Materials, 12(4), 2301439.

Liu, Y., Zhang, W., Xu, T., He, J., Zhang, F., & Li, F. (2011). Fiber laser sensing system and its applications. Photonic Sensors, 1(1), 43–53.

Maiman, T. H. (1960). Stimulated optical radiation in ruby. nature, 187(4736), 493–494.

Malik, A. M., Rohrer, J., & Albe, K. (2023). Theoretical study of thermodynamic and magnetic properties of transition metal carbide and nitride MAX phases. Physical Review Materials, 7(4), 044408.

Mansor, M., Zainol Abidin, N. H., Liew, J. Y. C., Alresheedi, M. T., Garg, A. K., Janyani, V., & Mahdi, M. A. (2022). Cerium oxide/polydimethylsiloxane composite tapered fiber saturable absorber for mode-locked pulsed erbium-

doped fiber laser. Infrared Physics & Technology, 125. https://doi.org/10.1016/j.infrared.2022.104220

Milani, A., LI BASSI, A., Russo, V., Tommasini, M., & Casari, C. S. (2019). Handbook of Graphene, Volume 3: Graphene-Like 2D Materials.

Nady, A., Ahmed, M. H. M., Latiff, A. A., Numan, A., Ooi, C. R., & Harun, S. W. (2017). Nickel oxide nanoparticles as a saturable absorber for an all-fiber passively Q-switched erbium-doped fiber laser. Laser physics, 27(6), 065105.

Naidu, R. R., Ahmad, A. D., Masruroh, Ali, H. N., Zakaria, R., Khudus, M. I. M., & Harun, S. W. (2025). Ultrashort pulse generation using tantalum aluminum carbide as a pulse modulator. Applied Optics, 64(2), 436–442.

Naidu, R. R. N., Masruroh, M., Diblawe, A. M. M., Khudus, M. I. M., & Harun, S. W. (2024). Generation of dark pulses in mode-locked erbium-doped fiber ring laser using Ti2SnC absorber. Physica Scripta.

Omar, S., Rosol, A. H. A., Jafry, A., Zulkipli, N. F., Jusoh, Z., Musa, B., Yasin, M., & Harun, S. W. (2021). Ti3AlC2 MAX phase thin film as saturable absorber for generating soliton mode-locked fiber laser. Optik, 245, 167767.

Pang, L., Jiang, L., Zhao, M., Zhang, J., Zhao, Q., Li, L., Wu, R., Lv, Y., & Liu, W. (2025). Ti3C2Tx/CuO heterojunction for ultrafast photonics. Journal of Materials Science & Technology, 223, 208–216.

Paschotta, R. (2008). Field Guide to Laser Pulse Generation. SPIE Press.

Popa, D., Sun, Z., Hasan, T., Torrisi, F., Wang, F., & Ferrari, A. (2011). Graphene Q-switched, tunable fiber laser. Applied Physics Letters, 98(7), 073106.

Razak, N. N., Abdul Latiff, A., Zakaria, Z., & Harun, S. W. (2017). Q-switched Erbium-doped Fiber Laser with a Black Phosphorus Saturable Absorber. Photonics Letters of Poland, 9(2).

Ren, J., Wang, S., Cheng, Z., Yu, H., Zhang, H., Chen, Y., Mei, L., & Wang, P. (2015). Passively Q-switched nanosecond erbium-doped fiber laser with MoS(2) saturable absorber. Opt Express, 23(5), 5607–5613.

Rokhsari, H., & Vahala, K. J. (2005). Observation of Kerr nonlinearity in microcavities at room temperature. Optics Letters, 30(4), 427–429.

Salah, M., Yoon, J., El-Desoky, M. M., Hussain, Z., Ju, H., & Mo, S.-K. (2022). Electronic structure of p-type transparent conducting oxide CuAlO2. Current Applied Physics, 39, 107–112.

Shakaty, A. A., Hmood, J. K., Mahdi, B. R., Mahdi, R. I., & Al-Azzawi, A. A. (2022). Q-switched erbium-doped fiber laser based on nanodiamond saturable absorber. Optics & Laser Technology, 146.

Shi, W., Fang, Q., Zhu, X., Norwood, R. A., & Peyghambarian, N. (2014). Fiber lasers and their applications. Applied optics, 53(28), 6554–6568.

Shiner, B. (2016). Fiber lasers continue to gain market share in material processing applications. Manuf. Eng., 156, 79–85.

Silvestroni, L., Melandri, C., & Gonzalez-Julian, J. (2021). Exploring processing, reactivity and performance of novel MAX phase/ultra-high temperature ceramic composites: The case study of Ti3SiC2. Journal of the European Ceramic Society, 41(12), 6064–6069.

Singh, S. P., & Singh, N. (2007). Nonlinear Effects in Optical Fibers: Origin, Management and Applications. Progress in Electromagnetics Research-pier, 73, 249–275.

Song, X., Diblawe, A. M., Tiu, Z. C., Salam, S., Ibrahim, F., & Harun, S. W. (2024). Domain-wall dark pulse generation with polyacrylonitrile as saturable absorber. Indian Journal of Physics, 1–6.

Tiu, Z., Suthaskumar, M., Zarei, A., Tan, S., Ahmad, H., & Harun, S. (2015). Generation of switchable domain wall and cubic–quintic nonlinear Schrödinger equation dark pulse. Optics & Laser Technology, 73, 127–129.

Travagnin, M. (2001). Effects of Pauli blocking on semiconductor laser intensity and phase noise spectra. Physical Review A, 64(1), 013818.

Wadi, N. I. S., Ab Kadir, R., Jusoh, Z., Ahmed, N., Khudus, M. I. M., & Salam, S. (2024). Q-switched EDFL with copper phthalocyanines saturable absorber. Optik, 296, 171547.

Wadi, N. I. S., Kadir, R. A., Jusoh, Z., Ahmed, N., Khudus, M. I. M., & Salam, S. (2024a). Utilizing Iron Phthalocyanines Absorber for the Generation of Q-switched and Mode-locked Pulses. Optik, 171665.

Wadi, N. I. S., Kadir, R. A., Jusoh, Z., Ahmed, N., Khudus, M. I. M., & Salam, S. (2024b). Utilizing iron phthalocyanines absorber for the generation of Q-switched and mode-locked pulses. Optik, 300, 171665.

Wang, G., Sheng, Q., Tang, S., Li, Q., Xiong, S., Lu, C., Bai, C., Zhang, W., Zhang, H., & Fu, S. (2023). Evolution between bright and dark pulses in a Mo x W1-x Te2 based fiber laser. Optics express, 31(16), 26145–26155.

Wang, R., Liu, Y., Jiang, M., Xu, X., Wu, H., Tian, Y., Bai, J., & Ren, Z. (2017). Passively Q-switched and mode-locked fiber laser research based on graphene saturable absorbers. Optical and Quantum Electronics, 49.

Wu, K., Zhang, X., Wang, J., Li, X., Zou, W., & Chen, J. (2019). WS2 based 523 MHz mode-locked erbium-doped fiber laser for microwave photonic application. Optical Materials Express, 9(12).

Wu, Q., Jin, X., Chen, S., Jiang, X., Hu, Y., Jiang, Q., Wu, L., Li, J., Zheng, Z., & Zhang, M. (2019). MXene-based saturable absorber for femtosecond mode-locked fiber lasers. Optics express, 27(7), 10159–10170.

Xu, X., Zhai, J., Li, L., Chen, Y., Yu, Y., Zhang, M., Ruan, S., & Tang, Z. (2014). Passively mode-locking erbium-doped fiber lasers with 0.3 nm Single-Walled Carbon Nanotubes. Scientific reports, 4(1), 6761.

Yang, S., Zhang, Q.-Y., Zhu, Z.-W., Qi, Y.-Y., Yin, P., Ge, Y.-Q., Li, L., Jin, L., Zhang, L., & Zhang, H. (2022). Recent advances and challenges on dark solitons in fiber lasers. Optics & Laser Technology, 152, 108116.

Zhang, B., Pan, H., Zhu, Y., Wang, D., Chen, C., & Li, R. (2024). Wavelength injection locking actively Q-switched with wide locking range random fiber laser based on single-mode fiber. Optical Fiber Technology, 84, 103732.

Zhang, K., Feng, M., Ren, Y., Liu, F., Chen, X., Yang, J., Yan, X.-Q., Song, F., & Tian, J. (2018). Q-switched and mode-locked Er-doped fiber laser using PtSe2 as a saturable absorber. Photonics Research, 6(9).

Zhang, K., Feng, M., Sun, G., Xie, J., Yang, J., Xu, R., Tian, Y., Song, F., & Huang, W. (2023). Q-switched and noise-like mode-locked fiber laser based on ternary transition-metal carbide Nb2AlC saturable absorber. Optics & Laser Technology, 162, 109237.

Zhang, L., Zhou, J., Wang, Z., Gu, X., & Feng, Y. (2014). SESAM mode-locked, environmentally stable, and compact dissipative soliton fiber laser. IEEE Photonics Technology Letters, 26(13), 1314–1316.

Zhang, Y., Qi, Y., Huo, X., Chen, B., Bai, Z., Yang, X., Ding, J., Wang, Y., & Lu, Z. (2021). Study of the influence of SESAM parameters on the evolution of mode-locked pulses at different repetition rates. Applied Physics B, 127(8), 1–10.

Zheng, J., Li, D., Liu, P., Cui, X., Zhang, B., Geng, W., Zhang, Q., Xu, Z., Kauppinen, E. I., & Sun, Z. (2023). Broadband synchronization of ultrafast pulse generation with double-walled carbon nanotubes. Nanophotonics, 12(17), 3397–3407.

Zheng, Z., Zhao, C., Lu, S., Chen, Y., Li, Y., Zhang, H., & Wen, S. (2012). Microwave and optical saturable absorption in graphene. Optics express, 20(21), 23201–23214.

Zuikafly, S. N. F., Ahmad, H., Ismail, M. F., Abdul Rahman, M. A., Yahya, W. J., Abu Husain, N., Abu Kassim, K. A., Yahaya, H., & Ahmad, F. (2023). Dual Regime Mode-Locked and Q-Switched Erbium-Doped Fiber Laser by Employing Graphene Filament-Chitin Film-Based Passive Saturable Absorber. Micromachines (Basel), 14(5).

AUTHOR'S PROFILE



Muhammad Nur Al Hafiz Bin Mohamad Husaini obtained his Bachelor of Engineering (Hons.) in Electrical and Electronic Engineering from Universiti Teknologi MARA in 2020. He later completed his Master of Science in Telecommunication and Information Engineering at the same university in 2023. He is currently pursuing his PhD at Universiti Teknologi MARA, Terengganu Campus, specializing in photonics. His research focuses on fiber laser technology, particularly passive Q-switched and mode-locked pulse generation in erbium-doped fiber lasers (EDFL). His work involves studying pulse formation mechanisms, stability, and performance optimization for applications in optical communication and photonic systems. Through his research, he has gained strong hands-on experience with various optical and electronic instruments, including radio-frequency spectrum analyzers, digital oscilloscopes, optical spectrum analyzers, optical power meters, and autocorrelators. He is also skilled in using fiber-optic equipment such as fiber splicers, fiber cleavers, and laser diode pump sources for building and maintaining fiber laser cavities. He is actively involved in experimental setup design, system alignment, troubleshooting, and data analysis related to photonic systems. His knowledge and experience in laser operation and fiber optics have contributed to the scientific community through the publication of several research papers in reputable journals.

LIST OF PUBLICATIONS

M. N. A. H. M. Husaini, N. I. S. Wadi, A. M. Markom, K. Dimyati, R. Apsari, and Z. Jusoh, "Mode-locked erbium-doped fiber laser based on Cr2GaC saturable absorber," Optik, vol. 311, p. 171902, 2024/09/01/ 2024, doi: https://doi.org/10.1016/j.ijleo.2024.171902.

M. N. A. H. M. Husaini, N. I. S. Wadi, Z. Jusoh, A. D. Ahmad, R. Apsari, and K. Dimyati, "Dark pulse generation in mode-locked erbium-doped fiber lasers using chromium gallium carbide film-based pulse transducer," Physica Scripta, vol. 100, no. 5, p. 055535, 2025/04/21 2025, doi: 10.1088/1402-4896/adcb76.

M. N. A. H. M. Husaini Aeriyn D. Ahmad, Masruroh, Sulaiman Wadi Harun ., "Copper Aluminum Oxide for enabling Q-switching and mode-locking in erbium-doped fiber lasers," Optik, vol. 339, p. 172545, 2025/11/01/ 2025, doi: https://doi.org/10.1016/j.ijleo.2025.172545.